People's Democratic Republic of Algeria
Ministry of Higher Education and Scientific Research
University of Oum El Bouaghi
Faculty of: Science and Applied Sciences

Thesis

Presented to obtain

3rd Cycle Doctorate

Branch: Electrotechnics

Specialty: Electrical Network

Title:

Integrated Energy Management Model of a Hybrid Renewable Energy System Connected to the Electrical Grid

Presented by:
Menzri Fatima

Publicly defended on 08/10/2024 in front of the following committee members:

01	SAKRI Djamel	MCA	University of Oum El Bouaghi	President
02	BOUTABBA Tarek	MCA	University of Abbes Laghrour Khenchela	Supervisor
03	LAIB Hichem	MCA	University of Oum El Bouaghi	Examiner
04	DRID Said	Prof.	HNS RE2SD Batna School	Examiner
05	SAIFI Rabie	MCA	University of Setif	Examiner
06	BELILA Hassen	MCA	University of Oum El Bouaghi	Examiner

Acknowledgements

At the end of this work, I would like to express my gratitude and thanks to all the people who contributed, each in their own way, to the completion of this thesis.

First of all, I would like to sincerely thank my thesis supervisor:

Mr. BOUTABA Tarek, doctor at the University of Khenchela, for his continuous support, guidance, and encouragement throughout my PhD journey.

I also extend my sincere thanks to ***Mr. SAKRI djamel*** , doctor at the University of Oum El Bouaghi, for accepting to be the president of the jury for this thesis.

I would also like to warmly thank the jury members:

Mr. LAIB Hichem, doctor at the University of Oum El Bouaghi, ***Mr. DRID Said***, Professor at the University HNS RE2SD Batna, ***Mr. SAIFI Rabie***, doctor at the University of Ferhat Abbas Sétif 1, ***Mr. BELILA Hassen***, doctor at the University of Oum El Bouaghi for honoring me by accepting to be the examiners of this thesis.

Abstract:

The increasing and continuous demand for electricity and its various uses in different fields, especially in industry, has prompted scientists and researchers to search for new and RES. This is because fossil energy sources are depleting on one hand, and they are among the main sources of environmental pollution on the other. Renewable energies have many advantages, but the unpredictable nature of weather conditions poses challenges that require the development of new strategies and methods for optimal exploitation. Our research addresses the proposal of a strategy for managing the energies of a hybrid system linked to the electrical grid, which consists of solar and wind energy as the main elements for energy production. A storage system was integrated as a secondary element to cover shortages through charging and discharging when the main system fails to meet the demands of an alternative load, taking into account the battery condition at specified values to avoid degrading its lifespan. Simultaneously, the proposed strategy aims to reduce the role of the electrical grid by prioritizing the hybrid system and the storage system in feeding the load. The outcomes achieved using MATLAB Simulink confirmed the proposed plan's effectiveness.

Key words: Renewable energy, Electrical grid, Wind turbine, Photovoltaic, Storage system, Energy management system.

Résumé :

L'augmentation et la demande continue en électricité et ses diverses utilisations dans différents domaines, notamment dans l'industrie, ont incité les scientifiques et les chercheurs à rechercher de nouvelles énergies renouvelables (ER). Cela s'explique par l'épuisement des sources d'énergie fossiles d'une part, et le fait qu'elles sont parmi les principales sources de pollution environnementale d'autre part. Les énergies renouvelables présentent de nombreux avantages, mais la nature imprévisible des conditions météorologiques pose des défis qui nécessitent le développement de nouvelles stratégies et méthodes pour une exploitation optimale. Notre recherche propose une stratégie de gestion des énergies d'un système hybride relié au réseau électrique, composé de l'énergie solaire et éolienne comme principaux éléments de production d'énergie. Un système de stockage a été intégré en tant qu'élément secondaire pour pallier les pénuries en chargeant et déchargeant lorsque le système principal ne parvient pas à répondre aux besoins d'une charge alternative, en tenant compte de l'état de la batterie à des valeurs spécifiées afin d'éviter de dégrader sa durée de vie. Simultanément, la stratégie proposée vise à réduire le rôle du réseau électrique en donnant la priorité au système hybride et au système de stockage pour alimenter la charge. Les résultats obtenus à l'aide de MATLAB Simulink ont confirmé l'efficacité du plan proposé.

Mots clés : Énergie renouvelable, Réseau électrique, Éolienne, Photovoltaïque, Système de stockage, Système de gestion de l'énergie.

ملخص:

إن الطلب المتزايد والمستمر على الكهرباء واستخداماتها المختلفة في مختلف المجالات، وخاصة في الصناعة، دفع العلماء والباحثين إلى البحث عن مصادر الطاقة الجديدة والمتجددة. وذلك لأن مصادر الطاقة الأحفورية آخذة في النضوب من جهة، وهي من المصادر الرئيسية للتلوث البيئي من جهة أخرى. تتمتع الطاقات المتجددة بالعديد من المزايا، لكن طبيعة الظروف الجوية التي لا يمكن التنبؤ بها تفرض تحديات تتطلب تطوير استراتيجيات وأساليب جديدة للاستغلال الأمثل. يتناول بحثنا مقترح استراتيجية لإدارة طاقات النظام الهجين المتصل بالشبكة الكهربائية والذي يتكون من الطاقة الشمسية وطاقة الرياح كعنصرين أساسيين لإنتاج الطاقة. تم دمج نظام تخزين كعنصر ثانوي لتغطية النقص من خلال الشحن والتفريغ عندما يفشل النظام الرئيسي في تلبية متطلبات الحمل المتناوب، مع مراعاة حالة البطارية عند قيم محددة لتجنب تدهور عمرها الافتراضي. وفي الوقت نفسه تهدف الاستراتيجية المقترحة إلى تقليص دور الشبكة الكهربائية من خلال إعطاء الأولوية للنظام الهجين ونظام التخزين في تغذية الأحمال. أكدت النتائج التي تم الحصول عليها باستخدام برنامج المحاكاة فعالية الطريقة المقترحة.

كلمات مفتاحية: طاقات متجددة، شبكة كهربائية، توربينات الرياح، الكهروضوئية، نظام التخزين، نظام إدارة الطاقة.

Table of contents

Chapter 2: Modeling of a hybrid system connected to the electrical grid

Chapter 3: Optimization and managing of hybrid renewable energy systems (HRES)

List of Figures

List of tables

Lists of acronyms and symbols acronyms	
RE	Renewable energy
RES	Renewable energy sources
HREMS	Hybrid renewable energy management system
HRES	Hybrid renewable energy system
HES	Hybrid energy system
PV	Photovoltaic
WT	Wind turbine
PMSG	Permanent magnetic synchronous generator
BSS	Battery storage system
MPPT	Maximum power point tracking
MPP	Maximum power point
SMC	Sliding mode control
FLC	Fuzzy logic control
DPC	Direct power control
P-DPC	Predictive direct power control
THD	Total harmonic distortion
P&O	Perturb and Observe algorithm
SOC	State of the charge
SOC_{max}	Maximum state of the charge of the battery
SOC_{min}	Minimum battery state of the charge
PD	Proportional-Derivative
PI	Proportional-Integral
Symbols	
I_{pv}	Current supplied by PV cell (A)

V_{pv}	Voltage at cell terminal (V)
I_{pv_n}	Photo current generated by irradiation at nominal condition (A).
G	Irradiation (W/m^2).
Gn	Nominal irradiation (W/m^2).
I_D	Current generated by the diode (A).
Ir	Current across the shunt or parallel resistor.
I_0	Diode saturation current (A).
Isc,n	Rated short circuit current (A).
Voc,n	Rated open circuit voltage (V).
R_s	Series resistance (Ω).
R_{sh}	Shunt resistance (Ω).
T	Cell temperature ($°K$).
T_n	Nominal cell temperature ($°K$).
$\boldsymbol{a}$	Ideality factor of the diode ($1 \leq a < 1.5$).
N_s	Number of photovoltaic cells connected in series
N_{ss}	Number of photovoltaic modules connected in series
N_{pp}	Number of Photovoltaic modules connected in parallel
K	Boltzmann constant (K=1.3806503 10−23 $J\ K$−1).
Ki	Short-circuit current coefficient/Temperature
q	Charge of the electron (q=1.60217646 10−19 C).
V_w	The output voltage of the wind turbine (V)
I_w	The output current of the wind turbine (A)

P_{aer}	Aerodynamic power (W)
Ω_t	Angular speed of the turbine (rad/s)
T_{aer}	Aerodynamic torque of the wind turbine (N·m)
Cp	Wind turbine power coefficient
$\boldsymbol{\lambda}$	Specific speed
β	Pitch angle (°)
ρ	Air density (kg/m^3)
V	Wind Speed (m/s)
J_t	Total moment of inertia of the turbine and generator assembly ($kg \cdot m^2$)
P	Number of pole pairs electromagnetic torque
T_{em}	Electromagnetic torque (N·m)
Tg	The effect of turbine torque on the generator shaft (N·m)
I_{w_opt}	Optimal Wind current (A)
$\boldsymbol{\lambda}_{opt}$	Optimal specific speed
G	The gain multiplier
V_{bat}	Battery voltage (V)
I_{bat}	Battery current (A)
V_{dc}	DC bus terminal voltage (V)

General introduction

According to a recent report by the international energy agency (IEA), 2023 has been a milestone year for the growth of global renewable electricity production capacity. An additional 510 gigawatts (GW) were added, a 50% increase from 2022, marking the highest growth seen in the past thirty years. China led this surge, adding as much photovoltaic solar energy in 2023 as was connected globally in 2022 (including China). Additionally, China's wind power capacity saw a remarkable 66% increase. Europe, the United States, and Brazil also achieved new highs in renewable energy capacity expansion. The IEA predicts that with existing policies and market circumstances, The global renewable energy capacity is anticipated to reach 7,300 GW between 2023 and 2028, a 2.5-fold increase. Solar and wind energy will dominate this expansion, accounting for 95% of the growth. With this trend, renewable energies are expected to surpass coal as the leading source of electricity production by 2025. However, despite this significant progress over the past year, the world must triple its renewable electricity capacity by 2030 to meet the commitments made at COP28 [1].

The previously mentioned statistics highlight the importance of utilizing renewable energy sources (RES) for electricity generation and reducing the reliance on fossil fuel sources, which are major contributors to environmental pollution. Fossil fuels are responsible for up to 40% of carbon dioxide emissions [2], prompting many researchers to seek new, non-polluting, and renewable energy sources. Their goal is to exploit these sources optimally and efficiently by developing methods and strategies that make them indispensable, unlike fossil fuel sources which are destined to deplete over time.

While RES have many advantages, they are not entirely free of drawbacks. One of the main disadvantages is the irregularity of weather conditions, which affects the consistent production of renewable energy [3]. This challenge has led researchers to combine multiple sources in a single system for electricity generation, leveraging the strengths of each source. This integrated approach is known as a hybrid system.

Our topic focuses on managing the energy of a hybrid system connected to the grid., which consists of two primary RES, including solar energy and wind energy. These sources are among the most widely used worldwide for electricity production. A battery is integrated as a secondary component in the hybrid system to supply alternating loads through static converters. Batteries serve as an excellent complement to the hybrid system, especially in isolated areas, by covering deficiencies of the primary system. Despite their importance, the relatively high cost and limited lifespan of batteries, due to deep discharge or excessive demand, affect the use of storage systems and their applications.

As mentioned before, while renewable energies have many advantages, their main weakness is the random variation in weather conditions. Furthermore, the diversity and differences in production sources and their dynamic composition led us to propose a strategy on how to manage different energy outputs to meet load requirements while maintaining system balance without faults and issues despite the challenges presented.

To address the raised issue, the thesis was divided into four chapters, the first one provides a technical overview and some statistics about renewable energy sources and their utilization worldwide, with a particular focus on Algeria. We also reviewed previous studies by researchers in the same context and examined the impact of integrating RES with the electrical grid.

In the second chapter, we present the mathematical models of the various components of the grid-connected hybrid system, which were adopted in the thesis. The third chapter provides an introduction to our topic, where we discuss the strategy for optimizing and managing a standalone hybrid system. We proposed a strategy for tracking the maximum power point (MPP) of RES and managing the energy required to satisfy demand by adjusting the continuous voltage according to the reference value using the bidirectional static converter for the storage system.

In the fourth chapter, the strategy for managing the grid-connected hybrid system was addressed and explained by optimizing and efficiently managing

different energy outputs, prioritizing renewable energy sources to meet load demands while minimizing the grid's role. This was achieved through the charging and discharging of the storage system, considering the state of the charge at specific values.

The main objective of our subject is to propose a strategy for the optimal management of energy in a grid-connected hybrid system. To achieve this main goal, we addressed several key points:

- Improving the quality of energy produced from various sources
- Reducing the dependency on the electrical grid with ensuring load demand is met.
- Automatically integrating the battery and improving its role

Chapter 1: State of the art on the HRES connected to the electrical grid

1. Introduction

Today, renewable energies are increasingly taking a significant role in our society. Faced with environmental challenges and concerns associated with the depletion of natural resources, renewable energies offer promising and sustainable solutions to meet our energy needs.

Renewable energies, also known as green energies, are sources of energy that naturally and continuously regenerate. They are mainly produced from natural resources like sunlight, water, wind, biomass, and geothermal energy. Unlike fossil fuels like oil, coal, and natural gas, which are non-renewable and contribute to greenhouse gas emissions, renewable energies have a reduced environmental impact and contribute to the fight against climate change [4].

In the first chapter, we provided a technical overview of renewable energies, focusing on two main sources: solar energy and wind energy, as they are the primary sources considered in our subject. We also presented some statistics on their utilization rates globally and specifically in Algeria. Moving on, we gave a brief definition of the storage system, particularly nickel-metal hydride batteries. The combination of more than one source led us to define the hybrid system and provide some details related to it and its impact when connected to the electrical grid. At the end of this chapter, an overview was provided of the strategy used to manage the proposed hybrid system's energy.

2. Diverse electricity production sources

There are two different technologies used in electricity production, where raw materials are used and converted into electrical energy through specific techniques. These include fossil energy sources and RES.

Fossil energy sources include coal, oil, and natural gas, which are extracted from underground and are non-renewable. They have been used for many years to generate electricity, but their use has led to air pollution and the emission of greenhouse gases, prompting the world to seek new RES [7].

On the other hand, RES include solar energy, biomass, wind energy, hydroelectric energy, and geothermal energy, as mentioned in detail in references [2][3]. Their main characteristics are their continuous renewability and reduced environmental impact, as they do not produce harmful greenhouse gases.

Today, RES are receiving increasing interest due to their long-term availability and low environmental impact. Many governments and companies are investing in the development of technologies to exploit these energy sources optimally and decrease reliance on fossil fuels. However, efforts continue to find innovative solutions to maximize the use of renewable energy sources and achieve a sustainable energy future [4]. The following graph illustrates the proportion of different energy sources used in electricity production [5].

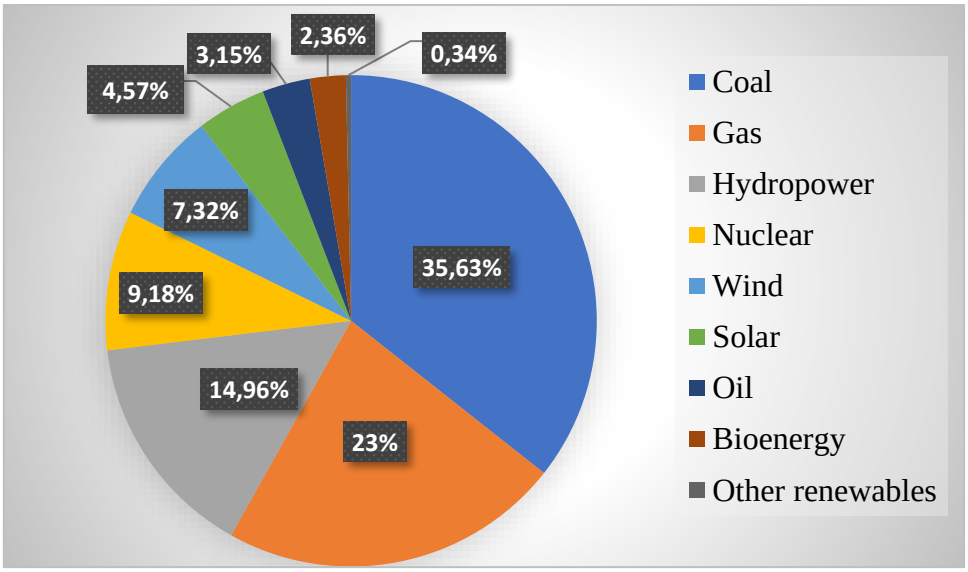

Figure 1.1. Different Sources for Electricity Production (2022)

3. Concept of a hybrid energy system (HES)

The combination of fossil energy sources with two or more RES such as solar, wind, and other sources mentioned earlier is referred to as a hybrid system [6]. Due to the complexity of its configuration resulting from the diversity of production sources, the system requires advanced energy control and management techniques, as well as optimal power supply to the load.

The primary objective of adopting a hybrid system instead of a single renewable energy source is generally to increase energy production efficiency and provide sufficient power supply to the load without interruption.
Hybrid systems generally operate in two modes: either they are connected to the electrical grid or they are isolated (autonomous).

The isolated hybrid systems, which are not connected to the electrical grid, are considered more prevalent compared to centralized systems [7]. This is due to its facility of control and its ability to meet the needs of remote sites through centralized networks. Here is an illustration to clarify the hybrid system:

Several references such as [8] have classifies hybrid systems based on the amount of energy produced, ranging from a few watts to several megawatts. Hybrid systems are used for a variety of applications, from small houses to large grids. Low-power HES, typically below 5 kW, are commonly used to power small houses and decentralized facilities. On the other hand, larger-scale systems with a capacity exceeding 500 kW are designed to connect to large-scale electrical networks, such as distribution networks or interconnected grids.

4. Advantages and disadvantages of a hybrid energy system

Like any natural system, the hybrid system has both advantages and disadvantages. The advantages of this system are numerous, while its disadvantages are relatively limited. They can be detailed as follows [9] [10]:

a. Advantages of a hybrid energy system

The hybrid system offers several advantages compared to a single energy source:

• Independence from a single energy source.
• facility of operation, requiring less maintenance and revisions.
• Cost-effectiveness, with reduced costs.
• The hybrid system stands out for its adaptability, flexibility, and capability to meet evolving load requirements.

b. Disadvantages of a hybrid energy system

The hybrid system also has a few disadvantages that can be mentioned as follows [9]:

- Higher initial cost compared to traditional diesel generators.
- On the other hand, the hybrid system is more complicated than single-source systems as it requires integrating different energy sources and implementing storage devices to ensure optimal energy management.

5. Different architectures of hybrid energy systems

There are three various types of RES integration in hybrid system design, which are as follows:

5.1. DC bus configuration

The configuration of the DC bus is widely used due to its ease and simplicity of control compared to other designs [10] as represents in figure 1.2. The hybrid system operates by supplying the DC bus using static converters (DC/DC - AC/DC) to power the subsequent load, whether it is DC or AC. This type of design is typically used in isolated or hard-to-reach areas.

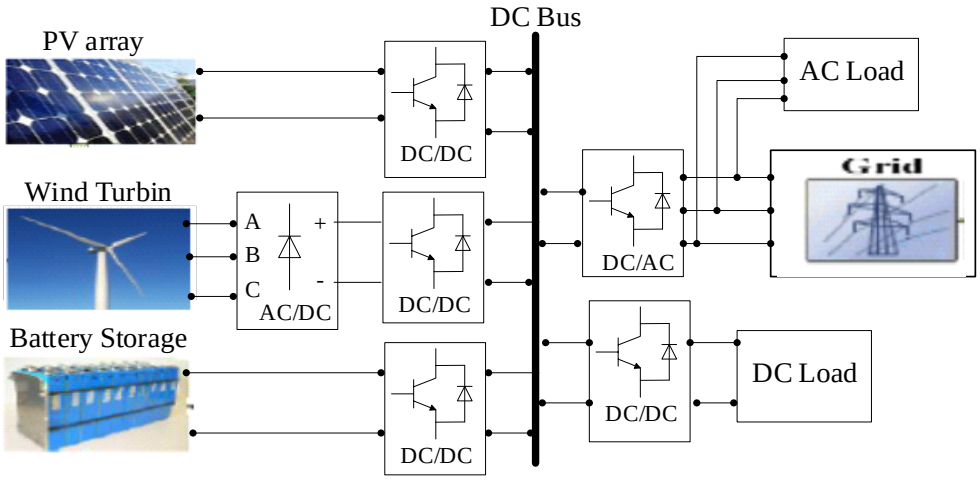

Figure 1.2. DC Bus Configuration

5.2. AC bus configuration

The configuration of the AC bus is considered more complex than the previously mentioned configuration (Figure 1.3). It relies on the use of

multiple static converters to connect different energy production sources and the AC bus, resulting in greater complexity of the overall control system design and has a negative impact on the power output efficiency [11].

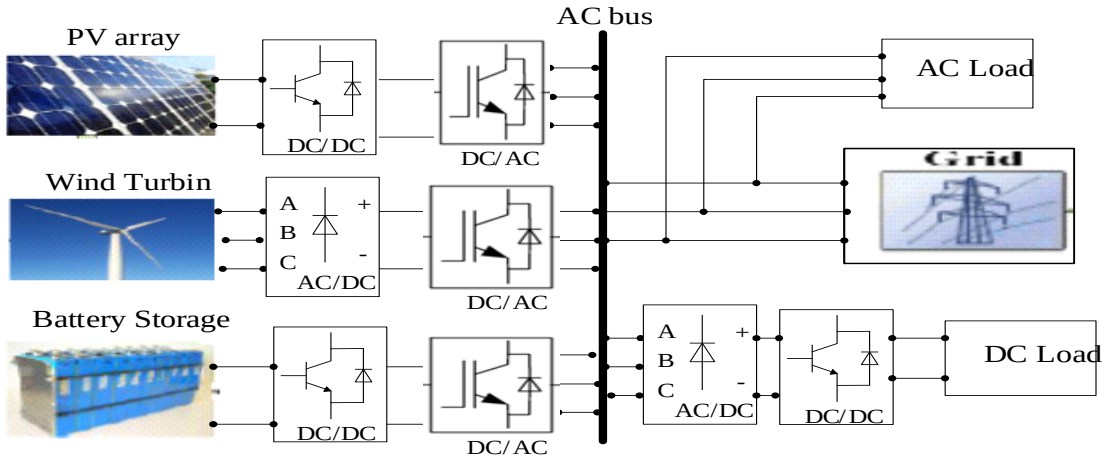

Figure 1.3. AC Bus Configuration

5.3. DC/AC mixed bus configuration

The mixed design, also known as DC/AC design, involves connecting the DC bus to the AC bus through a static converter, as shown in figure 1.4. One of the advantages of this design is that it allows for separate, easy, and efficient power supply to both DC and AC loads [12].

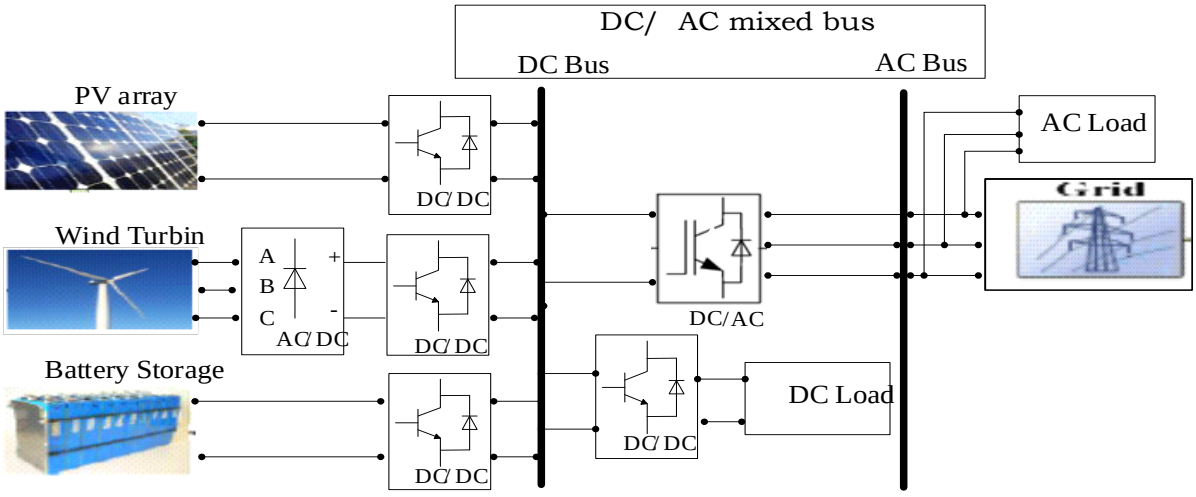

Figure 1.4. DC/AC mixed bus configuration

6. Hybrid system connected to the electrical grid

The integration of RE to the electrical grid involves the implementation of technical measures, advanced management systems, and compliance with

standards to ensure smooth and efficient integration. This transition promotes the transformation towards a sustainable energy system, reduces carbon emissions, and contributes to the development of a cleaner and more responsible energy future. The aforementioned is achieved through computer technologies or the so-called "smart grid." The static converter known as an "inverter" can serve as a link between the hybrid energy system (HES) and the electrical grid to perform power conversion (DC/AC) [13].

6.1. Definition of a smart grid

The term smart grid (SG) , refers to a network for the transmission and distribution of electrical energy that is connected to high-tech devices. These devices, including electronic meters, enable remote measurement, monitoring, and other controls, thereby providing greater benefits to utility companies such as system reliability, security, and efficiency. Current technological advancements offer significant opportunities for energy savings and improved management of electrical energy. With these new technologies, it is possible to smooth out consumption peaks by implementing intelligent strategies that distribute demand over a longer period. Furthermore, by promoting the use of decentralized production sources such as solar and wind energy, dependence on traditional and polluting energy sources is reduced. In summary, new technologies offer effective solutions for optimally managing the demand and production of electrical energy. This results in cost savings, improved power supply reliability, and reduced environmental impacts through a decrease in the use of polluting sources. The integration of these technologies into electrical grids paves the way for a more sustainable and economically advantageous energy future for all [14].

Figure 1.5 illustrates the concept of "smart grid," where decentralized generation and usage are optimally controlled locally through central control units. In this way, each local cluster of decentralized generators and loads, along with storage devices, appears to the distribution grid operator as a single entity that can act either as an electricity consumer or producer. This makes it easier to predict consumption and production in the short term,

thereby providing more information to other stakeholders in the electrical system, allowing for overall system improvement [29].

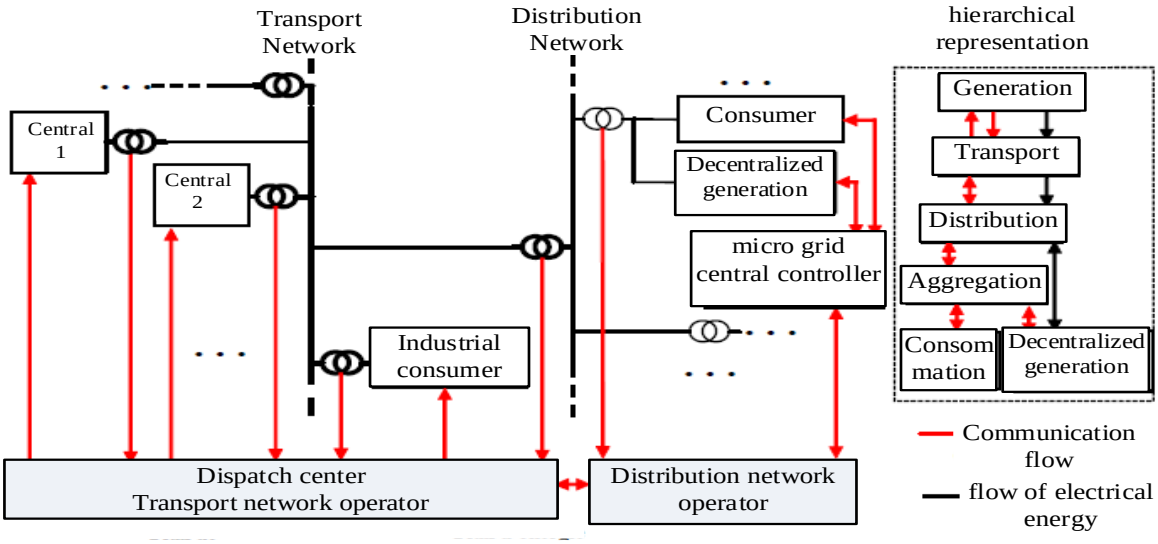

Figure 1.5. Smart grid structure [29]

6.2. Design of the proposed hybrid renewable energy system

The proposed hybrid generation system consists of two renewable energy sources and their accessories (solar and wind), each individually controlled for energy generation. The storage system is integrated as a secondary component to improve system efficiency and store excess energy. The various mentioned elements are connected to the (DC) bus via static converters as needed, and then integrated into the electrical grid through an inverter, which uses a filter to reduce harmonics in the inverter voltage before connecting to the load.

6.2.1. Solar energy

6.2.1.1. International and national potential of solar energy

The Earth's surface receives a substantial amount of energy from the sun, far exceeding current global energy consumption by 7900 times. On average, each square meter of sunlight-exposed land can generate 1700 kWh of power annually [15]. Most regions experience approximately 4380 daylight hours per year, representing half of the total annual duration.

Global horizontal irradiance (GHI) quantifies the solar resource available per unit surface area, with different regions receiving varying annual average

solar energy. In the Middle East, GHI ranges from approximately 1800 to 2300 kWh/m²/year, while in Europe it's around 1200 kWh/m²/yr. Regions like the United States, Latin America, Africa, Australia, India, China, and other Asian countries possess significant solar energy potential, aligning with anticipated increases in energy demand in the coming decades [16].

Areas with lower solar energy reception include Alaska, Canada, Russia, Northern Europe, and Southeast China. However, adjusting equator-facing solar collectors towards the sun can mitigate these differences and enhance energy yield, especially at higher latitudes. This adjustment's effectiveness depends on meteorological patterns and the balance of diffuse versus direct light [17].

Developing countries, due to their geographical positioning, exhibit high potential for solar radiation receipt compared to developed nations. This comparison underscores the abundant and seemingly inexhaustible nature of solar energy. Many developing countries possess sufficient solar radiation to make solar energy a viable utility option [18]. Recognized as a crucial clean energy source among renewables, solar energy holds promise in addressing climate change consequences and enhancing energy security.

Figures 1.6. describes the evolution of solar energy production in the leading solar-producing countries over several years.

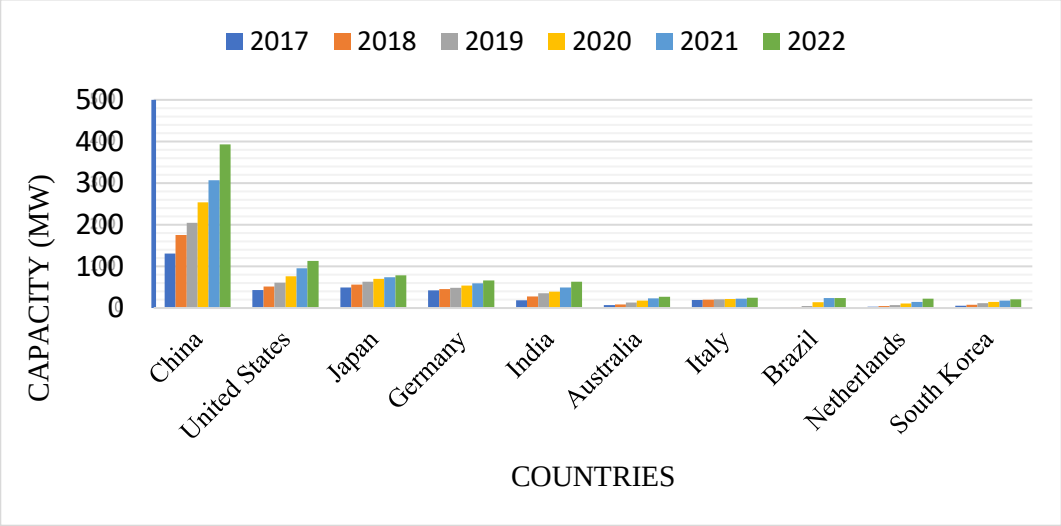

Figure 1.6. Chart illustrating the evolution of solar energy production in the top solar-producing countries over several years.

To understand the importance of renewable energies. in Algeria and the considerable stakes, they entail, it is first necessary to recall the substantial and untapped existing resources of these energies. Algeria possesses one of the highest solar potentials in the world (covering an area of 2,381,745 km2), with an average sunshine duration in the Algerian Sahara of 3,500 hours. This potential could be a significant factor in sustainable development in this region if economically exploited. Compared to solar energy, wind, biomass, and geothermal potentials are much less significant, while hydroelectric potential is very low. Faced with the dual challenge of decreasing fossil fuels and climate change, renewable energies represent a new alternative and a secure future for energy security in Algeria [19].

Algeria annually receives one of the world's most significant solar energies across its entire territory (Figure 1.7.). It totals around 5.2 quadrillion kilowatt-hours per year [18], equivalent to: 430 times Algeria's proven hydrocarbon reserves and 4.8 times the amount found globally proven oil reserves.

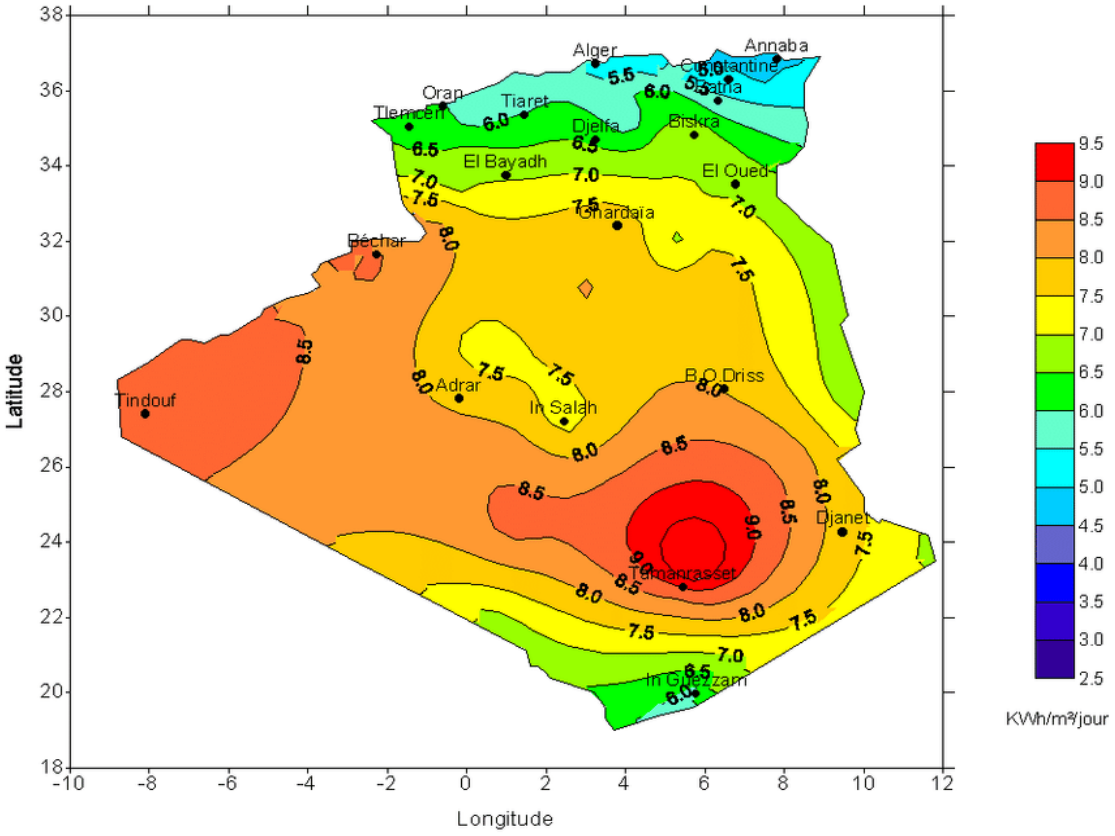

Figure 1.7. Global distribution of annual solar radiation in kWh/m2 [19]

Solar power represents the most significant potential among renewable energies in Algeria. It accounts for 169.44 TWh per year, which is 5000 times Algeria's electricity consumption. With over 2,000 hours of sunshine per year and up to 3,900 hours in the high plateaus and Sahara, the daily solar energy received in Algerian territory is around 1,700 kWh/m2/year in the North and 2,263 kWh/m2/year in the South. This averages more than 2,200 kWh/m2/year. From 2016 to 2020, four solar thermal power plants equipped with storage, totaling about 1200 MW, were commissioned. The program for the 2021-2030 phase plans to install 500 MW annually until 2023, followed by 600 MW annually until 2030 [20].

6.2.1.2. Operating principle of a photovoltaic cell

The basic unit of a photovoltaic panel is a cell, which can be either square or round in shape. The cell is a sensor made of a semiconductor material that absorbs light energy and directly converts it into electrical current [21]. Cells are linked together to form a module or panel, and these modules are then connected to create an array for generating the necessary electrical power. There are three primary types of cells: monocrystalline, polycrystalline, and amorphous:

- Monocrystalline cells: are composed of thin slices cut from a single silicon crystal. They have a higher efficiency (12-17%).
- Polycrystalline cells: are composed of thin slices cut from a block of silicon crystals. They have lower efficiency (11%-13%).
- Amorphous cells: are made up of very thin layers of a photosensitive material deposited on inexpensive substrate such as glass, stainless steel, or plastic. Thin-film technology has lower production costs compared to crystalline technology. Their efficiency is lower (5%-10%).

Solar energy is derived from sunlight, wherein photons from sunlight force free electrons to flow, converting it into direct current electricity, known as the photovoltaic effect (Figure 1.8)

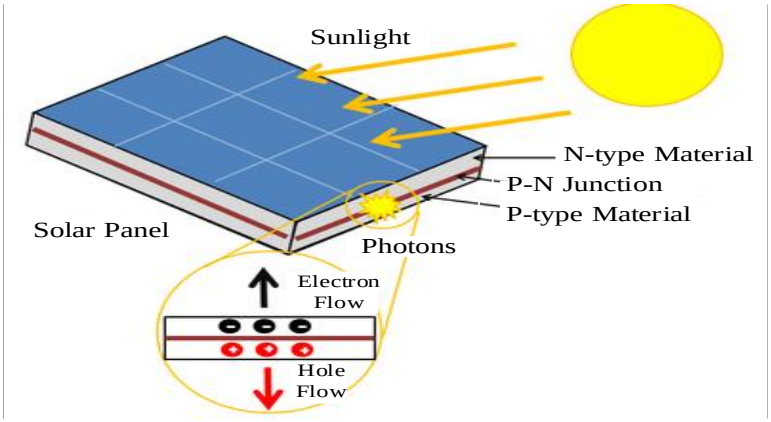

Figure 1.8. Operating principle of a photovoltaic cell [23]

Practically, each cell provides between 2 to 4 amps depending on its dimensions, providing an output voltage of 0.5 volts. Typically, a panel with cells linked in series provides 12 volts to charge batteries.

Connecting multiple modules in series increases the voltage of the PV system. Indeed, this arrangement ensures that all cells are traversed by the same electrical current. Whereas, in a grouping of several modules in parallel, they increase the current of the PV system for the same voltage. Figure 1.9. shows the resulting characteristics for different assemblies of identical PV modules [24].

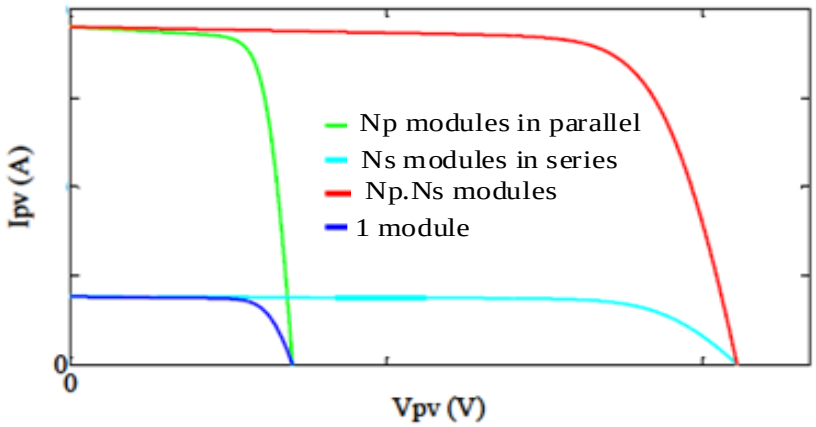

Figure 1.9. Resultant characteristics for different PV module assemblies [24]

6.2.1.3. Types of photovoltaic systems

Photovoltaic systems in the realm of solar energy have been classified into two types, based on the system's service or desired applications. The first

type is the standalone photovoltaic system. This type is typically used in remote areas where access to traditional electrical grids is difficult. Batteries are usually employed in these systems to store the generated energy. One of its advantages is the ease of supplying electrical energy to consumers. The second type is the grid-connected photovoltaic system, where the photovoltaic generator is connected to the electrical grid through static converters. This type is typically used to support electrical grids in power generation when demand is high on one hand, and to reduce fossil fuel usage on the other hand.

6.2.1.4. Advantages and disadvantages of a PV system

The photovoltaic system has many advantages [25]:

- Inexhaustible solar energy;
- Free fuel;
- Solar energy providing electricity to the most isolated rural areas;
- Solar panels requiring very little maintenance;
- Silent and non-disturbing solar panels;

However, photovoltaic sources also have some disadvantages [25]:

- Dependent on weather conditions: photovoltaic sources do not work when solar energy is not available;
- Manufacturing of PV modules involve high technology;
- Cost: PV installation requires high-cost investments;
- Efficiency: PV module conversion has low efficiency
- Size of installations: Solar energy is not competitive for large-scale energy production because it requires a large area.

6.2.2.Wind energy

6.2.2.1. International and national potential of wind energy

According to the global wind energy council (GWEC), the installed global capacity by the end of 2022 is approximately 906 gigawatts, with onshore wind power representing the majority at around 842 gigawatts. China leads

as the largest installer of wind power capacity globally, surpassing the United States by more than double. By 2022, China had installed over 395 gigawatts of wind energy, compared to 122.2 gigawatts in the United States. This significant increase in wind energy capacity reflects a growing trend over recent decades [26].

The potential of wind energy worldwide is immense, and with the availability of new technologies, renewable energy generation globally is steadily increasing. This underscores the promising future of RES in meeting the global energy demands in a sustainable manner.

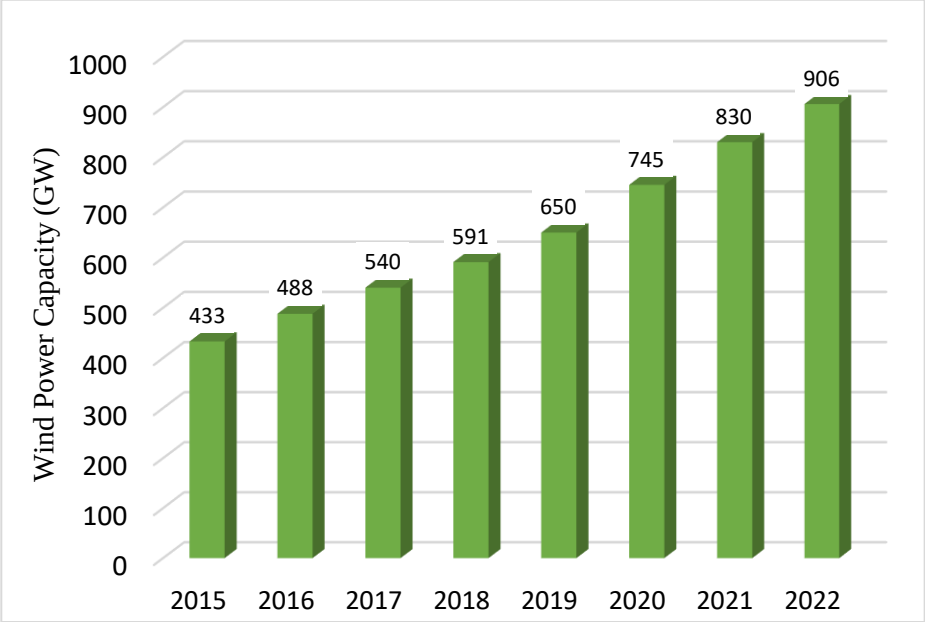

Figure 1.10. The total installed global capacity of wind power from 2015 to 2022.

Algeria has a moderate wind regime (2 to 6 m/s). In the North, it is generally observed that the average speed is relatively low. However, microclimates are noted on the coastal sites of Oran, Bejaia, and Annaba, on the high plateaus of Tiaret, and also in the region bordered by Bejaia in the North and Biskra in the South [27].

The South, conversely, is distinguished by higher speeds than the North.

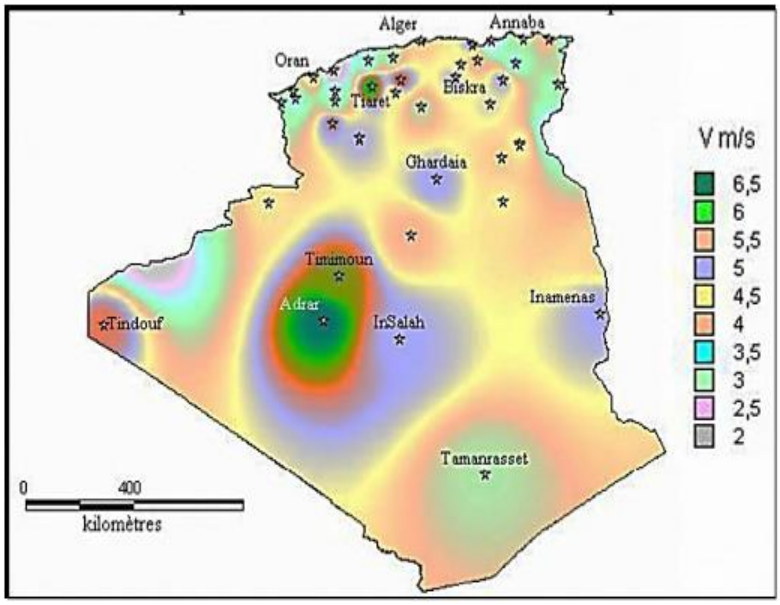

Figure 1.11. Wind speed map of Algeria [27]

6.2.2.2. Wind turbine system

A wind turbine is a mechanism that transforms the wind's kinetic energy into mechanical energy as presented in Figure 1.12. This energy is then typically transformed into electricity. Wind turbines operate for wind speeds generally ranging between 14 and 90 km/h, through a speed multiplier. The generator converts mechanical energy into electrical energy, directly injected into the electrical grid [28]. The amount of energy generated by a wind turbine primarily based on the wind speed, but also on the swept area of the blades and the air density

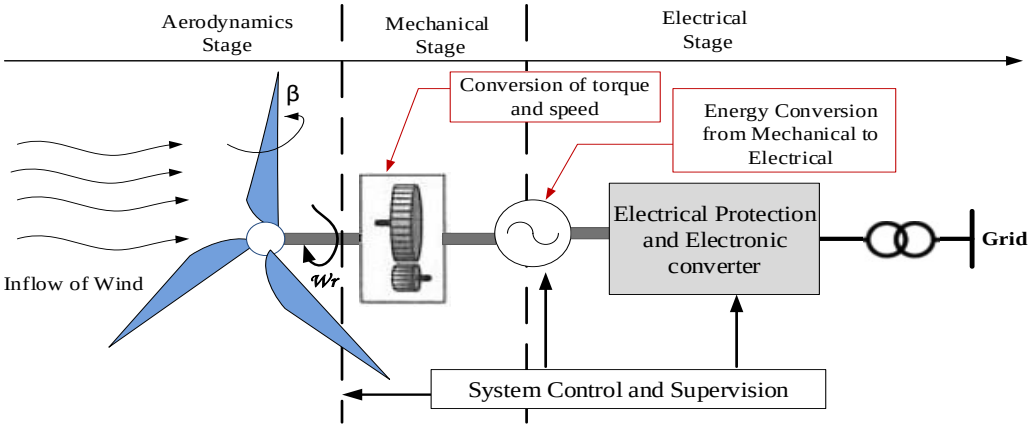

Figure 1.12. Main components of the wind conversion system [28]

6.2.2.3. Advantages and disadvantages of wind energy:

As with any form of energy present on the Earth's surface, wind energy has both advantages and disadvantages. Here are several advantages of wind energy:

- Similar to solar energy, wind energy is clean and does not contribute to air pollution.
- Wind energy is a cost-effective energy source because it relies on freely available natural wind.
- Wind energy can have great economic benefits, as it provides opportunities for countries that lack fossil fuels to limit the import of huge amounts of fuel to produce local energy.
- Wind turbines require only a small portion of land to operate, allowing the land to be used for agricultural or other purposes

along with several disadvantages listed in several points as follows:

- The energy harnessed by wind turbines is subject to weather conditions and its availability depends on the presence of wind gusts.
- Construction cost remains very high.
- Noise and visual impact.

6.2.2.4. Different types of wind turbines

There are two main categories of wind turbines:

- Vertical-axis wind turbines.
- Horizontal-axis wind turbines, based on speed criterion, this type of wind turbines is divided into two other classes:
  - Slow wind turbines (mainly used for pumping).
  - Fast wind turbines (used in electricity generation).

a. Vertical-axis wind turbines

Vertical-axis wind turbines were among the earliest structures developed for electricity generation, alongside the traditional horizontal-axis windmills. They offer the advantage of having control mechanisms and the generator

located at ground level. Thus, easily accessible. The peculiarity of this type of wind turbine is that they do not need to orient themselves with respect to the wind. Many variants have been tested, many without success, but both structures have been industrialized are the rotor of Savonius and the rotor of Darrieus [29].

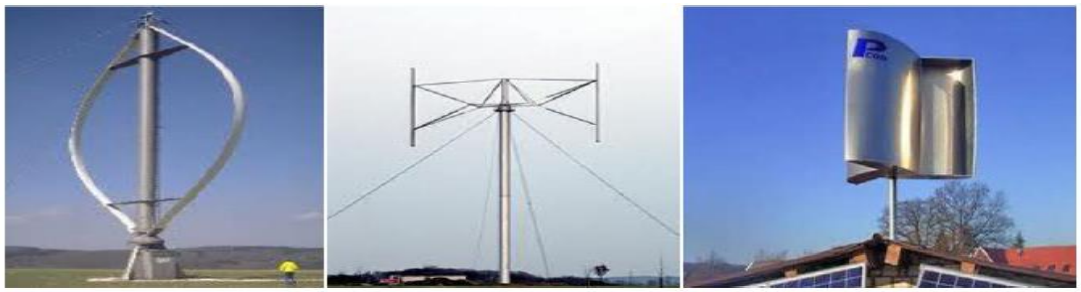

a) Classic Darrieus **b)** Turbines Darrieus turbines (H type) **c)** Savonius type turbine

Figure 1.13. Wind turbines with vertical axes [29]

b. Horizontal axis wind turbines

Horizontal-axis wind turbines are based on the ancestral technology of windmills [9]. They typically need a blade orientation mechanism, which enhances aerodynamic efficiency. They start autonomously and occupy a smaller ground footprint. In this type of turbine, the shaft is parallel to the ground. The number of blades used for electricity production varies between 1 and 3. The three-bladed rotor is the most commonly used since it balances power coefficient, cost, and wind sensor rotation speed [30]. This type of turbine has surpassed vertical-axis turbines due to their lower cost.

Figure1.14. Horizontal- axis wind turbines [30].

A horizontal-axis wind turbine is generally composed of three basic elements: the mast (tower or pylon), the rotor (hub and blades), and the nacelle (Figure 1.15) [31].

- ✓ **Mast (Tower):** It is typically a steel tube or sometimes a metal lattice, inside of which cables are arranged to carry electrical energy. It should be as tall as possible to avoid disturbances near the ground. Using the tower to support the entire assembly (rotor, nacelle), at a sufficient height to maximize wind energy utilization.
- ✓ **Rotor:** It is composed of blades mounted on a hub. The essential role of the rotor is to transform the wind's kinetic energy into mechanical energy.
- ✓ **Blades:** are a crucial part of wind turbines. They capture the kinetic energy of the wind and transfer it to the rotor hub. The number of blades directly affects the conversion efficiency of the rotor. More blades result in increased starting torque and the slower the rotation speed.
  - ✓**Hub:** This is the support for the blades, allowing them to be oriented to regulate the rotation speed.
  - ✓**Nacelle:** Mounted at the top of the mast, it houses all the mechanical elements necessary for coupling the wind turbine to the electrical generator.
  - ✓**Electrical generator:** It converts mechanical energy into electrical energy.
  - ✓**Gearbox:** It adjusts the rotation speed of the wind turbine to match that of the electrical generator.

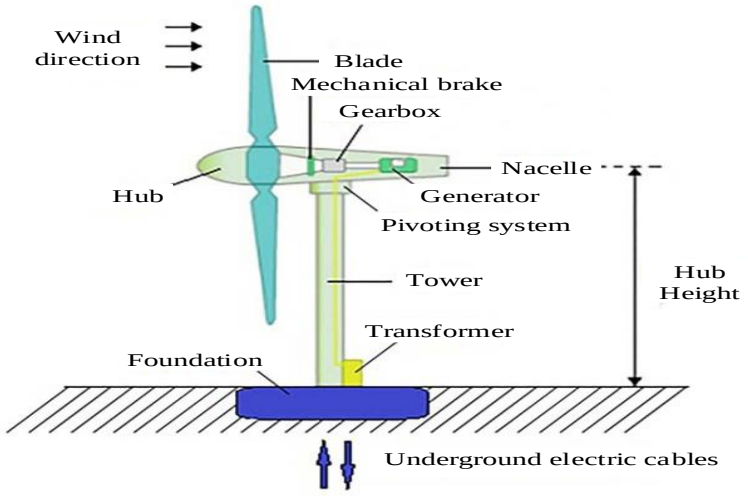

Figure 1.15. Parts of a horizontal-axis wind turbine

6.2.3. Storage energy

The storage system is a crucial component for enhancing the efficiency of the system and preventing the loss of excess production energy. Therefore, various types of storage systems are used in various applications depending on their characteristics and advantages, including lithium-ion batteries, flow batteries, nickel-based batteries, sodium-based batteries, lead-acid batteries, and metal-air batteries, you can refer back to this reference for more details. [32]. Despite the variety of batteries and the differences in their chemical nature and operational methods, they share several common characteristics, which include the following [33]:

- **Nominal capacity:** The total energy that can be stored in the battery, measured in ampere-hours (Ah).
- **Operating voltage**: The voltage at which the stored energy is typically delivered to the load.
- **Lifespan and cycle life:** These parameters indicate the durability of the storage system. Lifespan is measured in years, while cycle life is measured in the number of charge-discharge cycles.
- **Depth of discharge (DoD):** The percentage of the battery's total capacity that is used during each charge/discharge cycle.
- **Self-discharge**: The energy lost by the storage system during periods of non-use, measured as the ratio of energy lost over a specified period (hour, day, or month) to the energy capacity of the device.
- **Efficiency**: The ratio of the electrical energy output by the battery to the energy input.
- **State of charge (SOC**): The amount of available energy as a fraction of the battery's nominal capacity. An SOC of 1 means the battery is fully charged, while an SOC of 0 means it is empty.

In our subject, we utilized the category of nickel-based batteries, specifically metal hydride batteries. Below is a brief description of them:

6.2.3.1. Principle operation of a NiMH

The NiMH battery, a rechargeable secondary battery, operates through reversible reactions. Its negative electrode consists of metal hydride, while the positive electrode utilizes nickel oxyhydroxide, with potassium hydroxide serving as the electrolyte. The anode comprises a metal hydride alloy, such as zinc, vanadium, chromium, or titanium. The cathode is composed of nickel oxyhydroxide. An insulator made of polypropylene separates the anode and cathode. The NiMH battery is typically housed in a glass or steel container. These batteries find applications in various devices including electronic gadgets, electric vehicles (EVs), medical instruments, smart grids, and telecommunications [32]. The nickel-metal hydride battery was chosen for our research topic based on several characteristics and advantages, which we outline in the following points [34]:

a) General characteristics

- Can usually be recharged hundreds of times.
- Performs efficiently under high-rate discharge conditions.
- Offers significantly greater capacity compared to nickel-cadmium batteries.
- Expected lifespan ranges from 2 to 5 years.
- Functions effectively across a wide temperature range:
- Charging: 0°C to 50°C
- Discharging: 0°C to 50°C

b) Advantages of NiMH battery

Some of the benefits of nickel-metal hydride batteries include:

- High energy density, leading to longer run times or reduced battery space requirements.
- Avoidance of manufacturing, usage, and disposal restrictions associated with cadmium toxicity.
- Easy integration into products currently using nickel-cadmium batteries due to their similar design.

- Superior performance compared to other primary battery types in low temperature conditions, operating efficiently at -20°C.

7. Electrical Conversion System

A converter static is an electronic device that converts alternating current (AC) to direct current (DC) and vice versa. It has numerous applications, including connecting power sources to loads. It is divided into two types: DC/DC converters for DC power sources for DC load, and DC/AC inverters for AC loads [35].

7.1. Types of converters

7.1.1. DC-DC converter

A DC-DC converter is a power electronics circuit or electromechanical device that converts a direct current (DC) source from one specified voltage level to another. It is a type of electric power converter. The power levels handled by such circuits range from very low (small batteries) to very high (high-voltage or even extra-high-voltage power transmission) [36].

- High cost.
- The annual energy gain compared to a less complex system (such as voltage regulation) is not significant.

7.1.2. DC-AC converter

This device converts DC to AC. The formation of the output order can be achieved by two devices [37]:

a) Rotary

- Description: A DC motor coupled to an alternator.
- Efficiency: Ranges from 50% to 60% for 1kW up to 90% for 50kW.
- Advantages: Simplicity, sine wave output, good reliability.
- Disadvantages: High cost, low efficiency (especially for low power).

b) Static

Also known as an inverter. This device uses power transistors or thyristors. The simplest form of the output wave is square, which can be

suitable for some types of loads but has significant no-load losses, especially for low power. Inverters can be improved using filtering or PWM (Pulse Width Modulation) systems, which allow the modulation of pulse length to achieve a sine wave output. This system provides:

- High efficiency over a range of load rates.
- Low no-load losses.

8. Integration issues of an HES on the electrical grid

Many studies in the literature have focused on investigating the outcomes of decentralized production (DP) and suggesting remedies, as evidenced by references such as [38], [39], [40], In this context, we will briefly review and define the primary effects. Presently, most DP is integrated into the distribution network. We will initiate our analysis by assessing their influence on distribution networks before exploring their effects on the transmission network [38].

8.1. Impact on the distribution network

a. Influence on power flow direction:

Traditionally, networks are structured to facilitate power flow from the transmission network to the distribution network. However, the integration of decentralized production (DP) at the distribution level can lead to a reversal of these flows. Consequently, protection devices, initially designed for unidirectional flow, must be adapted for bidirectional operation. Moreover, the introduction of DP may exacerbate local congestion issues, necessitating network reinforcement.

b. Effects on voltage profile:

The incorporation of decentralized production is bound to affect the voltage profile near its connection point. Nevertheless, it is imperative for the network operator to uphold voltage levels within specified parameters. Power plants with a capacity exceeding 1 MW are mandated to adjust voltage at their connection point upon the network operator's request.

8.2. Impact on the transmission network

a. Ambiguity in the planning stage:

Intermittent energy sources like solar, wind and micro-hydro are pivotal in the realm of Decentralized Production (DP) [38]. The inability to predict wind speed variations is considered the primary challenge regarding this type of energy, which leads to indecisiveness regarding the construction of a wind farm. For instance, Denmark's case, as depicted in [41], showcases significant discrepancies in forecasts, with variation exceeding 50% less (under-production) or more (over-production) within a day timeframe [41], showing sudden changes throughout the day. This underscores the necessity of establishing controllable reserve production capacities, especially to fulfill demand during peak periods. ELTRA, the grid operator in western Denmark, which includes a large wind capacity (2400 MW in 2003) [41], faced critical scenarios due to overproduction of wind energy. The evacuation of this surplus energy to the Nordic grid (Nordel) or the UCTE grid (via Germany) posed challenges due to interconnection line saturation.

Overall, production magnitude forecasts are reliable, but uncertainty persists regarding the timing of reaching these production levels [39].

b. Grid reinforcement necessity

The capacity of electrical infrastructure, including lines and substations, is constrained. This limitation presents a significant challenge, particularly in the context of wind energy, as production sites (windy areas) are Usually far from consumption centers. To alleviate congestion on transmission lines and ensure network reliability, the construction of new electrical infrastructure, particularly at interconnection points between networks managed by different operators, is imperative. However, it's worth noting that the lead time for reinforcing substations can extend up to 5 years, while constructing new transmission lines may take up to 10 years and could face strong opposition from local communities [40].

c. Vulnerability to untimely decentralized production disconnections

The inability to control (DP) prompts transmission system operators (TSOs) to treat them as "negative loads," necessitating their disconnection in case of grid incidents [42], [43]:
For instance, in France, current regulations mandate disconnection of DP if:

- Voltage overtakes 85% to 115% of the rated voltage.
- The frequency deviates from the range of 49.5 to 50.5 Hz (for installations with less than 1 MW of power) or 47.5 to 51.5 Hz (for installations with more than 1 MW of power).

The adverse effects of such disconnections were evident during incidents like the one on November 4, 2006, and the blackout in Italy on September 28, 2003.

9. The criteria necessary to determine the optimal dimensions for a hybrid source system

Mixing various energy sources with different components, dynamic structures, operational principles, and under diverse climatic conditions is essential to meet consumer needs reliably and efficiently. Therefore, it is necessary to address a fundamental aspect, which involves determining the optimal size for a multi-source system. Determining the optimal dimension for such a system requires studying several criteria summarized in several points as follows:

a. Meteorological characteristics:

Analyzing the weather conditions at the project site is crucial before optimizing the system. Solar and wind resource data collected serve as the primary inputs for optimizing multi-source systems reliant on these energy sources. It's imperative to have a time series of meteorological data directly measured at the site, whether in minutes, hours, or days. If this data is unavailable, real or estimated satellite data can be utilized, although the latter may lack precision [44].

b. Demand profile

Establishing the electrical demand profile for the load is essential in crafting, organizing, and refining a multi-source system. It's challenging to accurately pinpoint and evaluate the load's real-time demand, considering its rapid fluctuations. Typically, hourly or daily load demand averages are employed. However, obtaining an accurate depiction of the load's variations throughout all seasons proves to be practically demanding. Precision is crucial in this endeavor, as any estimation inaccuracies can result in either over-sizing or under-sizing the system [45].

c. System configuration

After conducting pre-feasibility studies using meteorological data (such as wind speed, solar irradiation, and temperature) and analyzing load demand, it becomes possible to achieve improved component sizing. However, it's crucial to tailor this sizing process to suit the characteristics of the components. For instance, if the site being studied exhibits greater solar potential compared to wind, the hybrid system should prioritize a larger proportion of the photovoltaic system over the wind system [44].

d. Optimization results

The optimization outcomes must be sufficiently precise to prevent either power surplus or deficit. While electricity production from a multi-source system heavily relies on the project's specific location, it is still feasible to extrapolate optimization results for other sites with similar characteristics.

e. The cost of energy produced

Different methods are employed to determine this cost, which is contingent upon factors such as the energy required by the consumer, the initial investment outlay for procuring system components, installation expenses, maintenance charges, and replacement costs for components with shorter lifespans than the defining element of the hybrid system's lifespan, and so forth.

10. Energy flow control strategies in the HES

Many studies have delved into the topic of hybrid energy systems, whether in standalone or grid-connected forms. These studies vary based on the criteria under investigation, which can be summarized into four main points: optimization, sizing, control, and system management. Through these criteria, an efficient, practical, and ideal multi-source hybrid system can be established to continuously meet load requirements. Reference [46] compiled statistics on various publications addressed by researchers according to the studied criteria from 1999 to 2022. Based on these statistics depicted in Figure 1.16, we can say that the majority of studies focused on the optimization criterion, accounting for 40% of publications that addressed this criterion across different years. This is a fundamental criterion for the system as a whole and relies on improving system components for various sources and enhancing the resulting energy. Working on this criterion significantly reduces losses that may occur due to wasted energy if not optimized perfectly, in addition to reducing the overall system construction cost. Following this is the sizing criterion at 30%, which generally involves studying several characteristics (previously discussed in this chapter), the most important of which is knowing the load profile so that we can develop an ideal size for the produced sources.

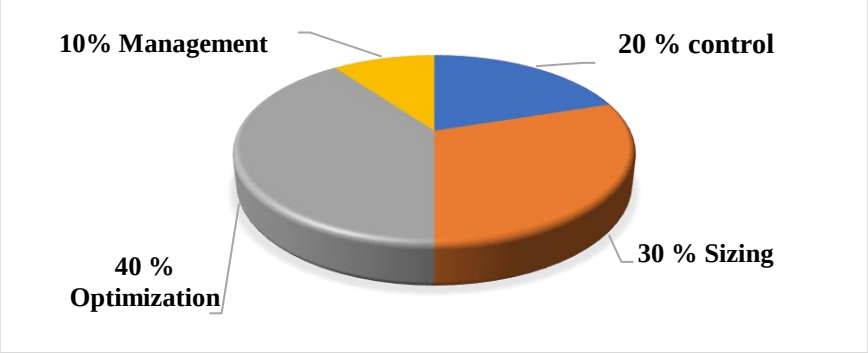

Figure 1.16. HRES publications (1999-2022 year)

The control criterion accounted for 20% of the publications that addressed or focused on this criterion in their studies. It is a sensitive criterion that requires proposing classic or advanced strategies to control various sources and ensure production aligns with consumption. Lastly, only a few studies addressed the management criterion in their research, accounting for 10% of

the studies that tackled energy management for the hybrid system, whether independent or grid-connected. This system relies on proposing strategies or algorithms to manage the various energy sources in the system as a whole to meet demand regardless of changing climatic conditions. If these criteria are effectively addressed, an optimal management of the multi-source hybrid system is achieved, regardless of changing climatic conditions or load profile variations throughout the day, ensuring the system is fully prepared for effective, instantaneous, and practical response.

In the proposed energy management system in our research topic, all the previously mentioned criteria have been addressed to achieve sufficiently optimized results. The four criteria were studied according to the following analysis:

- **Optimization:** In our research topic, this criterion was applied to various sources of energy production, whether from renewable energy systems (solar photovoltaic system, wind generator) or from the electric grid. The improvement criterion manifested in enhancing the quality of the produced energy by applying both classical and innovative methods to track the MPP of the energy produced from the renewable energy system (solar photovoltaic system, wind generator), in addition to proposing a new strategy to improve and estimate the energy output from the electric grid.
- **Control:** In our research, control of the grid-connected hybrid system primarily relied on controlling the DC bus through proposing a control unit connected to the bidirectional converter of the battery. Several intelligent methods, such as fuzzy logic and classical techniques, were applied to adjust the DC bus voltage at a specified value while considering the state of the charge of the battery storage system. On the other hand, control of the inverter was achieved through proposing direct power control technology to estimate the power output from the electric grid. (the first and second criteria are studied in more detail in the third chapter).

- **Sizing:** In this criterion, we relied on determining and prior knowledge of the load profile, as well as knowledge of meteorological characteristics (wind speed and sunlight). Subsequently, the optimal sizing of various system components was determined.
- **Management:** Managing the various energy sources of the grid-connected renewable hybrid system is considered the fundamental criterion in our research topic. This issue led us to propose an optimal management method for these sources (solar energy, wind energy, battery charging and discharging, grid integration or disconnection), all aimed at meeting load requirements without interruption. The criterion of energy management can be summarized in the following relationship (this criterion will be discussed in detail in Chapter Four).

$$P_{net} = P_l - (P_{pv} + P_w \pm P_g \pm P_{bat}) \quad (1.1)$$

The figure 1.17. provides an overview of the various criteria applied to the hybrid energy management system. Through it, one can identify the sources of energy production and consumption, as well as the locations that have been optimized and others that have been controlled.

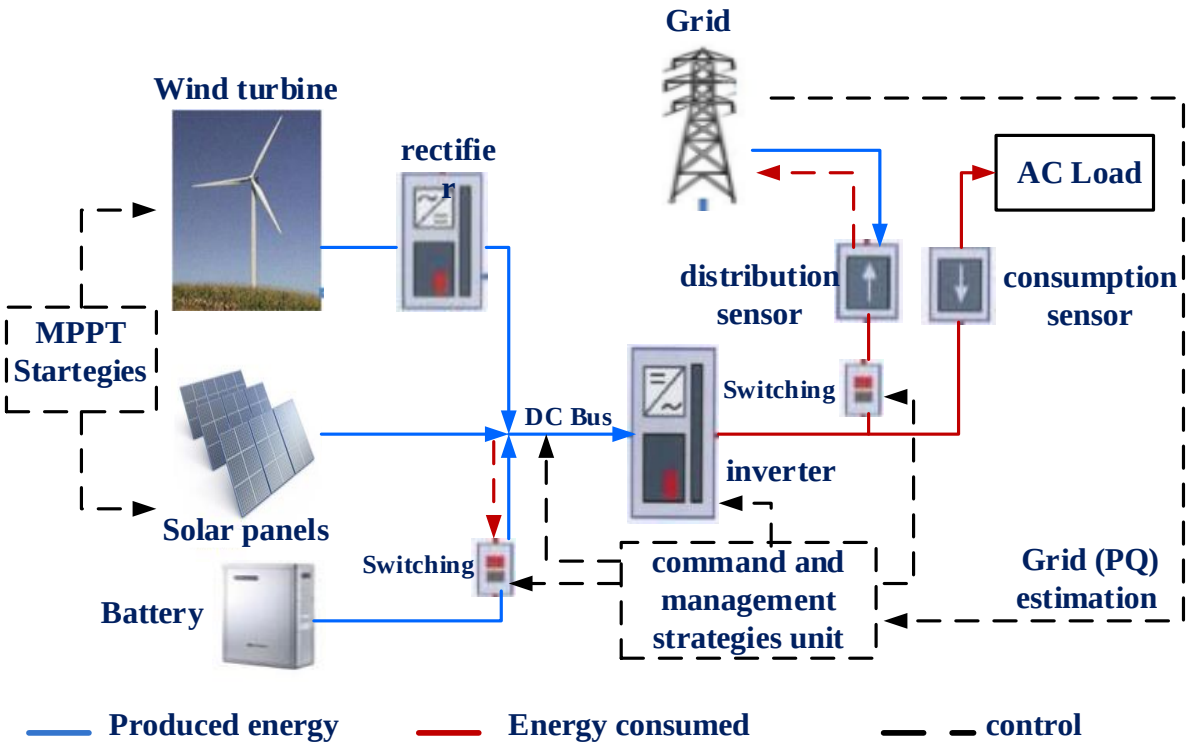

Figure 1.17. The proposed hybrid renewable energy management system

Many references have addressed various methods in managing hybrid renewable energy systems, which have been compiled and summarized in the reference [47]. Each method's advantages and disadvantages are provided, making the reference a valuable source for further exploration of this vast topic.

11. Conclusion

This chapter covers general aspects of hybrid renewable energy systems, highlighting their advantages and disadvantages. We also introduced the definition of grid-connected hybrid systems, which, in the context of our topic, comprise photovoltaic systems and wind turbines utilizing permanent magnet synchronous generators, along with storage. We also touched on presenting the extent of the impact of decentralization of production on the electrical network, and knowing the basic criteria for sizing a multi-source hybrid system, and examined how these criteria affect system efficiency and operation. Finally, we conclude the chapter by giving an overview of how the hybrid system is managed in the subject of our research and the proposed methods for addressing the various criteria on which the establishment of this system depends, in managing the various resulting energies to supply the load requirements perfectly and accurately.

Chapter 2:

Modeling of a hybrid system connected to the electrical grid

1. Introduction

Understanding the behavior of hybrid systems and proposing a strategy for managing the flow of energy from different sources requires detailed mathematical modeling of the different components that make up the system to be subsequently simulated in MATLAB.

In this chapter, we presented the mathematical modeling of several parts of the grid-connected hybrid system, starting with the modeling of the photovoltaic system, followed by the wind generator with an overview of the dynamic characteristics of each. Then, we modeled the storage system, which relies on a nickel-metal hydride battery. All the aforementioned components were connected to the electrical grid through a direct current bus using static converters to supply an alternating load, along with a detailed mathematical modeling of the connection method.

2. Modeling of Renewable Energy Production System

2.1. Modeling of the Photovoltaic module

2.1.1. Photovoltaic Generator Model

Photovoltaic (PV) generators are not considered to be voltage sources or current sources, but can be regarded as current sources controlled by voltage, with the solar module as the basic unit [48]. It consists of several monocrystalline solar cells, enabling the conversion of solar energy into electrical energy.

The equivalent circuit of a solar module can be found in the literature in various forms (single exponential, double exponential, etc...) [47][48][49], whereas the configuration depicted in Figure 2.1, known as the single diode model, remains the most common. It consists of a diode (D) representing the junction, a current source (G) representing the photocurrent, a series resistance (R_S) representing losses due to Joule heating, and a shunt resistance (R_{sh}) simulating leaks between the upper grid and the rear contact the element. The shunt resistance is typically much higher than R_S and can be placed interchangeably in the equivalent circuit [7].

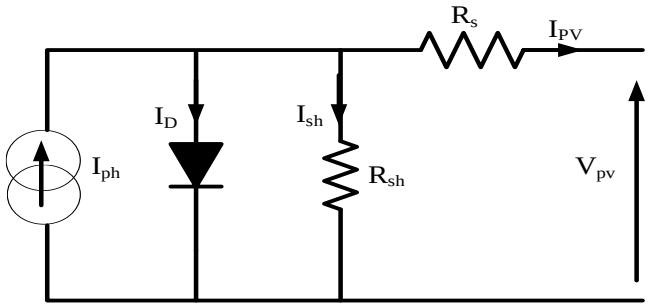

Figure 2.1. Equivalent Circuit of the solar module

According to Kirchhoff's law, the current delivered by a PV cell is given by:

$$I_{pv} = I_{ph} - I_D - I_{sh} \tag{2.1}$$

The current I_{ph} is given by the following formula:

$$I_{ph} = \left[I_{ph,n} + K_i \left(T - T_n \right) \right] \frac{G}{G_n} \tag{2.2}$$

The current of the diode is described by the following equation:

$$I_D = I_0 \left[\exp\left(\frac{V_{pv} + RI_{pv}}{\alpha . KT/q} \right) - 1 \right] \tag{2.3}$$

The current across the parallel resistance is expressed as:

$$I_{sh} = \frac{V_{pv} + R_s . I_{pv}}{R_{sh}} \tag{2.4}$$

The characteristic equation of a PV cell is provided by:

$$I_{pv} = I_{ph} - I_o \left[\exp\left(\frac{V_{pv} + R_s . I_{pv}}{a . V_t} \right) - 1 \right] - \frac{V_{pv} + R_s . I_{pv}}{R_{sh}} \tag{2.5}$$

With:

I_{pv}: Current delivered by the PV cell,

V_{pv}: Voltage across the PV cell,

I_o: Diode saturation current (A),

a: Diode ideality factor ($1 \leq a < 1.5$),

V_t: Thermal voltage,

R_s: Series resistance, and

R_{sh}: Shunt resistance (Ω).

The PV generator is formed by connecting multiple solar panels in series and parallel to achieve greater power output. In the case of N_{ss} panels

connected in series and N_{pp} panels connected in parallel, all operating under theoretically identical conditions, its current is given by the relationship [48]:

$$I_{pv} = N_{pp} I_{pp} - N_{pp} I_0 \left[\exp\left(\frac{V_{pv} + R_s . I_{pv} \left(N_{ss} / N_{pp} \right)}{a . V_t . N_s . N_{ss}} \right) - 1 \right] - \frac{V_{pv} + R_s . I_{pv} \left(N_{ss} / N_{pp} \right)}{R_p . \left(N_{ss} / N_{pp} \right)} \quad (2.6)$$

To plot the (I-V) characteristic, three measurement points provided by the manufacturer are required (Figure 2.2):

- Point (1): Known as the short-circuit point (I_{cc}, 0), corresponding to the maximum current the module can provide at zero voltage.
- Point (2): Known as the optimum point (I_{op}, V_{op}), where the module delivers its maximum power.
- Point (3): At open circuit (0, V_{oc}), according to the maximum voltage of the module without load.

Disregarding the specific values of voltage and current, the (I-V) characteristic depicted in Figure 2.2. can be interpreted in three different intervals:

1. **Interval I**: The solar module is considered as a current source, where the current is constant while the voltage is variable.
2. **Interval II**: The solar module is neither considered as a current source nor a voltage source. This part essentially represents the preferred operating zone.
3. **Interval III**: The solar module is considered as a voltage source, where the voltage is constant while the current is variable.

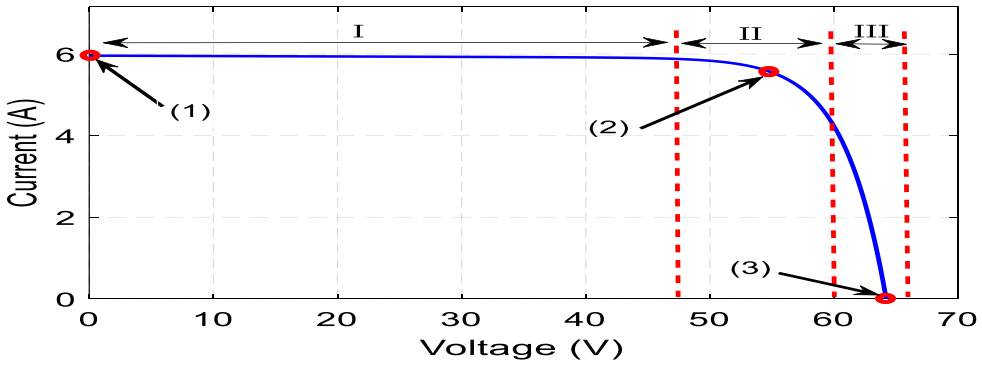

Figure 2.2. (I-V) behavior of the solar module under typical conditions (G=1000W/m², T=25°C (G=1000W/m², T=25°C).

- **Piece of identification of module SPR-305-WHT:**

In the study conducted, we relied on SunPower SPR-305-WHT solar panels that produced approximately 11 KW. Our choice of this type was based on several advantages, which we outline in the following points [21]:

- **Top Efficiency**: At 18.7% panel efficiency, it outperforms any commercially available panel on the market.
- **Increased Power Output**: SunPower 305 delivers 50% more power per unit area compared to conventional solar panels and twice as much as thin film solar panels.
- **Lower Installation Costs**: Higher power per panel reduces the number of panels required per installation, saving both time and money.
- **Dependable and Strong Design:** Utilizes proven materials, tempered front glass, and a robust anodized frame, ensuring reliable operation in various mounting setups.

2.1.2. Impact of weather Conditions on V-I Characteristics

According to the results provided by the figures below, we notice that the values The short-circuit current and power increase directly with the intensity of irradiance, whereas the open-circuit voltage varies slightly. For a changing temperature, it can be observed that the variation in voltage is greater than that of current. The voltage of a solar module is inversely proportional to the temperature.

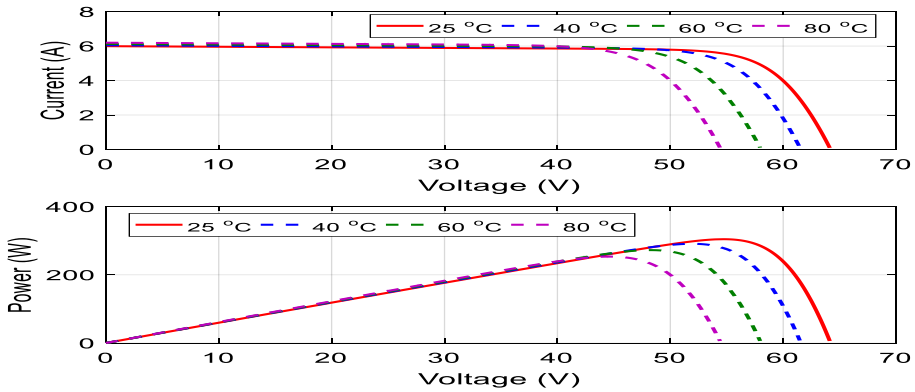

Figure 2.3. Electrical properties of the module at various temperature levels at G= 1000W/m²

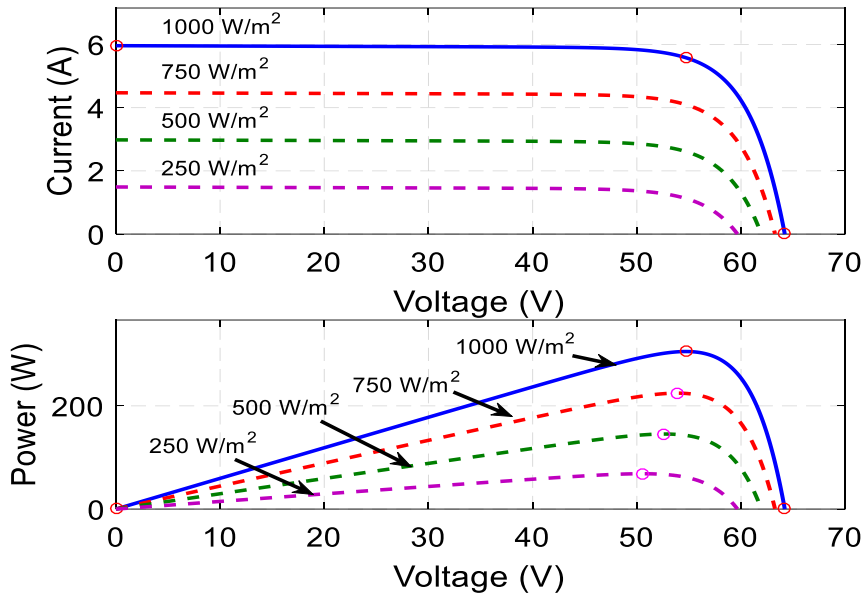

Figure 2.4. Electrical properties of the module at various irradiance values at T=25°C.

2.2. Modeling of the Wind system

The objective of this part is to model the wind turbine generator. The chosen wind turbine structure has already been the subject of several studies [32].

In our setup, this system mechanically comprises four components: Three adjustable blades with their own coefficients of inertia, elasticity, and air and turbine support friction.

- A blade-driving shaft with its own inertia, elasticity, and friction coefficient with respect to the gearbox.
- A speed multiplier with a gain factor G.
- A generator rotor with inertia Je and a friction coefficient De.

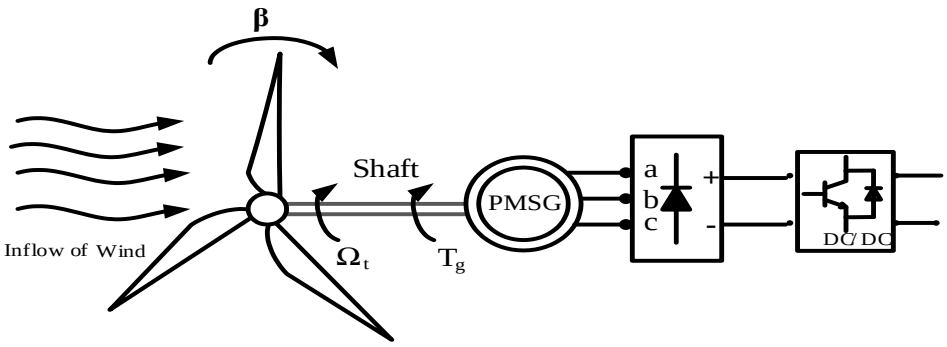

Figure 2.5. A block diagram representing a wind turbine

2.2.1.Decomposition of the Wind System Model

2.2.1.1. Modeling of the wind turbine

Based on the wind speed, air density, and the active surface area S of the blade, the power of the air mass is expressed as [49]:

$$P_v = \frac{1}{2}\rho S V^3 \tag{2.7}$$

The blades do not capture all of the wind power; hence the aerodynamic power is less than that of the wind. Both powers are connected by the following expression:

$$P_t = C_p P_v = \frac{1}{2} C_p(\lambda, \beta)\rho S V^3 \tag{2.8}$$

With Cp being the power coefficient. It depends on the pitch angle of the blades β and the tip-speed ratio λ. This coefficient reaches a maximum of 0.59 (16/27), known as the Betz limit, and is given by equation (2.9):

$$C_p(\lambda, \beta) = C_1\left(C_2\frac{1}{\lambda_i} - C_3\beta - C_4\right)\exp\left(\frac{-C_5}{\lambda_i}\right) + \lambda C_6 \tag{2.9}$$

With: $C_1 = 0.5176, C_2 = 116, C_3 = 0.4, C_4 = 5, C_5 = 21, C_6 = 0.0068$

$$\frac{1}{\lambda_i} = \frac{1}{\lambda + 0.08\beta} - \frac{0.035}{1+\beta^3} \tag{2.10}$$

$$\lambda = \frac{\Omega_t R}{V} \tag{2.11}$$

Figure 2.6 depicts the mechanical power for different wind speed and blade pitch angle values β =0 deg. The peak value of mechanical power (P_t = 0.8 pu occurs at β = 0° and wind speed=12 m/s)

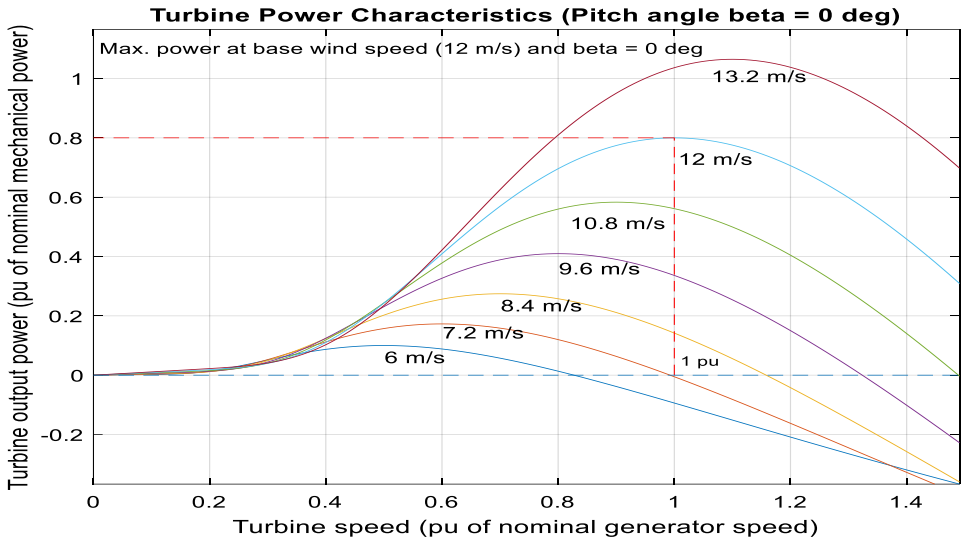

Figure 2.6. Output Mechanical Power as a function of the turbine speed

Given the turbine speed, the aerodynamic torque can be directly calculated by:

$$T_{aer} = \frac{P_t}{\Omega_t} = \frac{1}{2\Omega_t} C_p \rho S V^3 \tag{2.12}$$

Another parameter, referred to as the torque coefficient Ct, can also be defined, which depends on the wind speed and the specific turbine speed:

$$C_t = \frac{C_p}{\lambda} = C_p \frac{V}{R\Omega_t} \tag{2.13}$$

So we can write :

$$T_{aer} = \frac{1}{2} C_t \rho S R V^2 \tag{2.14}$$

2.2.1.2. Model of the gearbox

The gain multiplier G allows adjusting the mechanical quantities (speeds and torques) of the turbine and the generator, which are expressed by the following mathematical relationships:

$$\Omega_t = \frac{\Omega_e}{G} \tag{2.15}$$

$$T_g = \frac{T_{aer}}{G} \tag{2.16}$$

Where Tg: represents the effect of the turbine torque on the generator shaft;
G: The gain multiplier

2.2.1.3. Dynamic equation of the generator shaft

By transferring the mechanical characteristics of the turbine to the generator shaft, we establish the model expressed through the following equation:

$$J\frac{d\Omega_e}{dt} + D\Omega_e = T_g - T_{em} \tag{2.17}$$

With:

$$J = \frac{J_t}{G_2} + J_e \tag{2.18}$$

Where: J_t, D_t, J_e, D_e, $J\ et$, D : represent the inertia and friction coefficient of the turbine, generator, and those referred to the generator shaft, respectively.

Based on the equations presented earlier, the following figure can define a physical model of the turbine with inputs including the blade pitch angle, wind speed, and the electromagnetic torque provided by the generator.

$$D = \frac{D_t}{G^2} + D_e \tag{2.19}$$

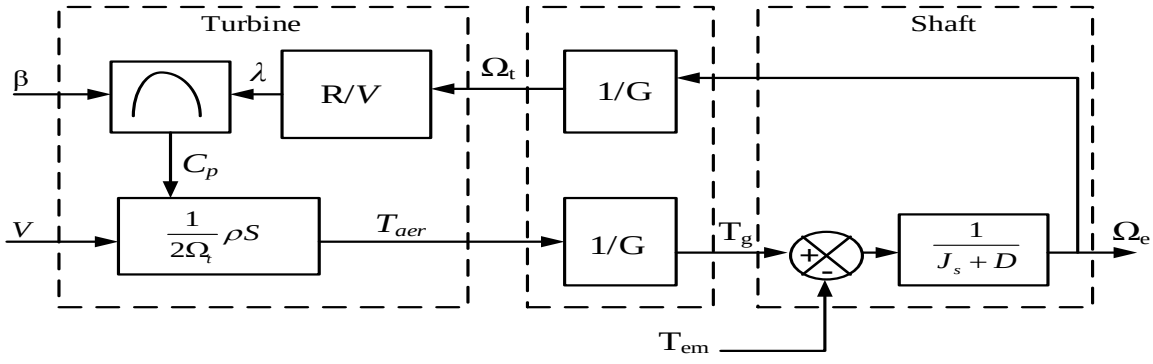

Figure 2.7. Model of the wind turbine shaft and blades.

2.2.1.4. Wind turbine generator

Generator technology is one of the constraints in wind turbines [50]. Historically, three primary types of wind turbine generators (WTGs) have

been used in different systems: direct current (DC), alternating current (AC) synchronous, and AC asynchronous generators. One of the advantages of these generators is their ability to operate at fixed or variable speeds. Due to the variable nature of wind power, to avoid physical stress on the turbine blades, it is preferable to operate the generators at variable speeds. This enhances the system's aerodynamic efficiency and torque transient behaviors [51].

a) DC generator

In traditional DC machines, the field is located on the stator while the armature is on the rotor. The stator contains several poles that are energized either by permanent magnets or by DC field windings. If the machine is electrically excited, it generally follows the principles of a shunt-wound DC generator[50], more detail about DC generator in [51].

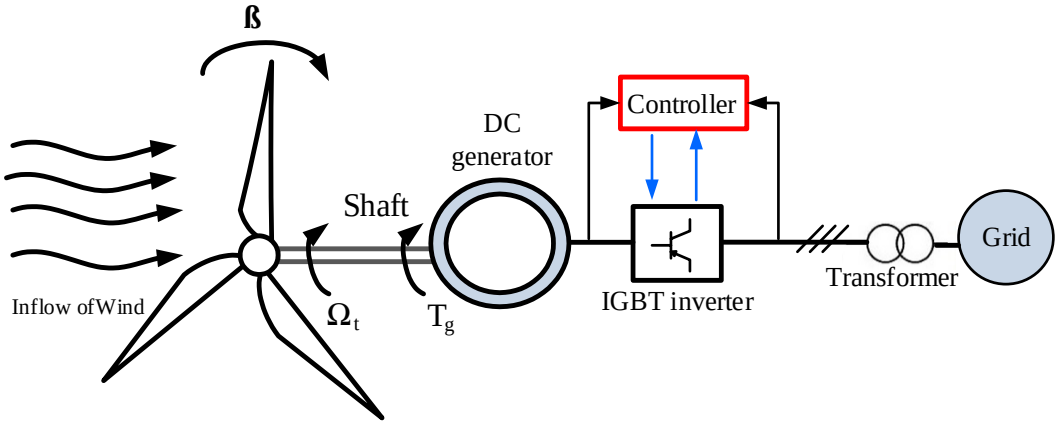

Figure 2.8. Diagram of a DC generator

b) AC asynchronous generator

Power generation usually requires synchronous machines, but wind power generation has recently become largely dependent on induction machines, which in turn are divided into two main types: fixed-speed induction generators (FSIGs) with squirrel-cage rotors (SQIGs) and double-fed induction generators (DFIGs) with Wounded rotors [52].

An induction machine functions based on the principle of electromagnetic induction. When three-phase AC power is supplied to the stator windings, it

creates a rotating magnetic field across the air gap between the stator and rotor. This rotating magnetic field induces a current in the rotor windings if there is a relative speed difference between the rotor and the magnetic field, known as slip [50]. The interaction between the magnetic fields of the stator and the induced currents in the rotor generates torque, causing the rotor to turn. Induction machines are valued for their robustness, simplicity, and cost-effectiveness, making them widely used in various applications, including wind power generation. They are capable of handling fluctuations in rotor speed and transients in the drive train, offering high damping capabilities and fault tolerance [53]. However, they require reactive power from the grid, necessitating compensation through capacitors or power converters to maintain efficient operation.

FSIGs connect the stator to the grid via a transformer and the rotor to the wind turbine through a gearbox, operating within a narrow speed range. These generators were prevalent until 1998 but were limited by their inability to control output voltage and need for external reactive power. They also had issues with size, noise, efficiency, and reliability, leading to significant maintenance needs [54].

c) AC synchronous generator

Since the early development of wind turbines, significant efforts have been made to utilize three-phase synchronous machines. These machines, known as PM synchronous generators (PMSGs) when using permanent magnets, and electrically excited synchronous generators (EESGs) when using electromagnets, can take constant or DC excitations [55]. When powered by the wind turbine, they generate three-phase power in the stator windings, where is then linked to the grid via electrical elements such as power converters and transformers. In the case of FSIGs, the rotor speed must precisely match the synchronous speed to maintain synchronization. [56].

Synchronous generators are well-established in power generation due to their long-studied and widely accepted performance. Their reactive power characteristics could be easily regulated through the field circuit for

electrical excitation. However, fixed-speed synchronous generators can pass random wind speed fluctuations and periodic disturbances onto the power grid [56]. They also have low damping effects, requiring additional damping elements like flexible couplings or gearboxes mounted on springs and dampers. Voltage control in electromagnet-excited synchronous machines occurs within the machine, while in permanent magnet machines, it is managed in the converter circuit [51].

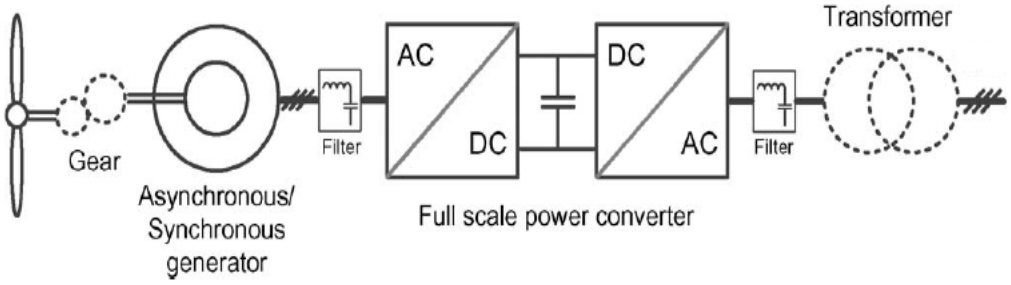

Figure 2.9. Diagram of a synchronous/asynchronous generator

Since the topic at hand deals with the PMSG, we will present the related mathematical modeling:

- **Modeling of the Permanent Magnet Synchronous Generator (PMSG)**

Because of the various benefits offered by the PMSG, we've become intrigued by its application in our system. Typically, the (PMSG) is represented by a voltage source with a series impedance. The equivalent circuit and vector diagram are depicted in Figure 2.10 [57].

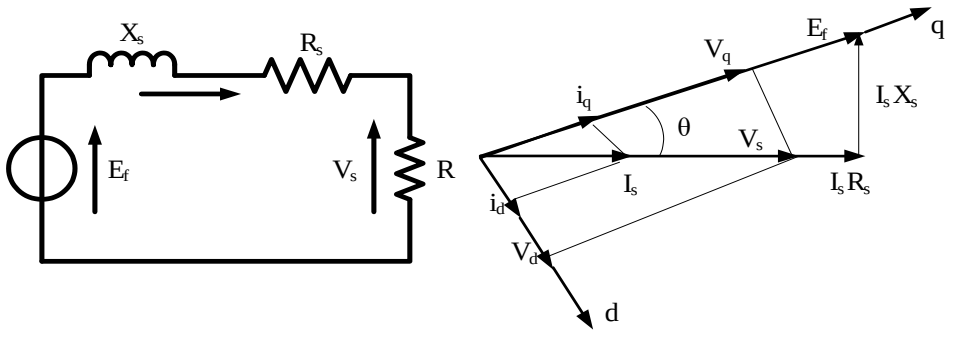

Figure 2.10. Equivalent diagram of the PMSG and the associated vector diagram

The dynamic model of the PMSG described in the d-q axis frame provided by [57]:

$$\begin{cases} v_q = -R_s i_q - L_q s i_q - w_e L_q i_d + w_e \phi_m \\ v_d = -R_s i_d - L_d s i_d + w_e L_d i_q \\ T_e = \frac{3}{2}\frac{P}{2}\left(\phi_m i_q + \left(L_d - L_q\right).i_q i_d\right) \end{cases} \quad (2.20)$$

With:

L_q, L_d: are the stator inductances in the d-q axes,

s: is the Laplace operator.

Using the vector diagram, equation (2.21) can be expressed in terms of the generator voltage Vs as follows:

$$\begin{cases} \frac{v_s i_q}{\sqrt{i_q^2 + i_d^2}} = -R_s i_q - L_q s i_q - w_e L_q i_d + w_e \phi_e \\ \frac{v_s i_d}{\sqrt{i_q^2 + i_d^2}} = -R_s i_d - L_d s i_d + w_e L_d i_q \end{cases} \quad (2.21)$$

On the other hand, we have $L_d = L_q = Ls$, so the torque equation (T_e) simplifies to:

$$T_e = \frac{3}{2}\frac{P}{2}\left(\phi_e i_q\right) \quad (2.22)$$

The voltage across The PMSG can be regulated by adjusting the duty cycle of the boost converter. Therefore, the voltage Vs is given by the following expression:

$$V_s = \frac{\pi V_{red}}{3\sqrt{3}} D_w \quad (2.23)$$

Therefore, equations 2.24 can be rewritten as:

$$\begin{cases} \dfrac{di_q}{dt} = \dfrac{1}{L_s}\left(-R_s i_q - w_e L_s i_d + w_e \phi_e - \dfrac{\pi V_{red} i_d}{3\sqrt{3} L_s \sqrt{i_q^2 + i_d^2}} D_w \right) \\ \dfrac{di_d}{dt} = \dfrac{1}{L_s}\left(-R_s i_d - w_e L_s i_q - \dfrac{\pi V_{red} i_d}{3\sqrt{3} L_s \sqrt{i_q^2 + i_d^2}} D_w \right) \\ \dfrac{dw_e}{dt} = \dfrac{P}{2J}\left(T_t - \dfrac{3P}{4} \phi_e i_q \right) \end{cases} \quad (2.24)$$

Where: i_d and i_q are the direct and quadrature stator currents respectively, ω_e is the electrical angular speed, R_s and L_s are the phase resistance and stator inductance respectively, P is the number of poles of the generator, J is the generator's inertia, Φ_e is the permanent magnet flux per pole, V_{red} is the rectified voltage, and D_w is the duty cycle of the boost converter.

- **Three-phase PWM rectifier**

To link the wind turbine generator to the DC bus, the output AC current must be converted into DC current through the PWM controller, which in turn is associated with the boost converter. This ensures smooth power conversion, where linking the WT generator to the PWM controller is essential as it regulates the output voltage and frequency of the wind turbine generator, making it compatible with the DC bus voltage. This contributes to the reliability and performance of the system.

Three-phase PWM rectifiers offer numerous advantages, including bi-directional power flow, minimal harmonic distortion, unity power factor, and the ability to control DC bus voltage [58]. The configuration of a three-phase PWM rectifier is illustrated in Figure 2.11. The voltage of the source phases is represented as:

$$\begin{aligned} V_a &= V_m \sin\theta \\ V_b &= V_m \sin\left(\theta - 2\pi/3\right) \\ V_c &= V_m \sin\left(\theta + 2\pi/3\right) \end{aligned} \quad (2.25)$$

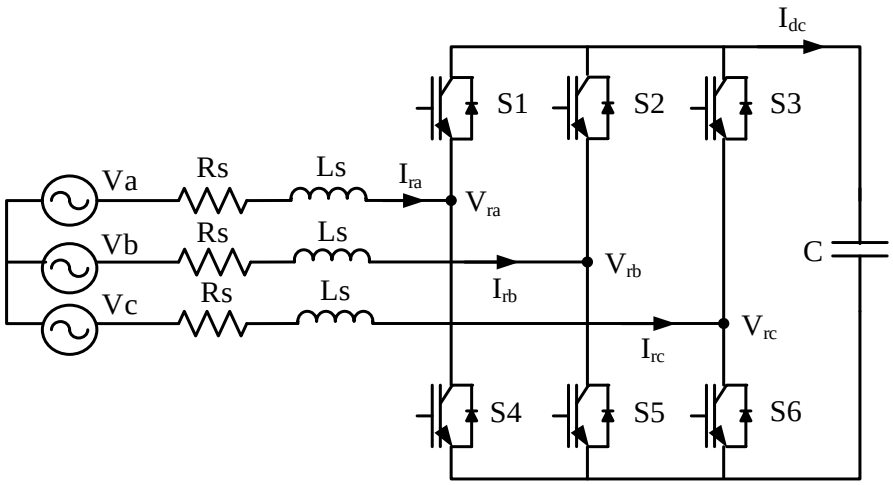

Figure 2.11. Schematic of a three-phase PWM rectifier

The mathematical representation of a PWM rectifier in the abc frame can be formulated as [58]:

$$\begin{bmatrix} L_s \dfrac{dI_{ra}}{dt} \\ L_s \dfrac{dI_{rb}}{dt} \\ L_s \dfrac{dI_{rc}}{dt} \\ L_s \dfrac{du_c}{dt} \end{bmatrix} = \begin{bmatrix} -R_s & 0 & 0 & 0 \\ 0 & -R_s & 0 & 0 \\ 0 & 0 & -R_s & 0 \\ S_a & S_b & S_c & -1 \end{bmatrix} \begin{bmatrix} I_{ra} \\ I_{rb} \\ I_{rc} \\ I_L \end{bmatrix} + \begin{bmatrix} V_a - V_{ra} \\ V_b - V_{rb} \\ V_c - V_{rc} \\ 0 \end{bmatrix} \tag{2.26}$$

$$\begin{bmatrix} V_{ra} \\ V_{rb} \\ V_{rc} \end{bmatrix} = \begin{bmatrix} 2/3 & -1/3 & -1/3 \\ -1/3 & 2/3 & -1/3 \\ -1/3 & -1/3 & 2/3 \end{bmatrix} \begin{bmatrix} S_a \\ S_b \\ S_c \end{bmatrix} V_{dc} \tag{2.27}$$

The wind generator inductance and resistance are represented by L_s and R_s respectively. The wind generator phase currents are denoted as I_a, I_b, and I_c, while V_{ra}, V_{rb}, and V_{rc} stand for the rectifier input voltages. These voltages are determined by the operation of the switching elements within the rectifier structure, alternately opening and closing to achieve the desired DC link voltage. The switching functions, Sa, S_b, and S_c, indicate whether the switches are off (0) or on (1). [58] express the Clark's matrix in the alpha-beta (α–β) framework as follows:

$$T = \begin{bmatrix} 1 & -1/2 & -1/2 \\ 0 & \sqrt{3}/2 & -\sqrt{3}/2 \end{bmatrix} \tag{2.28}$$

The dynamic characteristics of the PWM rectifier are found using the Clark transform:

$$\begin{bmatrix} V_\alpha \\ V_\beta \end{bmatrix} = L_s \begin{bmatrix} \frac{dI_\alpha}{dt} \\ \frac{dI_\beta}{dt} \end{bmatrix} + \begin{bmatrix} R_s & 0 \\ 0 & R_s \end{bmatrix} \begin{bmatrix} I_\alpha \\ I_\beta \end{bmatrix} + \begin{bmatrix} V_{r\alpha} \\ V_{r\beta} \end{bmatrix} \tag{2.29}$$

Applying Park's transformation to the rectifier system leads to the conclusion of the following equation:

$$\begin{bmatrix} V_d \\ V_q \end{bmatrix} = L_s \begin{bmatrix} \frac{dI_d}{dt} \\ \frac{dI_q}{dt} \end{bmatrix} + \begin{bmatrix} R_s & -\omega L_s \\ \omega L_s & R_s \end{bmatrix} \begin{bmatrix} I_d \\ I_q \end{bmatrix} + \begin{bmatrix} V_{rd} \\ V_{rq} \end{bmatrix} \tag{2.30}$$

The angle value (θ) necessary for the transformations mentioned above can be determined using a phase-locked loop (PLL) in MATLAB/Simulink, or it can be obtained through the abc–αβ transformation method.

2.3. Modeling of the Storage Unit (Ni-MH Model)

the equivalent circuit of a NiMH battery depicts in figure 2.12. In this circuit, E represents the no-load voltage, E_0 stands for the constant voltage, K represents the polarization constant or polarization resistance, q denotes the maximum battery capacity, and Q is the exponential voltage. A represents exponential capacity. All these parameters of the equivalent circuit type are determined consist on its discharge properties [59].

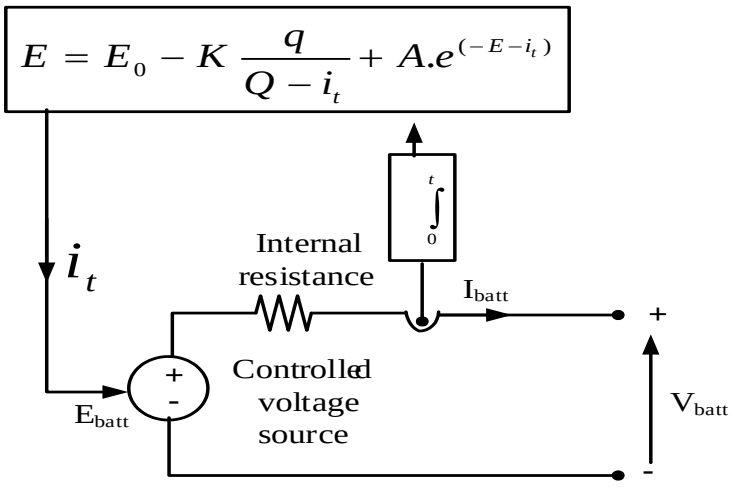

Figure 2.12. The NiMH battery equivalent circuit [59]

The battery voltage (V_{batt}) is given by the equation:

$$V_{batt} = E_{batt} - R_{batt}.I_{batt} \tag{2.31}$$

Where: I_{batt} is the battery current, R_{batt} is the internal resistance, and E is the open circuit voltage of the battery.

To prevent battery degradation and extend its lifespan, Its SOC must be kept within a specified range, as follows:

$$SOC_{\min}(t) \le SOC(t) \le SOC_{\max}(t)$$

SOC_{max}: Maximum SOC of the battery and SOC_{min}: Minimum SOC of the battery. The SOC of the battery is expressed as:

$$SOC = 100\left(1 - \frac{Q \times 1.05}{\int idt}\right) \tag{2.32}$$

Figure 2.13 illustrates various discharge curves. The initial section depicts the exponential voltage drop during battery charging. The width of this area varies depending on the battery type. The second segment indicates the amount of charge that can be drawn from the battery until the voltage falls below the nominal voltage. Finally, the third segment represents the complete discharge of the battery, characterized by a rapid voltage drop.

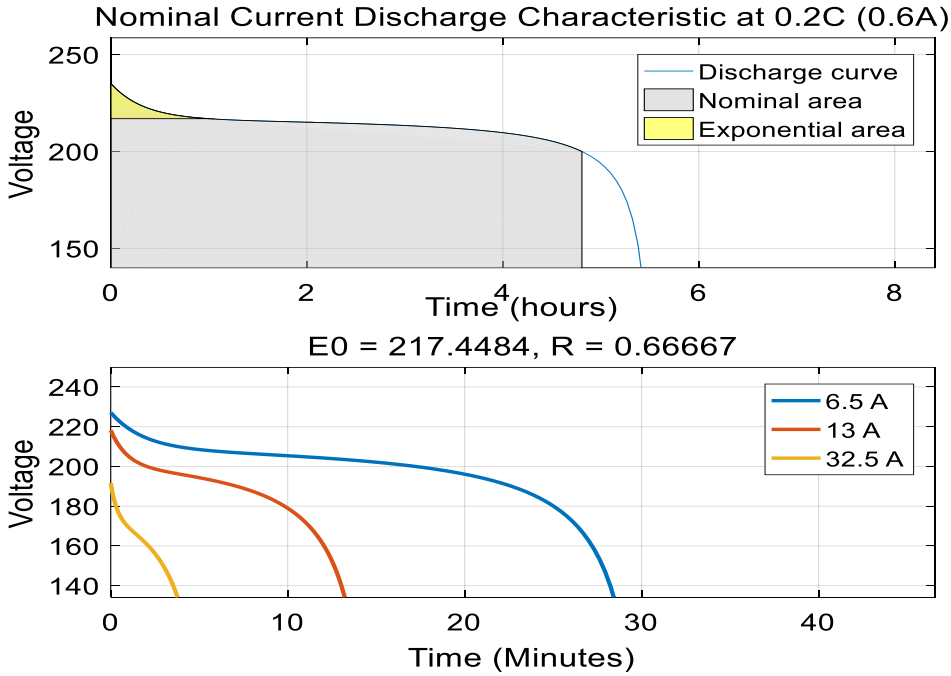

Figure 2.13. Characteristic discharge curve of a Nickel Metal Hydride battery.

The parameters of the NiMH battery used in the proposed propulsion system are shown in the table below (see annex).

3. Modeling of Electrical Components for the Link between the HRES and the Electrical Grid

3.1. Static Converters for the HRES

Choppers are converters made up of reactive elements: capacitors, inductors, and controlled switching devices (transistor, denoted as K in our study) and the other with spontaneous blocking and triggering (diode, denoted as D). We can distinguish the following types of choppers:

- Buck converter
- Boost converter
- Buck/Boost converter
- Bidirectional converter.

In the study we conducted, we used the second type to connect the photovoltaic generator and the wind turbine to the DC bus, while we used the fourth type for the same purpose.

During the operation of the DC/DC converter, the switch K will be switched at a constant frequency (f), with a closing time equal to DTs and an opening time of (1-D) Ts. Figure 2.14 shows the voltage across switch K (transistor).

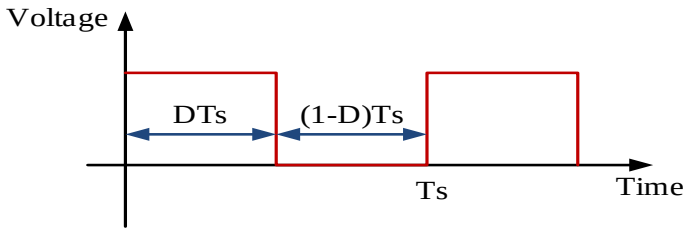

Figure 2.14. Voltage across switch K (transistor).

Where: Ts is the switching period, we have: Ts=1/f and D is the duty cycle of the switch, D∈ [0,1].

3.1.1. Boost Converter

We have two basic systems that use the boost converter:

- The photovoltaic generator is linked to the DC bus using a boost converter. This is to link the generator to the DC current on one hand and, on the other hand, to control the operation of the generator at the MPP that can be produced.
- The wind turbine itself is connected to the DC bus using a boost converter to operate the wind generator at the MPP.

Figure 2.15 illustrates the basic schematic of the boost converter. The operation of the boost converter can be divided into two switching phases based on the switch K's state (on/off). Each phase is described by a differential equation. [60].

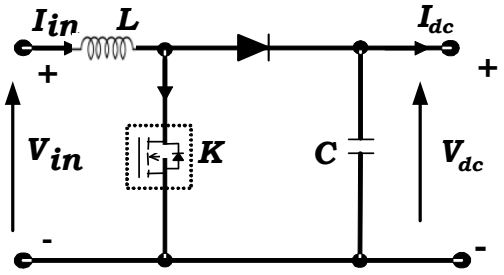

Figure 2.15. Block diagram of a boost converter

For the first period: K is closed

$$\begin{cases} V_{in} = L\dfrac{dI_{in}}{dt} \\ 0 = C\dfrac{dv_{dc}}{dt} + I_{dc} \end{cases} \tag{2.33}$$

For the second period: K is open

$$\begin{cases} V_{in} = L\dfrac{dI_{in}}{dt} + V_{dc} \\ I_{in} = C\dfrac{dv_{dc}}{dt} + I_{dc} \end{cases} \tag{2.34}$$

We assume that the switches used in this study are ideal. We can represent the converter by a system of equations (2.35):

$$\begin{cases} L\dfrac{dI_{in}}{dt} = V_{in} - (1-u).V_{dc} \\ C\dfrac{dV_{dc}}{dt} = -I_{dc} + (1-u).I_{in} \end{cases} \tag{2.35}$$

Where u is the state of switch K, it is given by:

- u = 1 when switch K is closed,
- u = 0 when switch K is open.

It can be replaced by its average value over one switching period, i.e., the duty cycle D, we can obtain the average value model [60]:

$$\begin{cases} \dfrac{dI_{in}}{dt} = \dfrac{V_{in}}{L} - (1-D).\dfrac{V_{dc}}{L} \\ C\dfrac{dV_{dc}}{dt} = -\dfrac{V_{dc}}{CR} + (1-u).\dfrac{I_{in}}{C} \end{cases} \quad (2.36)$$

3.1.2. Bidirectional Converter (Buck/ Boost)

The battery is connected to the DC bus through a bidirectional DC-DC converter of the current-reversible converter type to ensure energy transfer in both directions (charge/discharge).

Figure 2.16 illustrates the block diagram of a bidirectional converter.

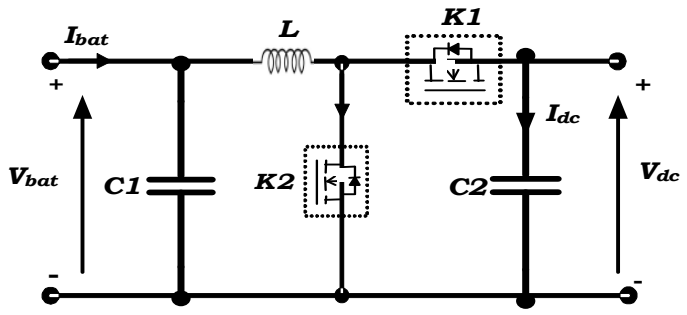

Figure 2.16. The block diagram of a bidirectional converter

The differential equations defining the operation of the bidirectional converter have been solved using an average value model. Knowing that the switches K1 and K2 are controlled simultaneously with complementary duty cycles D_b and 1 - D_b. The operation of the current-reversible chopper is described by [61]:

$$\begin{cases} \dfrac{dI_{bat}}{dt} = \dfrac{V_{bat}}{L} - \dfrac{V_{dc}}{L} D_b \end{cases} \quad (2.37)$$

The duty cycle D_b is obtained from a classical PI controller.

3.2. Modeling Elements for the Electrical Grid

To connect the proposed hybrid system in our study to the electrical grid and allow supplying the load with a sinusoidal waveform and active power,

the process is carried out through the static inverter. This is done after injecting the energy output by the hybrid system into the direct current bus (DC bus). The filter is used to reduce distortions in the current output from the static inverter.

Figure 2.17 illustrates the key elements linking the system to the network, which is done through the direct current bus, passing through the static inverter, and then the filter. This connection enables bidirectional flow of power with respect to the grid, allowing for effective integration of RE sources and smooth operation of the entire system. The static inverter plays a vital role in converting the DC output from the hybrid system into alternating current compatible with the grid's specifications, ensuring seamless interaction and optimal resource utilization.

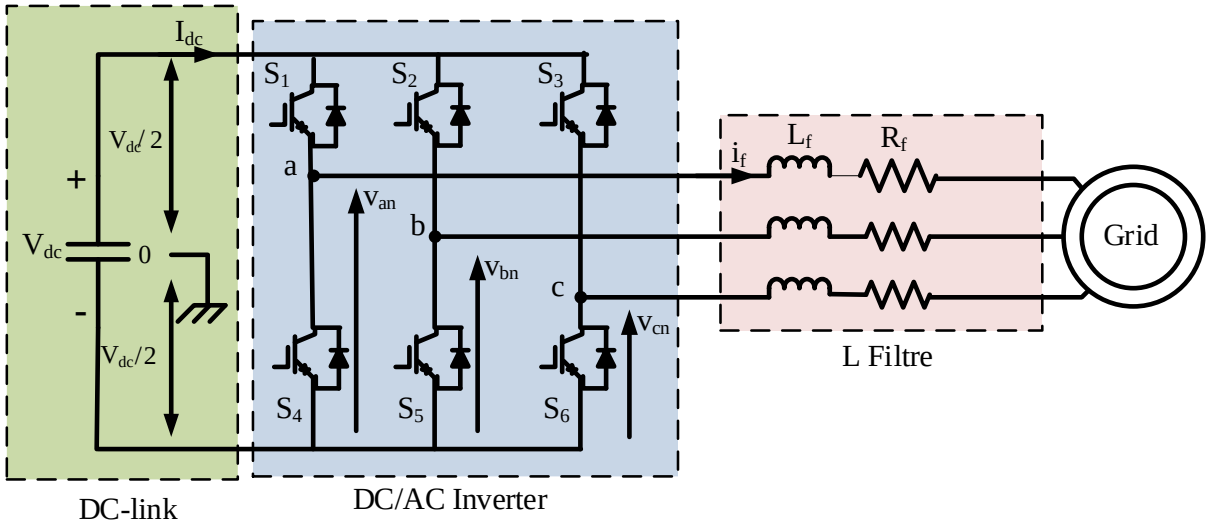

Figure 2.17. The diagram of the main components linking the system to the electrical grid

3.2.1. Modeling of the DC Bus

In general, in modeling, the DC bus is considered as a capacitor [7]. Figure 2.18 illustrates the centralization of the energy provided by each power source as well as the energy consumed by the load. We connected the sources according to the configuration of the DC bus. The arrows indicate the direction of energy transfer from the source to the DC bus or may be reversed, as is the case for the load.

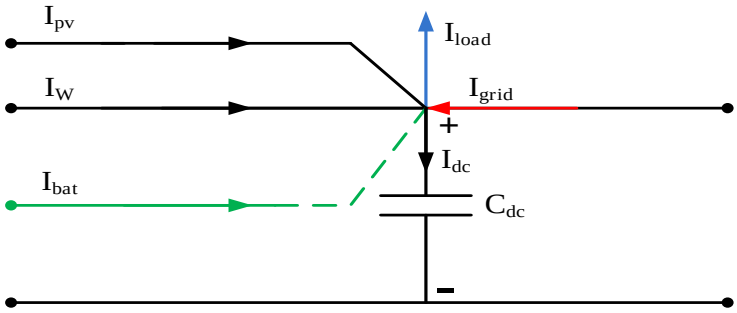

Figure 2.18. The Continuous bus model

The current in the DC bus is given by:

$$I_{dc} = C\frac{dV_{dc}}{dt} \tag{2.38}$$

With:

$$I_{dc} = I_{pv} + I_w \pm I_{bat} \pm I_g - I_{load} \tag{2.39}$$

Where: I_{pv} is the current of the photovoltaic system, I_w is the current of the wind system, I_{batt} is the charging/discharging current of the battery, I_{load} is the current of the load.

Setting the DC bus voltage (Vdc) to a reference value is crucial. It should exceed the maximum value (peak value) of the AC-side voltage from the inverter. When the adjustment coefficient is at its maximum (ma = 1), In our study, we fixed the constant voltage at reference value, the expression for Vdc-ref is described as [62]:

$$V_{dc} = 2\sqrt{2}.V_s \tag{2.40}$$

With V_s being the maximum phase voltage value at the output of the inverter.

3.2.2. Three-Phase Inverter (DC/AC)

The structural schematic diagram of a two-level three-phase inverter is shown in Figure 2.15. [63]. From the figure, we can observe that we used the three-phase inverter to connect the grid to the direct current bus by converting the incoming alternating current from the grid into a specified frequency and waveform, allowing for easy connection to the DC bus. This process is among the features of the inverter that greatly benefit renewable

energies in their integration with the electrical grid. The voltage inverter is a static converter generally consisting of switching cells using transistors or GTO thyristors.

Taking into account the fictitious point "o", the three compound voltages V_{ab}, V_{bc} and V_{ca} are defined by the following relationships [64]:

$$\begin{cases} V_{ab} = V_{ao} - V_{bo} \\ V_{bc} = V_{bo} - V_{ao} \\ V_{ca} = V_{co} - V_{ao} \end{cases} \quad (2.41)$$

Let "n" be the neutral point on the alternating side, the phase voltages of the inverter (V_{an},V_{bn} and V_{cn}) are given by:

$$\begin{cases} V_{an} = \frac{1}{3}(V_{ab} - V_{ca}) \\ V_{bn} = \frac{1}{3}(V_{bc} + 2V_{ab}) \\ V_{cn} = \frac{1}{3}(V_{ca} - V_{bc}) \end{cases} \quad (2.42)$$

By substituting equation (2.41) into equation (2.42), we obtain:

$$\begin{cases} V_{an} = \frac{1}{3}(2V_{ao} - V_{bo} - V_{co}) \\ V_{bn} = \frac{1}{3}(-V_{ao} + 2V_{bo} - V_{co}) \\ V_{cn} = \frac{1}{3}(-V_{ao} - V_{bo} + 2V_{co}) \end{cases} \quad (2.43)$$

Let Si denote the state of switch Ki, where:

- Si = 1 when the upper switch is closed and the lower one is open,
- Si = 0 when the upper switch is open and the lower one is closed.

Under these conditions, we can express the voltages V_{io} in terms of the control signals Si (i = a, b, c), taking into account the fictitious point "o" depicted in Figure 2.15:

$$V_{io} = V_{dc}\left(S_i - \frac{1}{2}\right) \quad (2.44)$$

Equation 2.45 enables the formulation of instantaneous equations for individual voltages based on the control variables:

$$\begin{bmatrix} V_{an} \\ V_{bn} \\ V_{cn} \end{bmatrix} = \frac{V_{dc}}{3} \begin{bmatrix} 2 & -1 & -1 \\ -1 & 2 & -1 \\ -1 & -1 & 2 \end{bmatrix} \begin{bmatrix} S_a \\ S_b \\ S_c \end{bmatrix} \quad (2.45)$$

3.2.3. Modeling of the L Filter

The output filter is designed to mitigate the harmonics present in the current generated by semiconductor switching. Various types of filters are utilized for this purpose. The most straightforward configuration involves a filter inductor connected to the output of the inverter. Additionally, combinations involving capacitors, such as LC or LCL configurations, can also be employed [65].

The first type of filter is the L filter, depicted in Figure 2.17 (a). It operates as a first-order filter with an attenuation rate of 20 dB/decade across the entire frequency spectrum. This type of filter is well-suited for converters operating at high switching frequencies. The second type is the LC filter, illustrated in Figure 2.17 (b). It functions as a second-order filter and exhibits superior damping characteristics compared to the L filter. This straightforward configuration is relatively easy to design and typically operates without significant issues. The second-order filter delivers a 12 dB/octave attenuation beyond the cutoff frequency [66]. The third variant is the LCL filter, illustrated in Figure 2.19 (c). LCL filters have an attenuation rate of 60 dB/decade for frequencies beyond their resonance frequency, allowing for the utilization of lower switching frequencies in the converter. Notably, the LCL filter effectively attenuates current ripple even when employing relatively small inductance values.

the LC filter can be defined as:

$$F(s) = \frac{1}{1 + s^2 LC} \quad (2.46)$$

The cutoff frequency (fc) for the LC filter can be computed as:

$$f_c = \frac{1}{2\pi\sqrt{LC}} \quad (2.47)$$

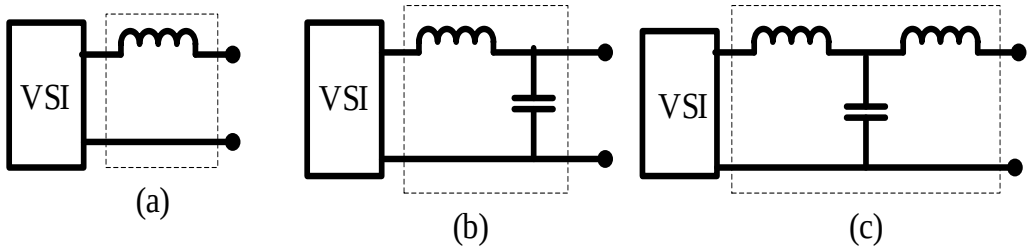

Figure 2.19. Different types of the passive filter

The representation of the L filter is depicted in the block diagram as illustrated in Figure 2.20 This model can be characterized by two equations: one detailing the dynamics of the inductance and the other outlining the dynamics of internal resistance of inductance [67].

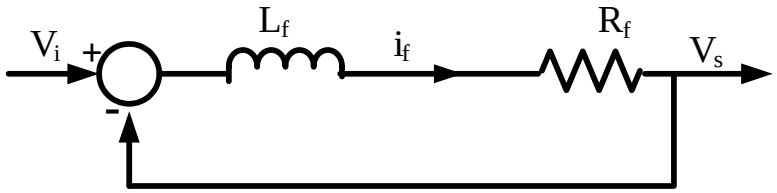

Figure 2.20. The scheme of L Filter

The equation representing the filter inductance in vector form is:

$$L_f \frac{di_f}{dt} + R_f i_f = v_i - v_s \tag{2.48}$$

With: The output voltage space vectors produced by the inverter are described by:

$$v_i = \frac{2}{3}\left(v_{an} + a v_{bn} + a^2 v_{cn}\right) \tag{2.49}$$

Vs: The output voltage of the L filter.

3.3.3. Modeling the Instantaneous Active and Reactive Power of the Electrical Grid

The purpose of connecting the hybrid system to the electrical grid is to supplement any shortfall in power if the RES and battery bank are unable to cover the load requirements. Modeling a grid-connected generator involves calculating the active and reactive power of the generator. It is widely acknowledged that calculating active power (P) necessitates a scalar product of voltages and currents, whereas determining reactive power (Q) entails a vector product of these quantities [68].

Where: $P = V_a i_a + V_b i_b + V_c i_c$ (2.50)

$$q = \frac{1}{\sqrt{3}}\left[(V_b - V_c) i_a + (V_c - V_a) i_b + (V_a - V_b) i_c\right] \quad (2.51)$$

in the dq frame express P and Q with:

$$\begin{cases} P = V_d i_d + V_q i_q \\ Q = V_d i_q - V_q i_q \end{cases} \quad (2.52)$$

4. Conclusion

In this chapter, we have modeled a multi-source system linked to the electrical grid, consisting of a photovoltaic generator, a wind generator, a storage system (NiMH), and converters to match the sources with the load. All these elements are interconnected through a continuous bus (DC bus) to feed an alternating current load by connecting it to the inverter.

Units of controllers developed will be connected to the static converters that modeled in this chapter to manage and optimize power generated from solar and wind energy sources.

In the next chapter, we will study the means to control all systems and optimize the utilization of the produced energies.

Chapter 3:
Optimization and managing of hybrid renewable energy systems (HRES)

1. Introduction

In this chapter, we studied an isolated hybrid renewable energy system by proposing a strategy for optimal management of the generated energy. This chapter serves as a gateway to understanding the grid-connected hybrid system, as studying the isolated system helped us address the main topic, which is the grid-connected hybrid system. We tackled the issue of managing the generated energy to meet load requirements through the following steps:

- Improving the energy generated from RES (solar generator and wind generator) by proposing a strategy for MPPT.

- Managing system energies by controlling the DC voltage according to the reference value using a bidirectional converter controller for the battery.

- Controlling the inverter**.**

2. Optimizing Power Generation of the Proposed HRES

the proposed design of a HRES shows in Figure 3.1, where the photovoltaic (PV) and wind turbine (WT) systems serve as the primary power sources, with a battery as a backup. To supply AC load requirements from these sources, static converters are connected to the DC bus voltage. Two controllers for MPP Trackers are used to control the boost converter, thereby enhancing the energy production efficiency from the primary sources. Additionally, the battery is integrated into the system to optimize energy management module (EMM) by managing charging and discharging through a bidirectional DC/DC converter.

Given the irregular nature of the investigated system, we aimed to maximize energy production by tracking the MPP of each source. This was achieved through both traditional and intelligent MPPT control methods. A battery was added and linked to the DC link via a converter, capable of regulating and stabilizing the DC voltage, ensuring the load demand is met under any operational condition. We then managed the controlled energy using an algorithm, which will be discussed later.

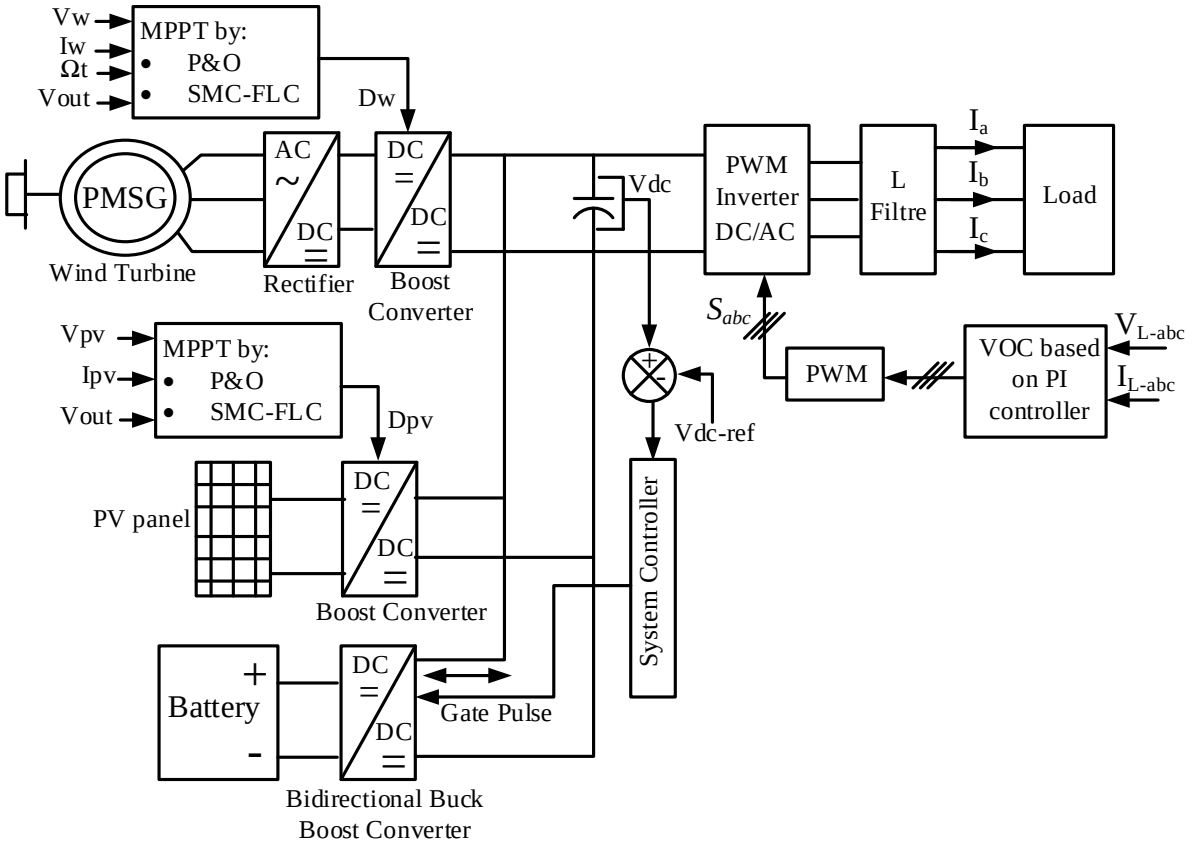

Figure 3.1. The proposed control system for HRES

2.1. MPPT methods for photovoltaic generator

The PV system experiences reduced energy efficiency during times of low irradiation or partial shading. The amount of electrical energy generated continuously fluctuates with changing weather conditions. This challenge drives researchers to create an MPPT controller to optimize power extraction from the PV system [69] [70].

In this study, we maximized the power output of the PV system using an MPPT controller that combines two intelligent control systems: a FLC and a SMC. This controller adjusts the duty cycle of the boost converter. The results obtained were then compared with the traditional (P&O) method, and it was also used to measure the reference voltage value of the PV generator (V_{ref}), as shown in Figure 3.2.

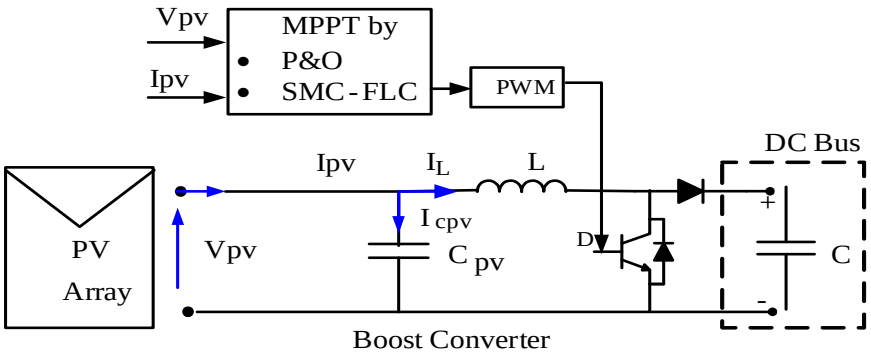

Figure 3.2. PV generator with MPPT control

2.1.1.A classical P&O algorithm

The P&O algorithm is the most widely used in photovoltaic systems, due to its simplicity and ease of implementation. In references [71] and [72], the Perturb and Observe (P&O) method has been employed. This approach involves adjusting the perturbation of the PV cell's harvest voltage, which in turn affects the PV output power, allowing the system to track MPP under any operating condition. In our research, we used the (P&O) algorithm to calculate (V_{ref}), which we then utilized as input data for the control unit composed of fuzzy logic and sliding mode control. Figure 3.3. illustrates the application flowchart of the P&O MPPT method.

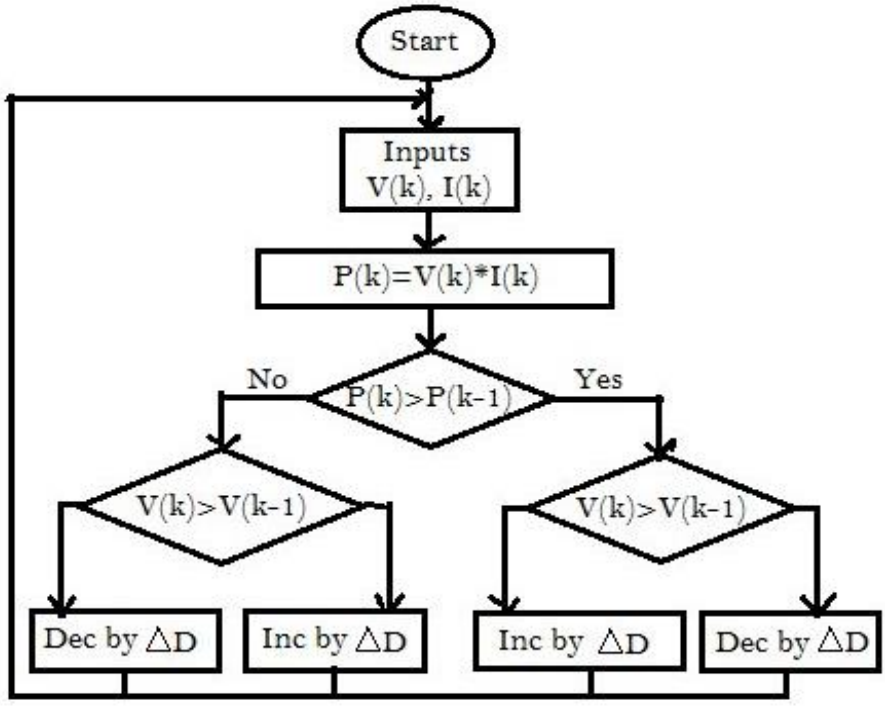

Figure 3.3. P&O's flow chart [73]

The flowchart illustrates how the P&O algorithm adjusts the reference voltage V(k) periodically with a constant step size C(k) to maximize power output. Initially, the algorithm measures the solar panel's output voltage V(k) and current I(k) to determine the instantaneous power P(k). This power value is then compared to the previously calculated power P(k-1) to decide whether to continue adjusting the voltage in the same direction. If P(k) is greater than P(k-1), the algorithm maintains the current adjustment direction; otherwise, it reverses the direction to find the optimal operating point [73].

The disadvantage of the P&O technique is that, at steady state (equilibrium), the operating point oscillates around the MPP, causing a loss of some available energy. Additionally, in the event of a sudden increase in irradiation, the P&O algorithm reacts as if the increase was caused by the previous perturbation. As a result, it continues in the same direction, which is incorrect, leading it further away from the true maximum power point [71].

2.1.2.The hybrid MPPT (SMC- Fuzzy logic control)

This approach was introduced in [74]. Figure 3.4 demonstrates how this method utilizes P&O, SMC, and FLC to establish the Upv control for a PV system.

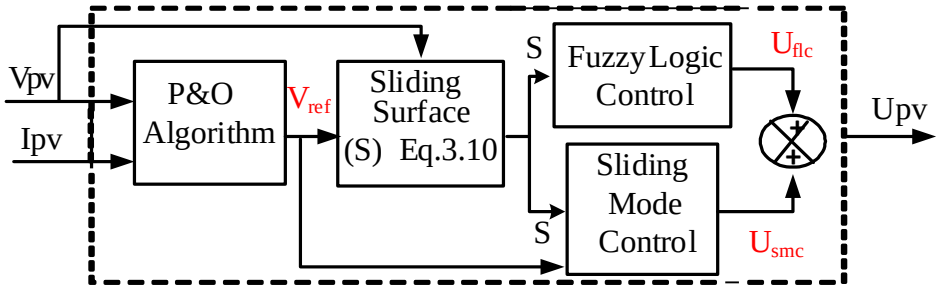

Figure 3.4. Schematic of the mixed MPPT for PV systems.

The control law enables the PV system to achieve its (MPP) as follow:

$$U_{pv} = U_{smc} + U_{FLC} \tag{3.1}$$

To compute the aforementioned control law, as illustrated in Figure.3.4, this strategy involves three crucial steps, which will be detailed in three sections: first, a P&O algorithm is utilized specifically to calculate the reference voltage

of the PV system (V_{ref}). This reference voltage is then used to determine the sliding surface (S) and the equivalent commands for the U_{smc} and U_{FLC} controls.

2.1.2.1. Structure block of SMC for photovoltaic generator

a) Sliding mode control (SMC) theory

The theory of Variable Structure Systems (VSS) and sliding modes has been extensively studied for the past thirty years [75]. The SMC aims to steer the system's state trajectory onto a specific surface. Here, adaptive switching mechanisms adjust the trajectory until it stabilizes at an equilibrium point on this surface figure 3.5. SMC stands out for its simple implementation and robustness compared to other methods. The switching between two values is determine by equation (3.2) [76]:

$$u = \begin{cases} u_{\min} \ pour & s < 0 \\ u_{\max} \ pour & s > 0 \end{cases} \tag{3.2}$$

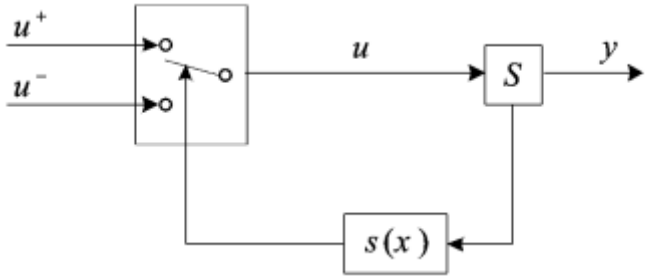

Figure 3.5. Variable structure control system with structure change through switching [77]

The synthesis of a SMC law involves, first and foremost, choosing the sliding surface that ensures the convergence of the system's state trajectory towards the desired equilibrium point, then establishing the condition for the presence of the sliding mode, which is associated with the state trajectory's convergence and determining the control law whose role is to maintain the sliding conditions (attractiveness). In other way, the design of the SMC law is carried out in three steps:

- Step 1: Choosing the sliding surface;
- Step 2: Developing the convergence condition;
- Step 3: Determining the control law.

1. Choice of the Sliding Surface

The choice of the sliding surface concerns the number and shape of the necessary functions. These two factors depend on the application and the objective.

For a system defined by equation (3.3), the sliding surface vector S has the same dimension as the control vector u.

$$\frac{dx}{dt} = f(x,t) + B(x,t)u \tag{3.3}$$

The sliding surface is a scalar function where the variable to be controlled moves along this surface, gradually approaching the origin of the phase plane. [78, 80].

The non-linear form is a function of the error on the variable to be regulated x. A general form proposed by J.J. Slotine that ensures the convergence of the variable to its reference is given by [78, 80]:

$$S(x) = \left(\frac{d}{dt} + \lambda \right)^{r-1} .e(x) \tag{3.4}$$

Where:

- e(x) represents the error between the variable to be regulated and its reference.
- λ is a positive constant.
- r is the relative degree, representing the number of times the output needs to be derived to reveal the control.

2. Conditions of Existence and Convergence

The attractiveness condition permits the system's dynamics to converge towards the sliding surface. This requires defining a scalar Lyapunov function V(x) > 0 for the state variables of the system. The control law must be designed to reduce this function. To achieve this, a scalar function S(x) is selected to attract the controlled variable to its target value. A control u is then designed so that the square of the sliding surface serves as a Lyapunov function as follows [77]:

$$V(x) = \frac{1}{2} S^2 \tag{3.5}$$

Its derivative is:

$$\dot{V}(x) = S(x).\dot{S}(x) \tag{3.6}$$

For V(x) to decrease, its derivative must be negative. Equation (3.5) demonstrates that $S^2(x)$ represents the squared distance from a specific point in the phase plane to the sliding surface, The reduction continues while the derivative of the Lyapunov function remains negative, directing the system's trajectory towards the surface from both directions. This scenario assumes an optimal sliding regime with an infinitely high switching frequency [78].

3. Determination of the Control Law

Achieving a sliding regime requires a discontinuous control. The sliding surface must be attractive from both sides. Therefore, if this discontinuous control is necessary, a continuous part can be added [77]. In the presence of disturbances, the discontinuous control ensures the attractiveness conditions. The structure of SMC comprises two components: one involving exact linearization u_{eq} and the other aimed at stabilization Δu, denoted as:

$$u = u_{eq} + \Delta u \tag{3.7}$$

The equivalent control proposed by Filippov and Utkin [77] maintains the variable to be controlled on the sliding surface S(x) = 0. The discontinuous control drives this variable towards its reference point when it deviates from the sliding surface [78], ensuring compliance with the convergence requirement.

- **Equivalent Control**

For relation (3.3), depending on setting the time derivative of the switching function to zero, an equivalent control vector can be developed:

$$\dot{S}(x,t) = \left(\frac{\delta S}{\delta x}\right)^T \left(f(x,t) + B(x,t)u\right) + \frac{\delta S}{\delta x} = 0 \tag{3.8}$$

Thus, the equivalent control is defined by:

$$u_{eq} = -\left[\left(\frac{\delta S}{\delta x}\right)^T \times B(x,t)\right]^{-1} \left\{\left(\frac{\delta S}{\delta x}\right)^T \times f(x,t) + \frac{\delta S}{\delta x}\right. \tag{3.9}$$

With the existence condition:

$$\left(\frac{\delta S}{\delta x}\right)\times B(x,t)\neq 0 \tag{3.10}$$

- **Discontinuous Control**

When the state trajectories deviate from the sliding surface S(x) = 0 due to disturbances or changes in parameters of the system, the function presented by (3.11) is a discontinuous function (two-level switch) capable of pulling these trajectories towards their references. This control is defined as follows [81]:

$$\Delta u = -ksign(S(x)) \tag{3.11}$$

With K>0

$$\text{And}\quad sign(S(x)) = \begin{cases} 1 \ if\ S(x) > 0 \\ -1 if\ S(x) < 0 \\ 0 \ if\ S(x) = 0 \end{cases} \tag{3.12}$$

- **Sliding Mode with Integral Effect**

In this method, the sliding surface could be optimized by inserting an integral action in its formulation, defined as [81]:

$$S(x) = \left(\frac{d}{dt}+\lambda\right)^{r-1} e(x) + k_1 \int e(t)dt \tag{3.13}$$

Where k_i is a positive integral gain. For a second-order system with r = 2, the solution is found within a plane, whereas in the traditional sliding mode, the solution occurs along a line.

b) Application of the proposed MPPT

Many studies have utilized (SMC) [79], [80] to enhance the performance of PV systems due to its robustness and simplicity compared to conventional methods. SMC is employed to track the (MPP) by following two key steps [80]. The first step involves defining the sliding surface, as shown in equation (3.15), to ensure that the system converges towards it. The second step is to regulate the equivalent control law, as described in equation (3.1), which ensures that the system remains on that surface, thereby reaching

the MPP. A diagram illustrating how to implement the sliding mode controller (Figure 3.6.):

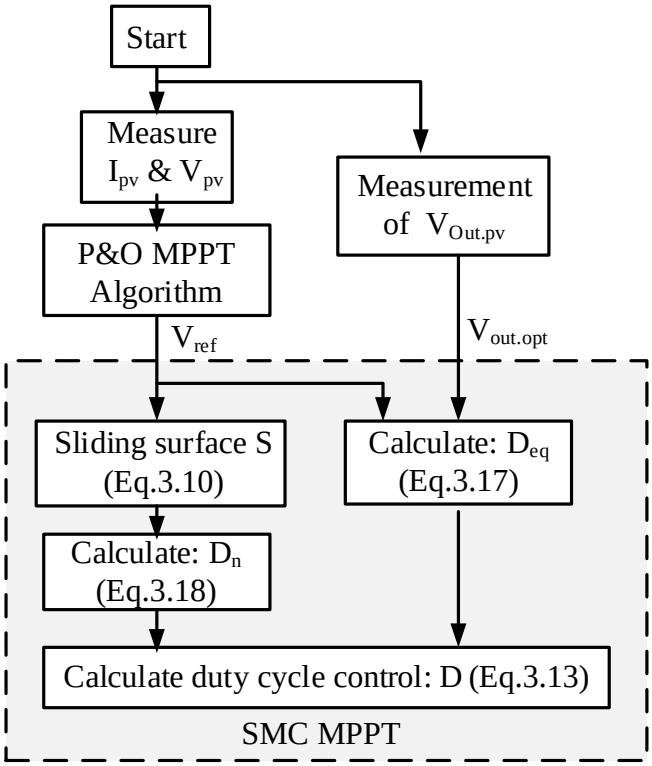

Figure 3.6. SMC MPPT approach for PV generator.

The sliding surface S can be expressed as follows [79]:

$$S = \frac{dP_{pv}}{dV_{pv}} = I_{pv} + V_{pv}\frac{dI_{pv}}{dV_{pv}} = 0 \tag{3.14}$$

The objective of the (P&O) method is to calculate V_{ref} to establish a new sliding surface, as defined in equation (3.15):

$$S = \frac{\Delta P}{\Delta V} = \frac{P_{pv} - P_{ref}}{V_{pv} - V_{ref}} = I_{pv} + V_{ref}\frac{dI_{pv}}{dV_{ref}} \tag{3.15}$$

With:

$$P_{ref} = I_{pv}.V_{ref} \tag{3.16}$$

This S enables us to define the boost converter duty cycle of the PV converter, expressed as [71]:

$$D_{k+1} = \begin{cases} D_k - \Delta D, if & S < 0 \\ D_k + \Delta D, if & S > 0 \end{cases} \tag{3.17}$$

The actual control signal is characterized by:

$$D=\begin{cases} 0 & , for \quad D_{eq}+D_n \le 0 \\ D_{eq}+D_n & , for \quad 0 < D_{eq}+D_n < 1 \\ 1 & , for \quad D_{eq}+D_n \ge 0 \end{cases} \tag{3.18}$$

D_{eq}, representing equivalent control, and D_n, discrete control, where: $D=U_{smc}$

D_{eq} is determined based on the condition outlined in [71]:

$$\dot{S}=\left[\frac{dS}{dX}\right]^T \dot{X}=0 \tag{3.19}$$

$$\dot{X}=\frac{dI_{pv}}{dt}=f(x)+g(x)D_{eq} \tag{3.20}$$

Based on Equation (2.35) of the boundary condition, we can derive the expression for equivalent control as defined by:

$$D_{eq}=\frac{\left[\frac{dS}{dX}\right]^T.f(x)}{\left[\frac{dS}{dX}\right]^T.g(x)}=1-\frac{v_{pv}}{V_{out-pv}} \tag{3.21}$$

The (P&O) method is employed to establish the (V_{ref}) for configuring this control to enhance the (MPPT). Consequently, the revised expression for equivalent control is as follows:

$$D_{eq}=1-\frac{v_{ref}}{V_{out-pv}} \tag{3.22}$$

The D_n is selected as [71]:

$$D_n=K.Sat(s) \tag{3.23}$$

With:

$$Sat(s)=\begin{cases} \frac{S}{\varepsilon}, if \quad |S|<\varepsilon \\ Otherwise, sign(s) \end{cases} \tag{3.24}$$

Here, K represents a constant positive value, while ε denotes the width of the limit layer.

2.1.2.2. Structure block of FLC for photovoltaic generator

a) Fuzzy logic control theory

The Principle of a Fuzzy Logic Controller consists of the following main parts [82]:

- Fuzzification

- Fuzzy inference system

- Knowledge base

- Defuzzification

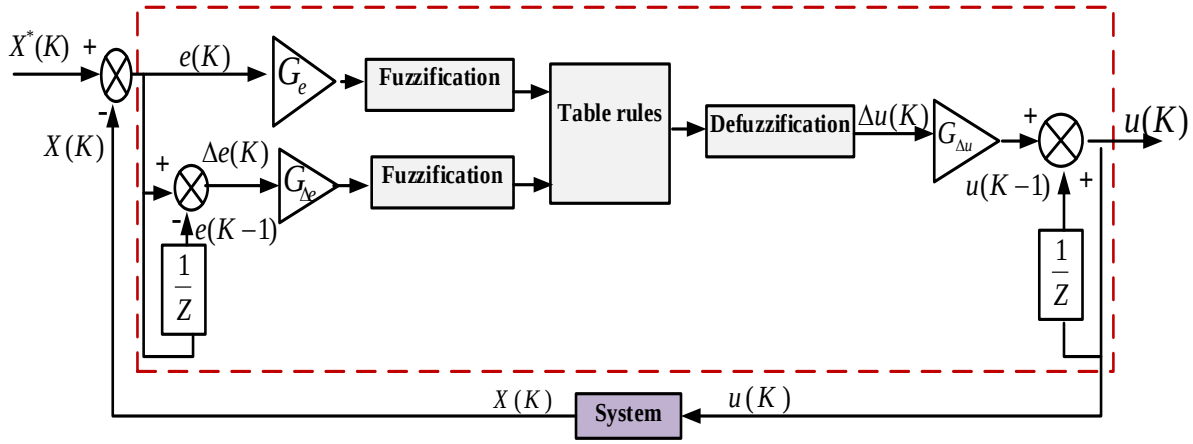

Figure 3.7. Internal structure of the fuzzy logic controller [82]

The controlled variable is compared to its reference value. The obtained error $e(k) = x*(k) - x(k)$ and its variation $\Delta e(k) = e(k) - e(k-1)$ are normalized by a normalization gain G_e for the error and G_{Δ_e} for the change in error).

The output of the fuzzy logic controller is the variation in the control law. The final control law is obtained as follows:

$$u(k) = u(k-1) + G_u \Delta u(k) \qquad (3.25)$$

Where: $G\Delta_u$ is a denormalization gain.

- **Fuzzification**

The process of converting a numerical variable (real number) into a linguistic variable (fuzzy number) is called fuzzification [83].

- **Fuzzy Inference System**

The basic structure of a fuzzy inference system consists of three components: a rule base, which contains a selection of rules, a database, which defines the membership functions used in the fuzzy rules, and a reasoning mechanism [84].

- **Defuzzification**

The rules of the fuzzy logic controller generate an output in a linguistic variable (fuzzy number) [82]. However, according to real-world requirements, the output linguistic variable must be transformed into a crisp output (real number). The most commonly used defuzzification method is the center of gravity. To find a crisp output value from the fuzzy set B having the universe of discourse y, the following equation can be used [82]:

$$u = \frac{\int_y \mu_B(y) y dy}{\int_y \mu_B(y) dy} \tag{3.26}$$

With a discretized universe of discourse, expression (3.26) can be rewritten as follows:

$$u = \frac{\sum_{j=1}^{q} u_B(y_j) y_j}{\sum_{j=1}^{q} u_B(y_j)} \tag{3.27}$$

Where: q is the number of quantization intervals of the function $\mu_B(y)$ and the corresponding center of the membership function (point b in Figure (3.8)):

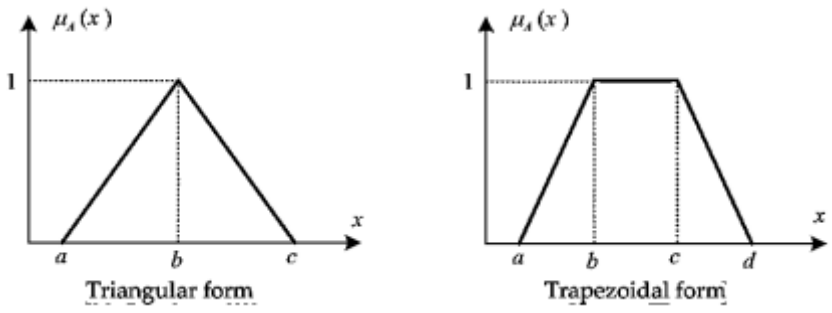

Figure 3.8. Common shapes of membership functions

b) Application of the proposed MPPT

To calculate the equivalent control U_{flc}, the two proposed inputs are S (represented as Error E) and its change dS (depicted as error variation dE). computed using equations (3.28) and (3.29). Figure 3.9 illustrates the structure of the FLC adopted in our study:

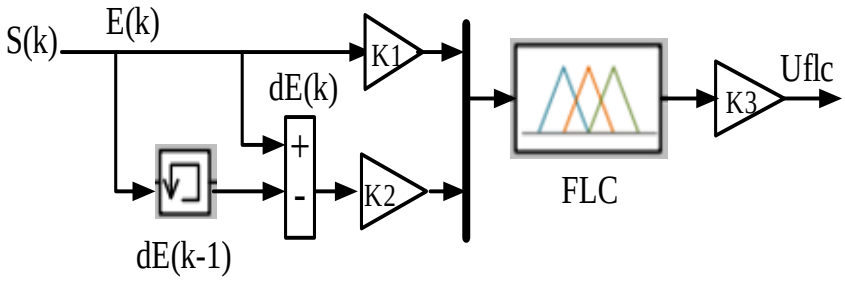

Figure 3.9. The structure of the proposed FLC

$$E(k) = S(k) = \frac{P_{pv}(k) - P_{ref}(k)}{V_{pv}(k) - V_{ref}(k)} \tag{3.28}$$

$$dE(k) = dS(k) = E(k) - E(k-1) \tag{3.29}$$

Variables are defined using five fuzzy subsets: negative small (NS), negative big (NB), zero (ZE), positive small (PS), and positive big (PB). The fuzzy system's rule base is detailed in the table of the inference engine step, with (E) and (dE) serving as inputs and Uflc as the output. Mamdani's method is employed for the fuzzy inference of the FLC, utilizing max-min composition. In the final defuzzification step, the controller computes the actual value of U_{flc}.

Table.3.1. (b) Fuzzy rules.

	dE					
E	NB	ZE	ZE	PS	PB	PB
	NS	ZE	ZE	ZE	PS	PS
	ZE	PB	PS	ZE	ZE	NS
	PS	NS	NS	NB	ZE	ZE
	PB	NS	NB	NB	ZE	ZE

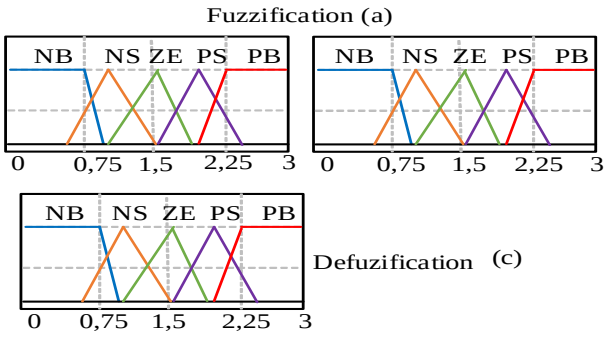

Figure 3.10. FLC Rules

2.1.3. Efficiency test of the MPPT algorithm

This test conducted under climatic conditions as illustrated in figure 3.11, where the temperature is kept constant at 25°C. Meanwhile, the solar radiation varies according to the profile shown. The radiation remains constant at 200 W/m², then decreases to 0 W/m², and subsequently increases again to 600 W/m², followed by a rise to 1000 W/m².

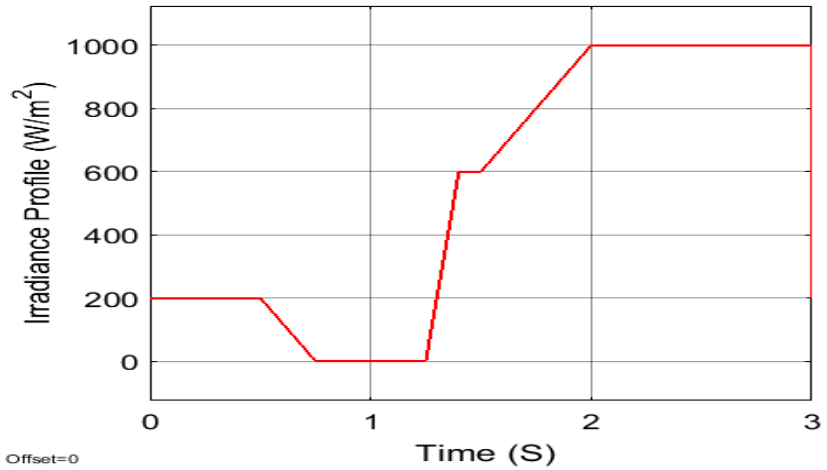

Figure 3.11. Solar irradiance

The figure 3.12. shows the voltage and current output from the photovoltaic generator. The results illustrate the disparity between the output voltage and the reference voltage calculated using the P&O algorithm, while the output current value follows the shape of the radiation profile.

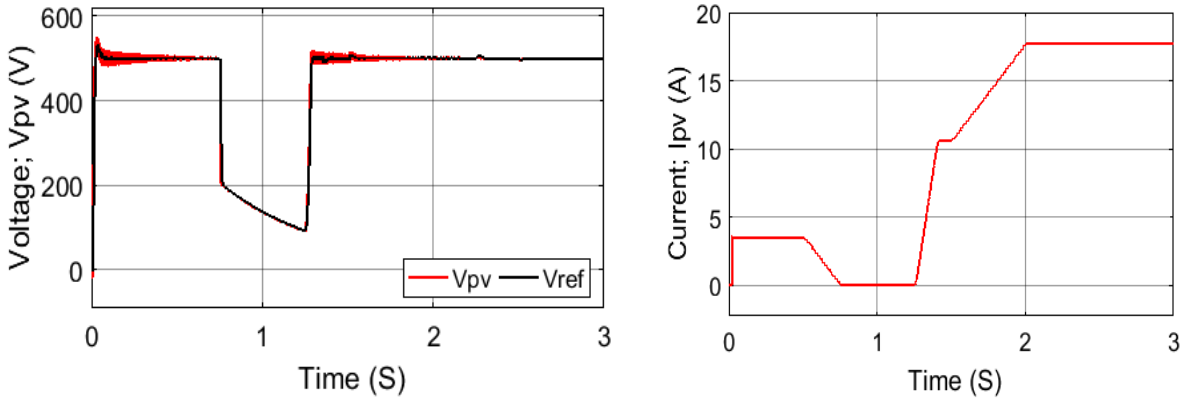

Figure 3.12. The voltage and current of the PV generator

Figure 3.13. demonstrates how the power output from solar panels varies with changing weather conditions. Compared to the P&O method, the proposed approach shows strong performance in PV generators. While P&O

can track the MPP, it exhibits noticeable oscillations in the output power between 1.51 to 2 seconds and 2.51 to 3 seconds. In contrast, the hybrid method combining robust SMC and FLC has proven effective, successfully tracking the MPP, stabilizing the system, and improving performance, particularly between 1.51 to 3 seconds.

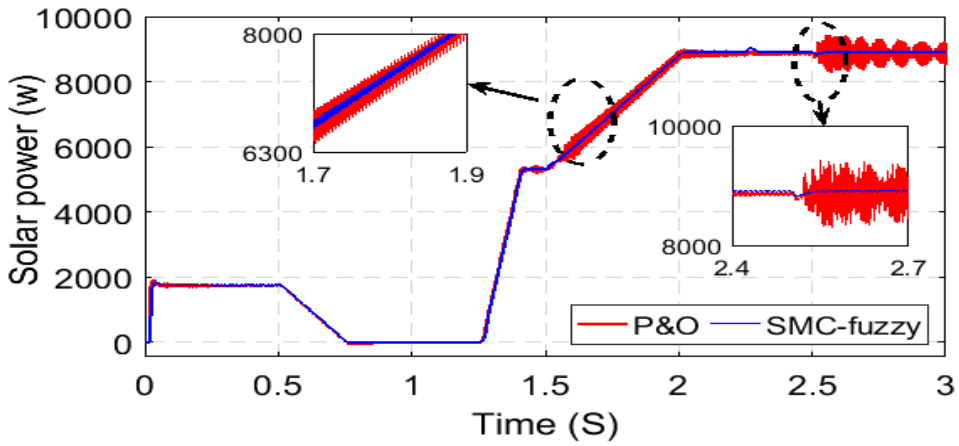

Figure 3.13. The power output of the PV generator

2.2. MPPT methods for the wind generator

As previously discussed, the importance of the control unit in a photovoltaic system for tracking the MPP is equally relevant for wind turbines. It is essential to implement a strategy or control unit to track the maximum power point of the generated energy, despite the random variation of weather conditions. A strategy combining fuzzy logic and SMC has been proposed for tracking the MPP. This involves inputting the data and distinctive attributes of the wind turbines. The results obtained using the proposed method are compared with those obtained using the P&O algorithm to verify the effectiveness of the proposed method, as illustrated in Figure 3.14.

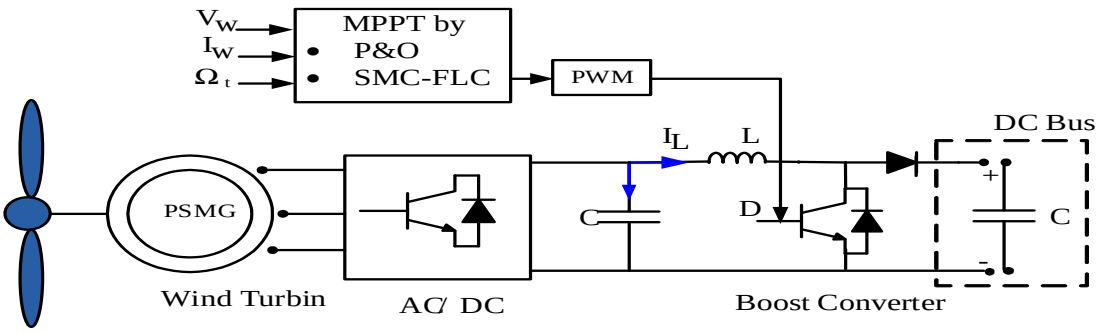

Figure 3.14. The WT generator with MPPT control

2.2.1.A classical P&O algorithm

The P&O MPPT method is commonly used to track a wind turbine's MPP. A detailed explanation of this strategy can be found in [85]. This method is specifically utilized to determine the reference rotor speed (Ω reference) for the new hybrid MPPT approach proposed in this study. The figure 3.15 illustrates the decision-making process flowchart of the P&O method, which facilitates the determination of Ω reference.

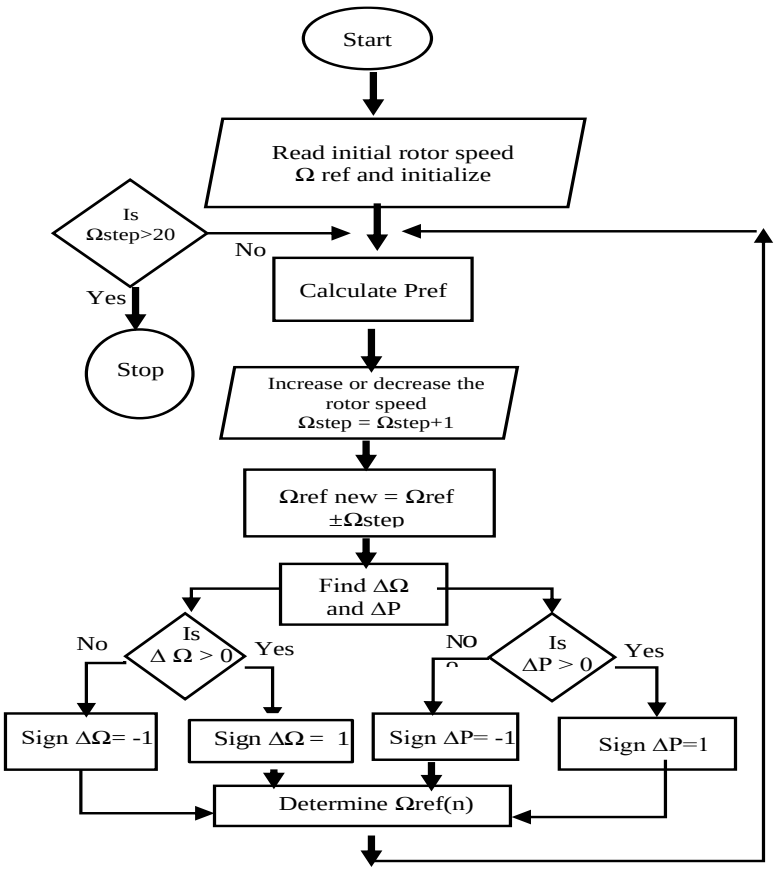

Figure 3.15. P&O's flowchart for WT

2.2.2.The hybrid MPPT (SMC- Fuzzy logic control)

This part introduces a novel technic aimed at improving MPPT of wind power generators, inspired by the MPPT techniques used in photovoltaic systems. As previously discussed, this method utilizes three fundamental components to control the wind for optimizing the power output of wind generators. The figure 3.16. presents the schematic diagram of the new MPPT strategy for wind turbines.

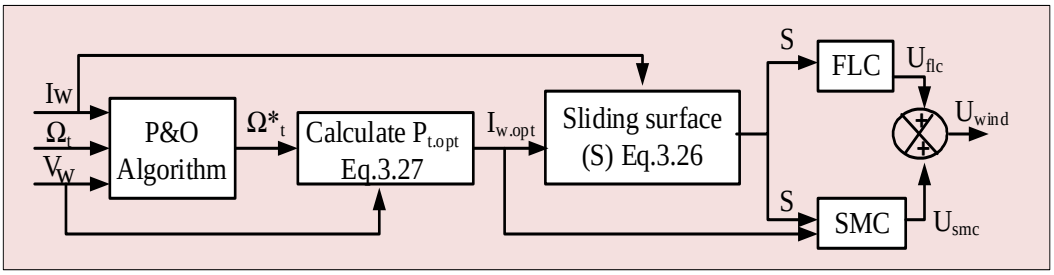

Figure 3.16. The schematic diagram of the new MPPT strategy for wind turbines.

To calculate the MPP for a (WT), we use the following equation:

$$U_{wind} = U_{flc} + U_{smc} \tag{3.30}$$

The wind control law is implemented in three steps: first, it requires understanding the characteristics of the wind turbine (WT). Second, SMC is employed to determine S, which is then used to estimate the equivalent commands U_{smc} and U_{flc}. The final step involves calculating the U_{wind} control using Equation (3.30).

a. Structure block of SMC for wind generator

First, we calculated the proposed S from [77] using SMC to determine the equivalent commands U_{smc} and U_{flc}. This calculation is based on the reference current ($I_{w\text{-}opt}$) (figure 3.17). The following equation expresses S:

$$S = I_{w\_opt} - I_w \tag{3.31}$$

Calculating the reference current necessitates knowing the optimal power value [77]:

$$I_{w\_opt} = \frac{P_{t-opt}}{V_w} \tag{3.32}$$

With: $$P_{t-opt} = \frac{1}{2}\rho\pi R^2 C_{p-opt} V^3 = K_{opt}\Omega_t^* \tag{3.33}$$

$$\lambda_{opt} = \frac{\Omega_t^* R}{V} \tag{3.34}$$

$$K_{opt} = \frac{1}{2}\frac{\rho\pi R^5 C_{p-opt}}{\lambda_{opt}^3} \tag{3.35}$$

The D of a (WT) can be represented by:

$$D_{k+1} = \begin{cases} D_k - \Delta D, if & S < 0 \\ D_k + \Delta D, if & S > 0 \end{cases} \tag{3.36}$$

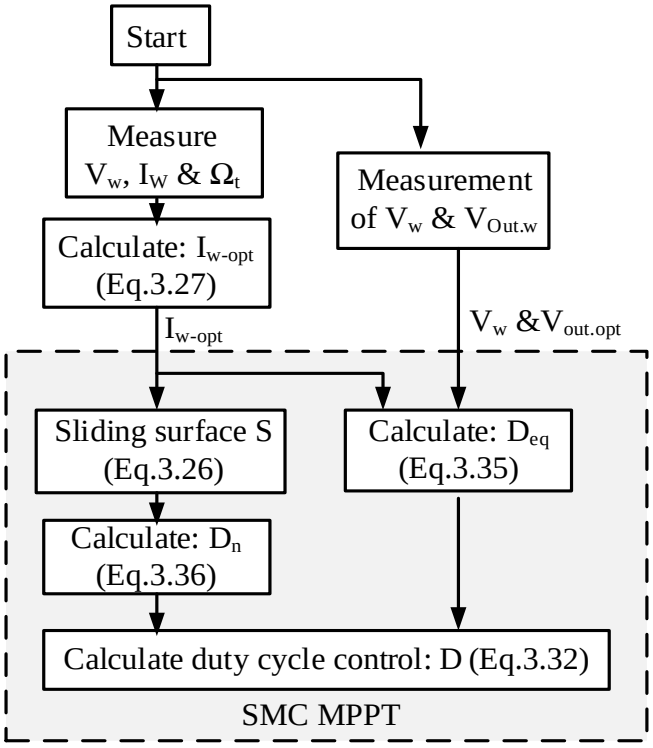

Figure 3.17. SMC MPPT approach for wind turbine generator.

The control signal is represented as:

$$D = \begin{cases} 0 & , for \quad D_{eq} + D_n \le 0 \\ D_{eq} + D_n & , for \quad 0 < D_{eq} + D_n < 1 \\ 1 & , for \quad D_{eq} + D_n \ge 0 \end{cases} \tag{3.37}$$

The equivalent control D_{eq} is defined by the following equation:

$$\dot{S} = \frac{dS}{dt} = \frac{dI_{w\_opt}}{dt} - \frac{dI_w}{dt} = 0 \tag{3.38}$$

From the boost converter equation [77], we derive the following expression:

$$\frac{dI_w}{dt} = \frac{di_L}{dt} = \frac{1}{L}\left[V_w - V_{out\_w}(1 - D_{eq})\right] \tag{3.39}$$

Thus, the equivalent control can be expressed as:

$$D_{eq} = \frac{1}{V_{out-w}}\left(\frac{dI_{w\_opt}}{dt}\right) + \left(1 - \frac{V_w}{V_{out\_w}}\right) \tag{3.40}$$

The discrete control is:

$$D_n = K.Sat(s) \tag{3.41}$$

$$\text{With: } Sat(s) = \begin{cases} \frac{S}{\varepsilon}, if & |S| < \varepsilon \\ Otherwise, sign(s) \end{cases} \tag{3.42}$$

b. Structure block of FLC for wind generator

The desired Fuzzy Logic Control (FLC) method plays a crucial role in optimizing Maximum Power Point Tracking (MPPT) by minimizing oscillations around the MPP, thus enhancing overall energy production. Figure 3.18 shows the three key steps of the FLC used to determine the equivalent command U_{flc}. In determining the equivalent control U_{flc}, we relied on the two proposed inputs: error (E) and its change (dE), which were calculated using equations (3.43) and (3.44):

$$E(k) = S(k) = I_{w\_opt} - I_w \tag{3.43}$$

$$dE(k) = E(k) - E(1-k) \tag{3.44}$$

Table.3.2. (b) Fuzzy rules.

		dE				
E	NB	ZE	ZE	PS	PB	PB
	NS	ZE	ZE	ZE	PS	PS
	ZE	PB	PS	ZE	ZE	NS
	PS	NS	NS	NB	ZE	ZE
	PB	NS	NB	NB	ZE	ZE

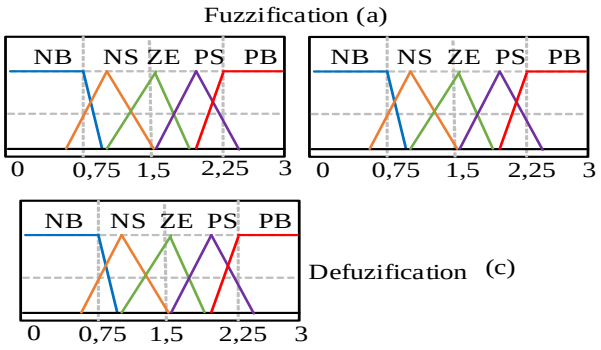

Figure 3.18. FLC's rules for WT

2.2.3. efficiency test of the MPPT algorithm

the power output from the wind generator illustrates in the figure 3.19, reaching a value of 6000 watts. We can see that the generated power follows the wind speed profile, which varies from 6 m/s to 12 m/s, then decreases to 9 m/s, in both control methods used (P&O algorithm, and Proposed Control).

However, the proposed method yielded more accurate results in tracking the MPP, confirming the effectiveness of the proposed approach.

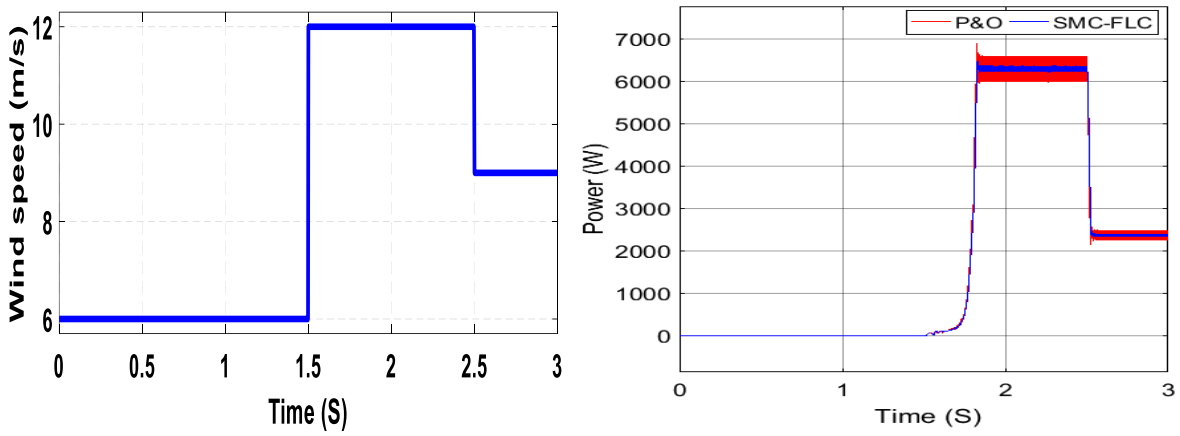

Figure 3.19. The wind speed, Output power of wind generator respectively

In figure 3.20 illustrates the output current of the rectifier (AC/DC) that used to connect the WT with DC bus, On the other hand, the figure illustrates the optimized output current ($I_{w\text{-}opt}$) of the wind generator using the proposed method compared to the output current (I_w) without optimization.

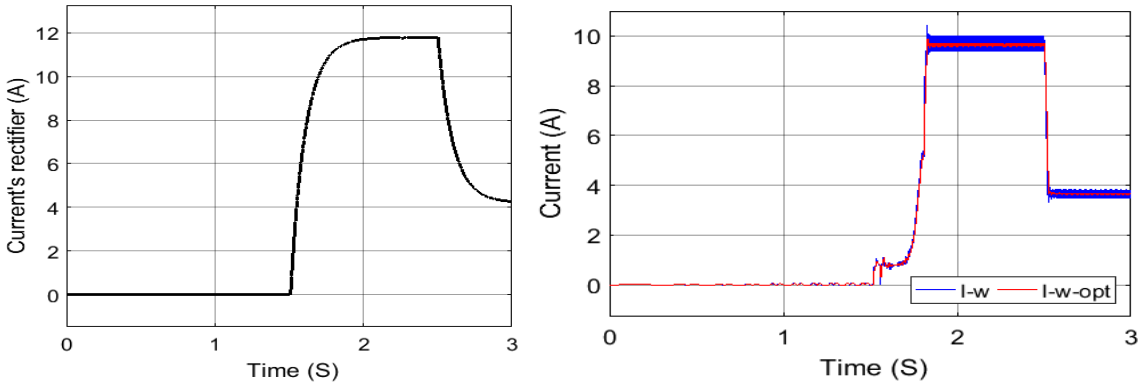

Figure 3.20. The current rectifier, Wind generator's current respectively

2.3. THD analysis for HRES

To assess the power quality obtained from the system using both conventional and proposed methods, which aim to enhance (MPPT), we studied the pulse values of the techniques in terms of Total Harmonic Distortion (THD). The results indicated that the proposed method improves power quality. The reduction ratio of THD values decreases when solar irradiation is at 1000 W/m², whereas the conventional method exhibits a

lower reduction ratio. In contrast, the proposed method achieves a higher reduction ratio, reaching 0.01% for solar generators and 0.98% for wind generators. As solar irradiation and wind speed increase, the reduction ratio in THD current values also rises. This suggests that the proposed method is more effective in reducing harmonic distortion and improving power quality. The notable decrease in THD values highlights the effectiveness of the proposed strategy in enhancing power quality in renewable energy systems.

Table 3.3. Total Harmonic Distortion for PV and WT

		THD (%)							
		P&O				***SMC-FLC***			
PV SYSTEM	***G (w/m²)***	0	200	600	1000	0	200	600	1000
	P_{pv}	2.22	1.19	1.49	3.15	2.19	0.26	0.42	0.01
	I_{pv}	1.11	0.01	0.01	0.02	1.10	0	0	0
	V_{pv}	1.11	1.19	1.49	3.15	1.10	0.14	0.55	0.01
WIND SYSTEM	***Wind speed (m/s)***	6		9	12	6		9	12
	P_w	4.93		2.4	1.02	2.02		1.07	0.98
	V_w	4.9		3.48	2.91	1.24		1.78	0.99
	I_w	3.53		1.07	1.08	1.07		0.7	0.62

3. Management using Fuzzy Logic controller

3.1. Control of the DC bus voltage (Vdc) by using the storage system

If the power available from RES is insufficient to meet the changing requirements, the DC bus voltage falls below the set reference value. The remaining power is then drawn from the battery, provided the battery's state of charge (SOC) is within the preset limits. Typically, the SOC of a Ni-MH battery ranges between 20% and 80%. In this study, during normal battery operation, the SOC at shore is considered within (SOC_min = 20%) < SOC < (SOC_max = 80%). On the other hand, when there is excess power, the DC bus voltage reaches the reference value without charging the battery from multiple sources [59]. In our particular case, we suggest using a fuzzy logic controller (FLC) to manage the DC bus voltage, taking into account the state of charge as illustrates in figure 3.21. Maintaining constant bus voltage regulation optimizes the battery, which serves as the storage element.

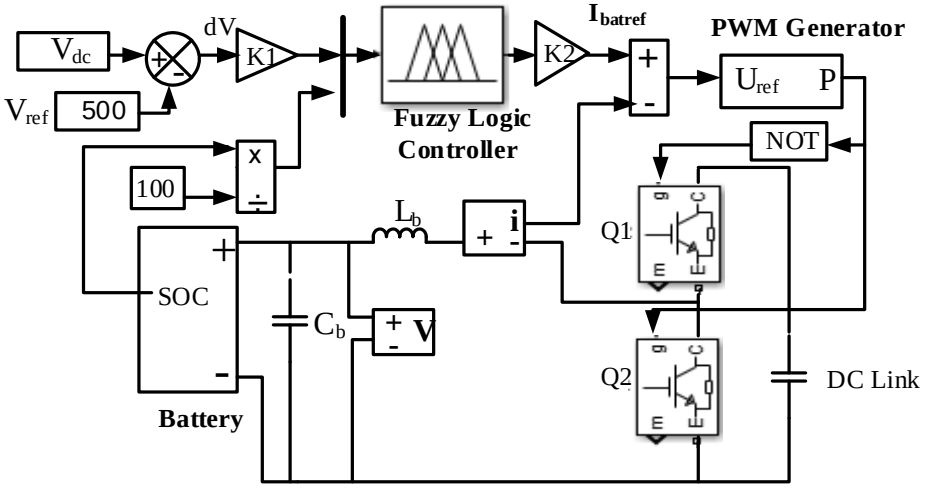

Figure 3.21. Bidirectional chopper control structure

The range of values for the first input variables (dV_{dc}) and (SOC) is defined using seven fuzzy subsets for their linguistic variables. The membership functions for these variables are illustrated in figure 3.22, which shows the range of values for the output variable ($I_{bat\text{-}ref}$) [86].

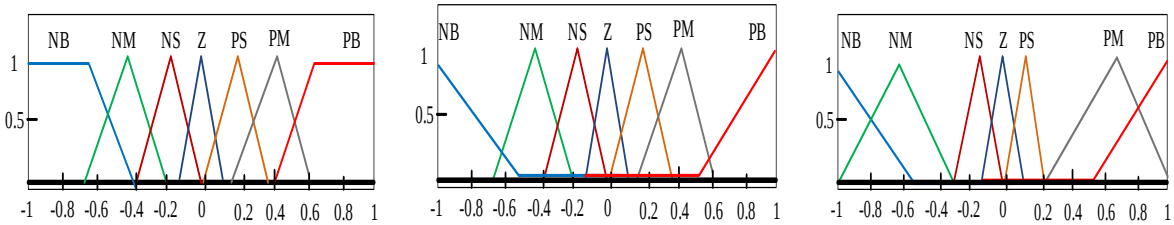

(a) (b) (c)

Figure 3.22. (a): Input dV_{dc}; (b): Input SOC; (c): Output $I_{bat\text{-}ref}$

The fuzzy system rule base is constructed according to Table 3.4, using (ΔV_{dc}) and (SOC) as inputs, and $I_{bat\text{-}ref}$ as the output. The fuzzy inference of the FLC employs Mamdani's method, utilizing max-min composition.

Table.3.4. Fuzzy Rules

SOC \ dV_{dc}	NB	NM	NS	Z	PS	PM	PB
NB	NB	NB	NB	NB	NM	NS	Z
NM	NB	NB	NB	NM	NS	Z	PS
NS	NB	NB	NM	NS	Z	PS	PM
Z	NB	NM	PS	Z	PM	PS	PB
PS	NM	NS	Z	PM	PS	PB	PB
PM	NS	Z	PS	PM	PB	PB	PB
PB	Z	PS	PM	PB	PB	PB	PB

3.2. Results analysis

The different parts of the HRES with the proposed controller were simulated in MATLAB/Simulink. we test the effectiveness of the proposed strategy in managing the power generated from various sources by adjusting the DC voltage to the reference value of 500 volts using a FLC, as illustrated in the figure 3.23 Meanwhile, the figure 3.24 illustrates the key characteristics of the battery throughout the simulation duration.

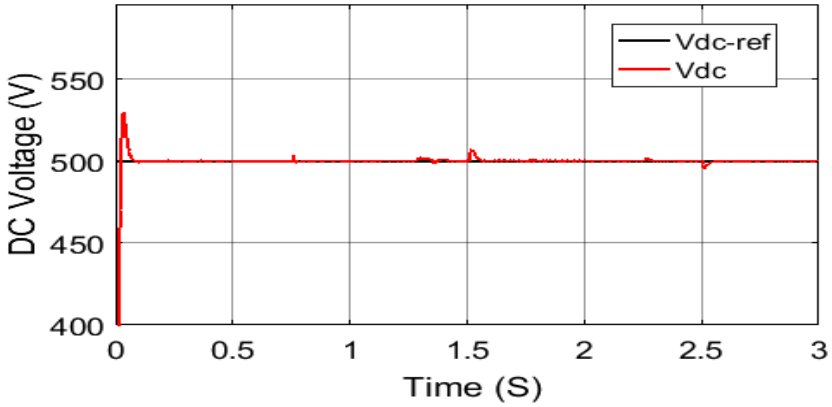

Figure 3.23. DC bus voltage

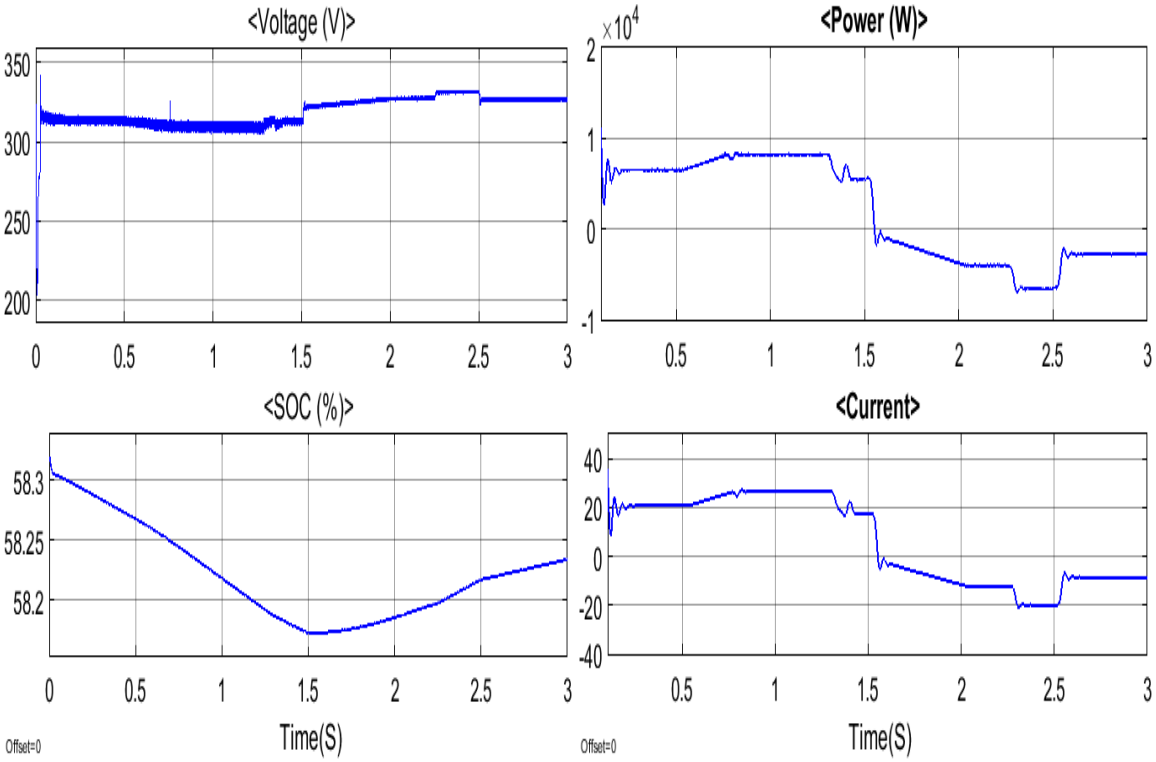

Figure 3.24. Battery's characteristics

The system has been tested on a load of up to 10 kilowatts, which led us to derive several scenarios for managing the generated power based on changing weather conditions (solar irradiation and wind speed).

- **Scenario 1**: Complete absence of wind power and low solar power production, requiring the storage system to compensate for the deficit, as the load demanded approximately 9 kilowatts of power.
- **Scenario 2:** Complete absence of RES (due to total lack of solar irradiation and wind speed) resulted in the full intervention of the storage system. This scenario highlights the critical importance of the storage system in ensuring the system's effectiveness and its ability to meet consumer demands without interruption.
- **Scenario 3:** Production of approximately 15 kilowatts of renewable energy, resulting in an excess over the consumption value of about 5 kilowatts. This surplus led to the storage system being charged with the excess energy to prevent it from being wasted.

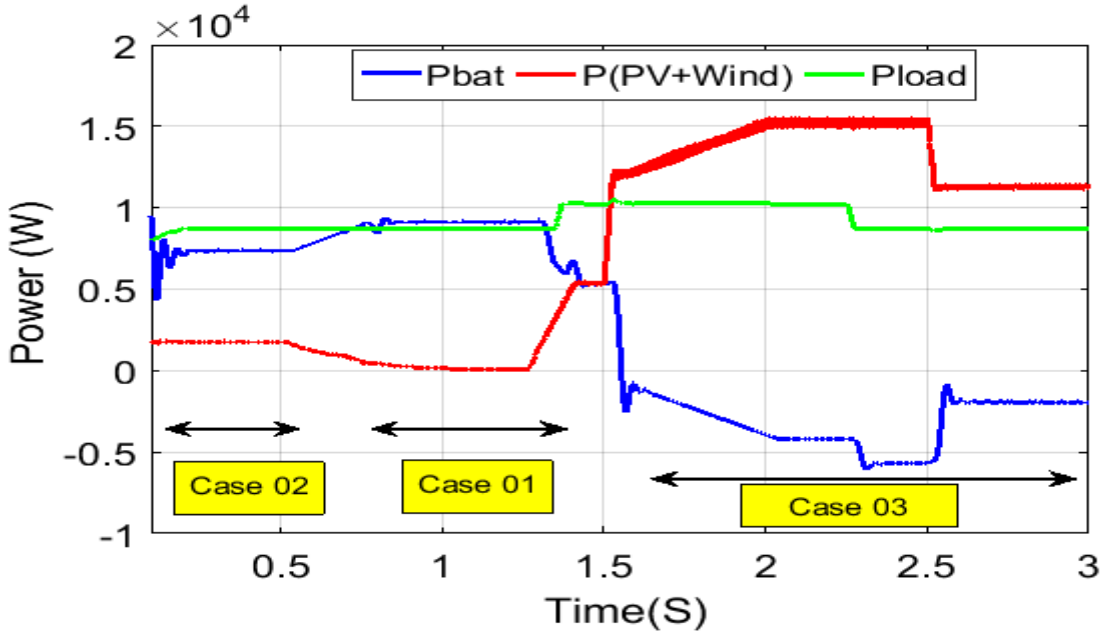

Figure 3.25. The System power management

The figure 3.26 illustrates the current and voltage of the load, both of which optimally take on a sinusoidal form.

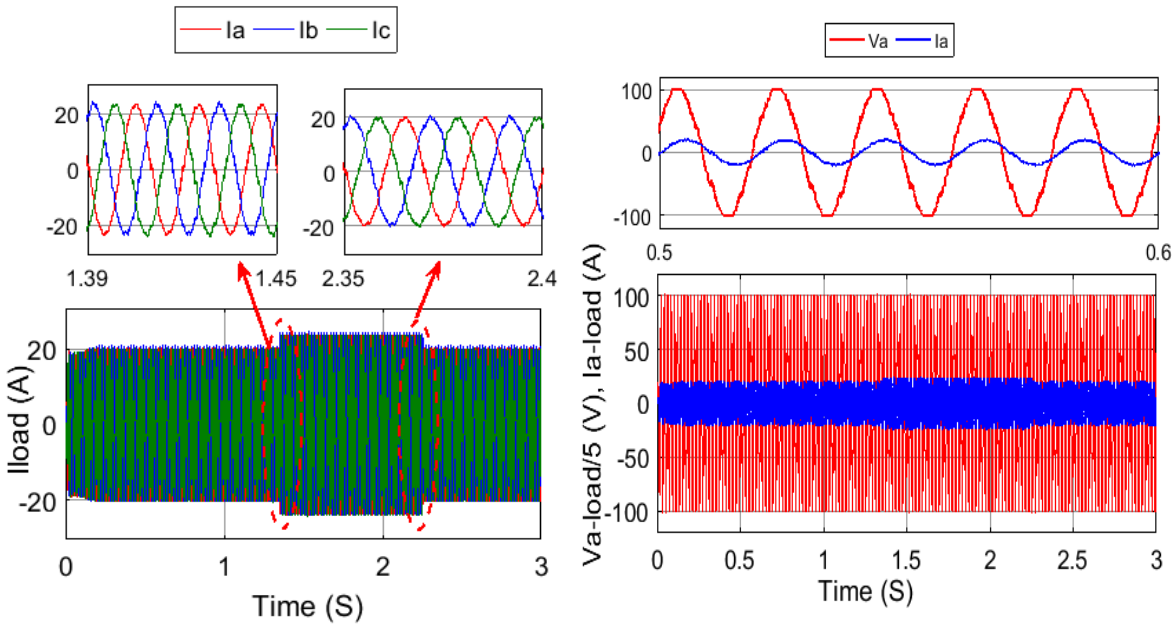

Figure 3.26. The current and voltage load respectively

In the figure 3.27 shows the output voltage of the inverter and the electrical impulse :

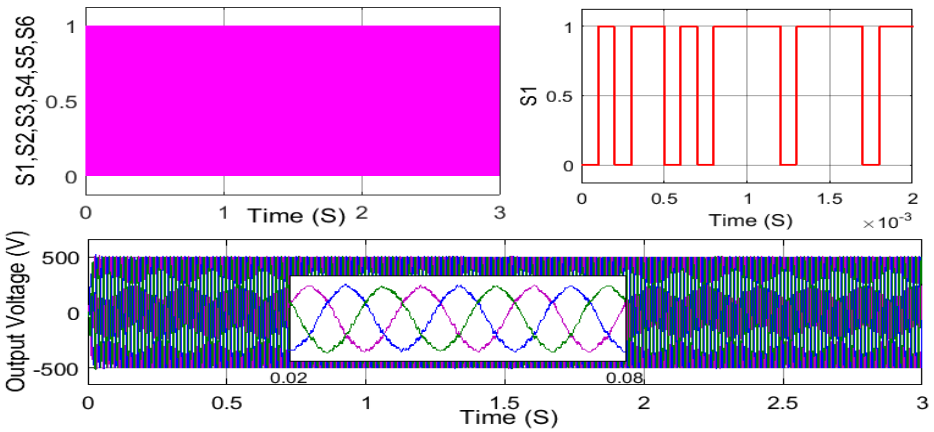

Figure 3.27. Inverter output voltage

4. Conclusion

In this chapter, we addressed a method to improve the MPPT strategy for RES able energy sources by combining two intelligent controls: SMC and FLC. The results obtained were good compared to the classical method of Perturb and Observe. We also examined the Total Harmonic Distortion (THD) for both strategies. Additionally, we proposed a method to manage the power generated from renewable sources to meet load requirements by adjusting

the reference DC voltage using a storage system, while considering the battery state at specific values (20% <SOC< 80%). This was achieved by applying Fuzzy Logic. The chapter concludes with an analytical study of the results obtained using MATLAB.

Chapter 4: Proposed Grid-connected hybrid renewable energy management strategy (HREMS)

1. Introduction

In this chapter, we conducted a comprehensive study on the management of renewable energies for a grid-connected hybrid system, which consists of a solar energy system, a wind generator, and a nickel-metal hydride battery. To achieve optimal energy management, we examined and improved several aspects of the proposed system:

- Enhancing the energy output of the hybrid system using the PD (1+PI) controller.
- Proposing a strategy to improve the energy output of the electrical grid.
- Developing a strategy to manage all the system's energies using the storage system, where priority is given to the renewable energy system to supply the load demand. If the renewable energy system fails, the electrical grid intervenes, provided the storage system cannot cover the shortfall of the renewable energy system, ensuring the battery operates under specific regulatory conditions.

2. Proposed strategy for grid-connected hybrid renewable energy system (HRES)

A hybrid system connected to a grid illustrates in figure 4.1. This system primarily relies on solar and wind power, with an energy storage system serving as a backup. The energy storage system enhances the primary system by managing the processes of battery charging and discharging. The main goal of this work is to propose a control method aimed at improving the quality of energy produced from the various sources within the system.

The proposed method aims to enhance energy quality and optimize energy management in HRES linked to the electrical grid by leveraging insights from recent advances in control theory and renewable energy system modeling. This study introduces a comprehensive control strategy centered on integrating a PD (1+PI) controller to address voltage and current errors in PV and wind systems, thereby improving the efficiency of MPPT technology. Additionally, the control strategy includes managing battery charging and discharging using a PD (1+PI) control unit and optimizing grid performance through a P-

DPC-PD (1+PI) approach. By incorporating advanced control algorithms and employing energy storage systems, this approach has the potential to enhance the effectiveness, reliability, and longevity of renewable energy systems.

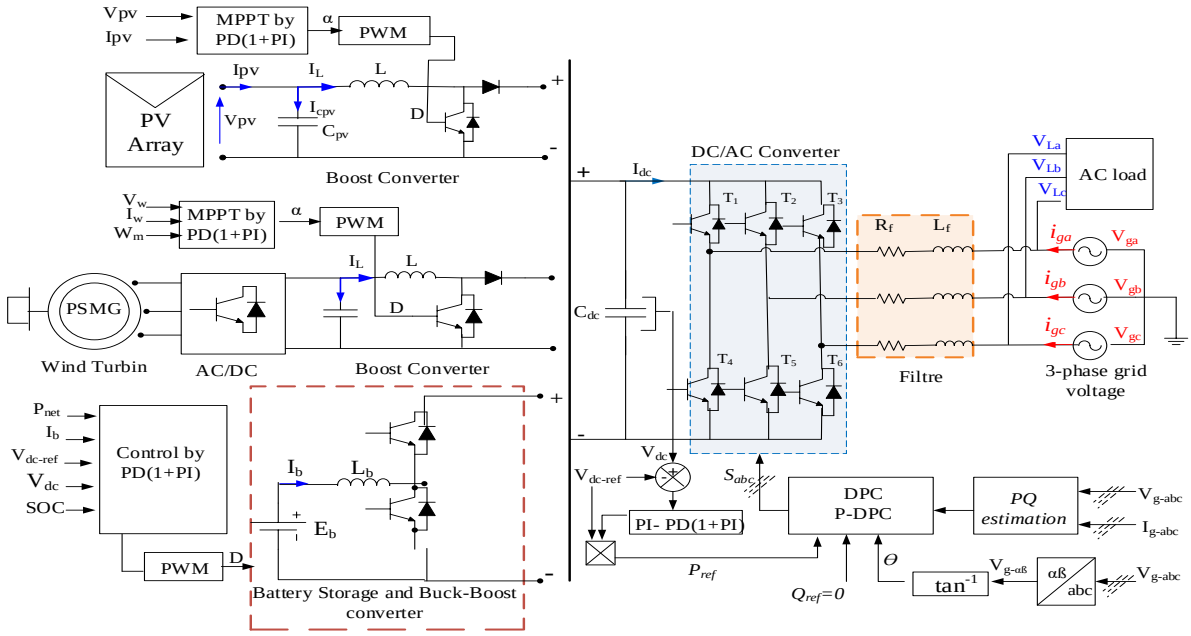

Figure 4.1. The proposed system designs

2.1. Hybrid renewable energy system control

2.1.1.PD(1+PI) controller

The Proportional (P), proportional-integral-derivative (PID), and proportional-derivative (PD) controllers are widely recognized and used in industrial applications due to their affordability, simplicity, and ease of use compared to other types. These controllers are employed in various techniques, such as vector control, field-oriented control (FOC) [87], direct torque control (DTC) [88], and direct power control (DPC)[89]. These types of controllers can be represented by Equation (4.1).

$$\begin{cases} u_1(t) = K_i \int_0^t S.dt + K_p.S \\ U_2(t) = K_d \dfrac{dS(t)}{dt} + K_p.S \\ u_3(t) = K_i \int_0^t S.dt + K_p.S + K_d \dfrac{dS(t)}{dt} \end{cases} \quad (4.1)$$

Equation (4.2) depicts the controller introduced in this section of the paper [87]:

$$w(t) = \left(K_1.S + K_2 \frac{dS(t)}{dt} \right) \left(1 + K_3.S + K_4 \int_0^t S.dt \right) \quad (4.2)$$

where, K1, K2, K3 and K4 are the constants gains, S is the surface or error $(S = X^* - X)$

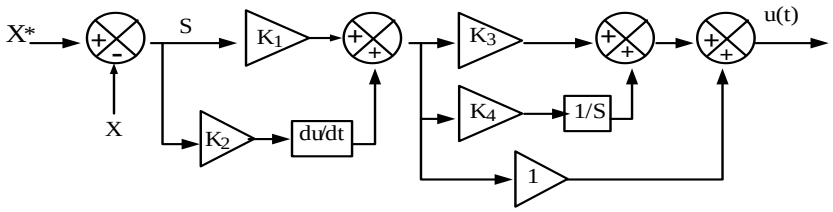

Figure 4.2. Structure of PD (1+PI) Controller

In the proposed P-DPC scheme figure 4.2, the magnitude of the fundamental input currents is delivered from the outer PD(1+PI) dc-bus voltage controller and will be multiplied by the dc voltage to obtain the reference of the instantaneous active power. To maintain unity power factor, the reference reactive power is set to zero.

The regulation function is now ensured by the PD(1+PI) controller as shown in the figure below. The PD(1+PI) controller is a combination of a Proportional-Derivative (PD) component with an embedded Proportional-Integral (PI) structure for improved transient response and steady-state error correction. The transfer function of the PD(1+PI) controller can be expressed as:

$$G_{PD(1+PI)}(s) = K_p(1 + T_d s) + \frac{K_i}{s} + \frac{K_d s}{1 + T_f s} \quad (4.3)$$

Where:

K_p is the proportional gain,

T_d is the derivative time constant,

K_i is the integral gain,

K_d is the derivative gain,

T_f is the filter time constant (used to reduce noise amplification from the derivative action).

-The **PD** component $K_P(1 + T_d s)$ handles fast transient responses and reduces overshoot.

-The **PI** component $K_P + \frac{K_i}{s}$ eliminates steady-state error.

-The derivative part with a filter $\frac{K_d S}{1+T_f s}$ ensures that high-frequency noise is filtered out, improving stability.

To determine the parameters of the PD(1+PI) controller, we perform the following mathematical analysis:

The power absorbed by the DC-bus capacitor is given by:

$$P_{ref}(t) = C.U_{dc}(t).\frac{dU_{dc}(t)}{dt} \tag{4.4}$$

In the Laplace (frequency) domain, this becomes:

$$P_{ref}(s) = C.U_{dc}(s).s.U_{dc}(s) \tag{4.5}$$

Simplifying for $U_{dc}(s)$, we have:

$$U_{dc}^2(s) = \frac{P_{ref}(s)}{C.s} \tag{4.6}$$

We find:

$$U_{dc}(s) = \sqrt{\frac{P_{ref}(s)}{C.s}} \tag{4.7}$$

(where, C: represents the capacitance of the capacitor for DC bus)

The transfer function of the closed-loop system with the PD(1+PI) controller is now:

$$F(s) = \frac{{\omega_0}^2}{s^2+2\xi\omega_0 s+{\omega_0}^2} \tag{4.8}$$

Where:

-ω_0 is the natural frequency,

-ξ is the damping ratio.

The controller parameters are tuned as follows:

$$K_p = \frac{2\xi}{\omega_0.C}\ ,\ K_i = \frac{1}{{\omega_0}^2.C}\ ,\ K_d = \frac{T_d.K_p}{1+T_f.s}\ , \tag{4.9}$$

- **The proposed PD(1+PI) controller**

The proportional, integral, and derivative actions in a closed-loop system serve to reduce overall error, eliminate steady-state error, and minimize overshoot and ringing, respectively [88]. The PD(1+PI) controller employs a two-stage structure: a PD controller in the first stage and a PI controller in the second stage, which governs the converter's duty cycle. The input-to-output transfer function of this cascade controller is defined as [89]:

$$U(s)=\left(K_p+K_d s\right)\left(1+K_{pp}\frac{K_i}{s}\right)E(s) \tag{4.10}$$

Figure 4.3 shows the controller design adopted in our study using mayfly optimization algorithm (MOA), the proposed controller is applied on three distinct systems: a solar system, a wind system, and a battery storage system. The controller is designed to eliminate the steady-state error and enhance the system's dynamic performance. To achieve this, it is essential to minimize the integral of the deviation e(t) of the system response from the desired value by defining the objective function as follows:

$$OF=\int_0^{T_{sim}} t\left|X^*(t)-X(t)\right|dt \tag{4.11}$$

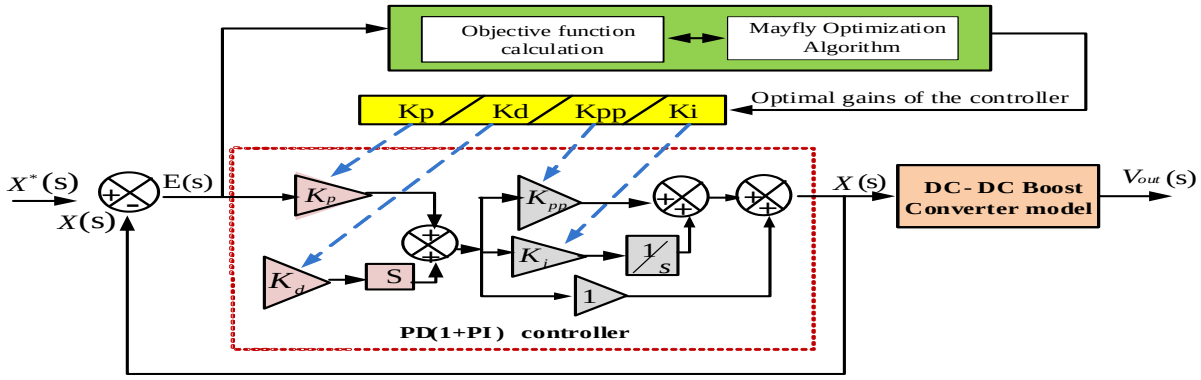

Figure 4.3. The controller design of PD(1+PI)

Different closed-loop system

The closed-loop system studied consists of the signal boost converter transfer function, the introduced PD(1+PI) controller, and negative feedback, as shown in figure 4.3. In this configuration, $X^*(s)$ represents the desired output magnitude, and $X(s)$ denotes the controlled output. The difference between them forms the input signal to the controller, $E(s)$.

✓ PV system

To define the transfer function of the solar power system, the input of the closed-loop system is considered to be the reference voltage V_{ref}, which is estimated using the Perturb and Observe algorithm, and V_{pv} denotes the controlled output.

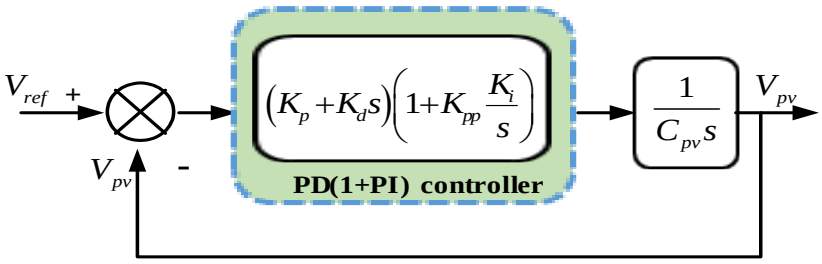

Figure 4.4. The PD(1+PI) controller for PV system

The closed-loop system transfer function, relating V_{ref} (s) to V_{pv} (s), can be expressed in a compact form as:

$$\frac{V_{pv}(s)}{V_{ref}(s)} = \frac{K_d s^2 + (K_p + K_d K_{pp} K_i)s + K_p K_{pp} K_i}{(K_d + C_{pv})s^2 + (K_p + K_d K_{pp} K_i)s + K_p K_{pp} K_i} \tag{4.12}$$

$$\begin{cases} where & K_d K_{pp} K_i = K_1 \\ & K_p K_{pp} K_i = K_2 \end{cases} \tag{4.13}$$

When we replaced equation (4.12) into equation (4.13), we find:

$$\frac{V_{pv}(s)}{V_{ref}(s)} = \frac{K_d s^2 + (K_p + K_1)s + K_2}{(K_d + C_{pv})s^2 + (K_p + K_1)s + K_2} \tag{4.14}$$

- ✓ **Wind system**

To define the transfer function of the wind system, the input of the closed-loop system is considered to be the optimal current $I_{w\text{-}opt}$, which is estimated using the Perturb and Observe (P&O) algorithm, and I_{pv} denotes the controlled output as shown in figure 4.5:

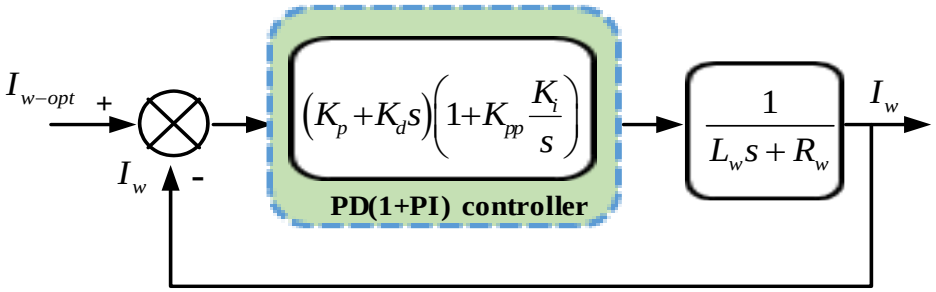

Figure 4.5. The PD(1+PI) controller for wind system

The closed-loop system transfer function, relating $I_{w\text{-}opt}$ (s) to I_w (s), can be expressed in a compact form as:

$$\frac{I_W(s)}{I_{W-opt}(s)} = \frac{K_d s^2 + (K_p + K_1)s + K_2}{(K_d + L_w R_w)s^2 + (K_p + K_1)s + K_2} \quad (4.15)$$

✓ **DC link**

To determine the transfer function of the solar power system, the input of the closed-loop syetm is taken as the reference voltage $V_{dc\text{-}ref}$, estimated using the Perturb and Observe algorithm, while V_{dc} represents the controlled output.

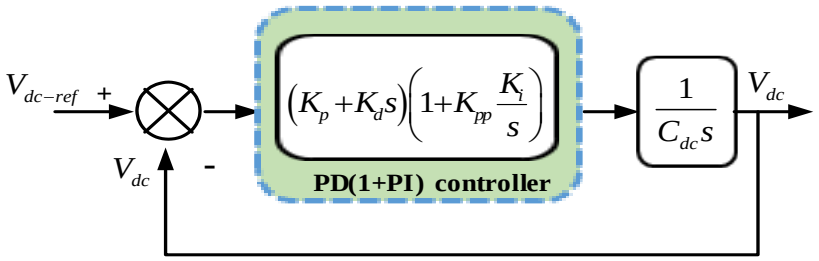

Figure 4.6. The PD(1+PI) controller for DC link

The closed-loop system transfer function, relating $V_{dc\text{-}ref}(s)$ to $V_{dc}(s)$, can be expressed in a compact form as:

$$\frac{V_{dc}(s)}{V_{dc-ref}(s)} = \frac{K_d s^2 + (K_p + K_1)s + K_2}{(K_d + C_{dc})s^2 + (K_p + K_1)s + K_2} \quad (4.16)$$

Mayfly optimization algorithm (MOA)

The MOA is employed to design the optimal controller. This nature-inspired algorithm incorporates concepts from the Genetic Algorithm (GA) and Particle Swarm Optimization (PSO) to enhance performance, effectively balancing exploration and exploitation [90]. Its efficiency in solving complex technical and engineering challenges has been validated, with its operational process depicted in the flowchart shown in Figure. 4.7 [91]. When utilizing this algorithm, the upper and lower bounds for the controller design decision must be defined.

The parameters are considered as follows:

$0 \le K_p \le 150$; $0 \le K_d \le 10$

$0 \le K_i \le 20$; $0 \le K_{pp} \le 10$

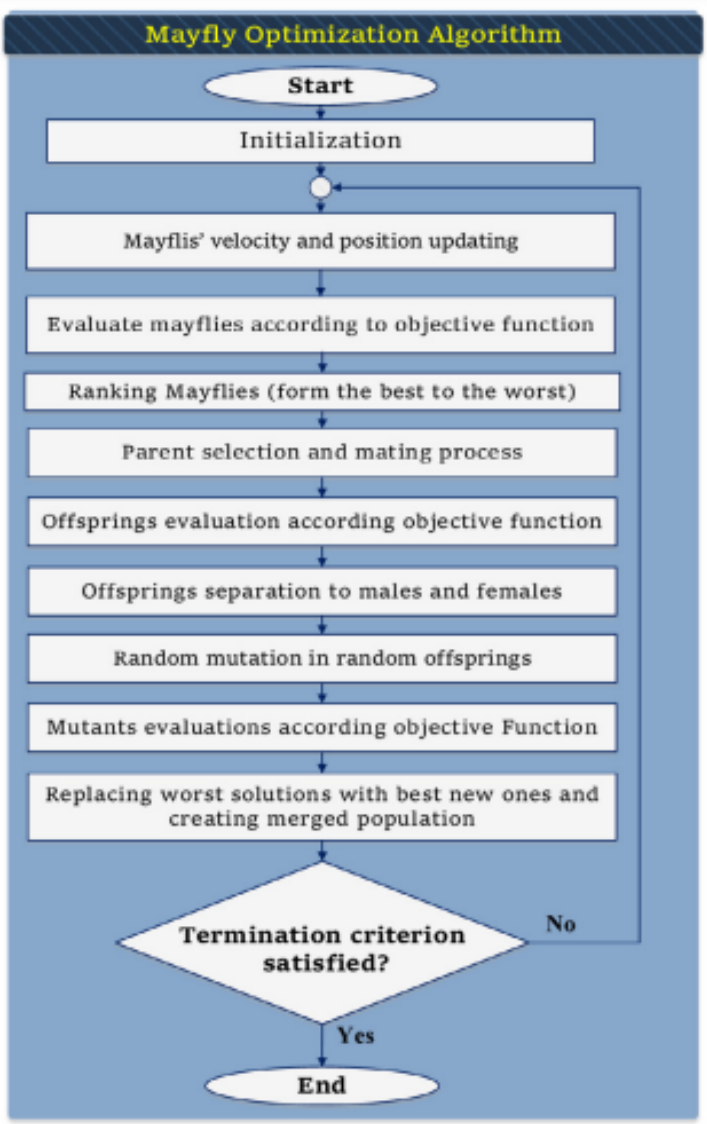

Figure 4.7. The flowchart for MOA algorithm [91]

2.1.2.MPPT based on PD (1+PI) controller for PV solar

To optimize power extraction, the DC-DC boost converter is commonly employed in solar PV systems to elevate and regulate the PV panel's voltage to a specified level. Figure 4.8. illustrates the configuration that integrates the MPPT approach with PD(1+PI) control.

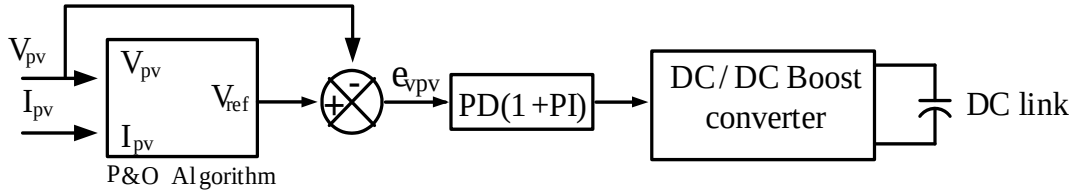

Figure.4.8. Structure diagram of MPPT-PD(1+PI) for PV generator

The reference voltage value was obtained using the (P&O) technique, which is discussed in [92]. The equation 4.17 was then used to compare the result with the PV generator's predicted voltage.

$$e_{V_{pv}} = V_{ref} - V_{pv} \tag{4.17}$$

The PD(1+PI) controller is in charge of producing the inductance reference current and controlling the PV voltage (V_{pv}). Equation 4.18 illustrates how this method generates the duty cycle for the DC/DC boost converter and guarantees the lowest possible level of steady-state error in the inductance current regulation:

$$u(t) = \left(K_1 . e_{v_{pv}} + K_2 \frac{de_{v_{pv}}(t)}{dt} \right) + \left(1 + K_3 . e_{v_{pv}} + K_4 \int_0^t e_{v_{pv}} dt \right) \tag{4.18}$$

2.1.3.MPPT based on PD (1+PI) controller for Wind turbine

The wind generator has been incorporated into the smart grid as an additional energy source. Given the system's variability, a control unit has been proposed to track the MPP and improve the quality of the generated energy. This is accomplished by integrating the control unit to adjust the current error value for the wind generator, which is then modified based on the reference current value derived from the reference torque value, as depicted in the figure 4.9.

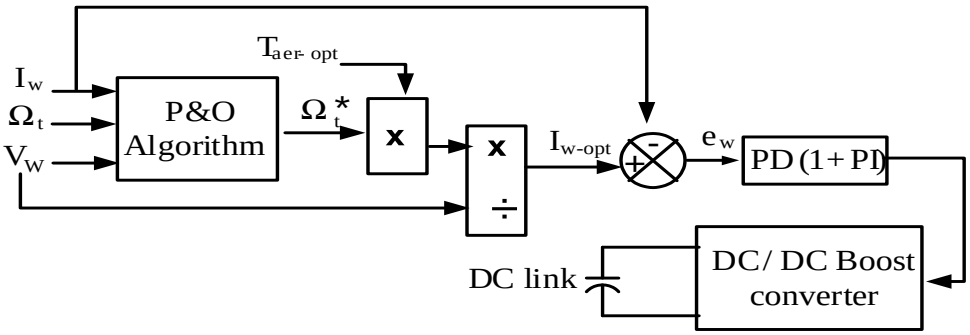

Figure.4.9. Structure diagram of MPPT-PD(1+PI) for WT generator

The reference value of the rotor speed (Ω_t^*) is extracted using the algorithm mentioned in the reference [93], followed by the calculation of the reference aerodynamic torque (T_{aer_opt}) for the wind generator using Equation 4.19 [94].

$$T_{aer\_opt} = \frac{p_{aer}}{\Omega_t^*} \tag{4.19}$$

The reference current of the wind ($I_{w\text{-}opt}$) is calculated by dividing the reference value of aerodynamic torque ($T_{aer\text{-}opt}$) that in Equation (4.20) by V_w as follows:

$$I_{w-opt} = \frac{P_{aer}}{V_w} = \frac{T_{aer-opt}.\Omega_t^*}{V_w} \tag{4.20}$$

The error in tracking the current of the wind generator is defined as:

$$e_w = I_{w-opt} - I_{out} \tag{4.21}$$

Where the duty cycle of DC-DC boost converter as presents in equation (4.22):

$$u(t) = \left(K_1.e_w + K_2 \frac{de_w(t)}{dt} \right) + \left(1 + K_3.e_w + K_4 \int_0^t e_w dt \right) \tag{4.22}$$

2.1.4.Bidirectional converter control

The local control unit for storage adjusts the battery current to manage the charging and discharging of the battery by supplying a duty cycle to the converter, as illustrated in Figure 4.10. Thus, ensuring the power balance of the hybrid system and maintaining a stable DC bus voltage.

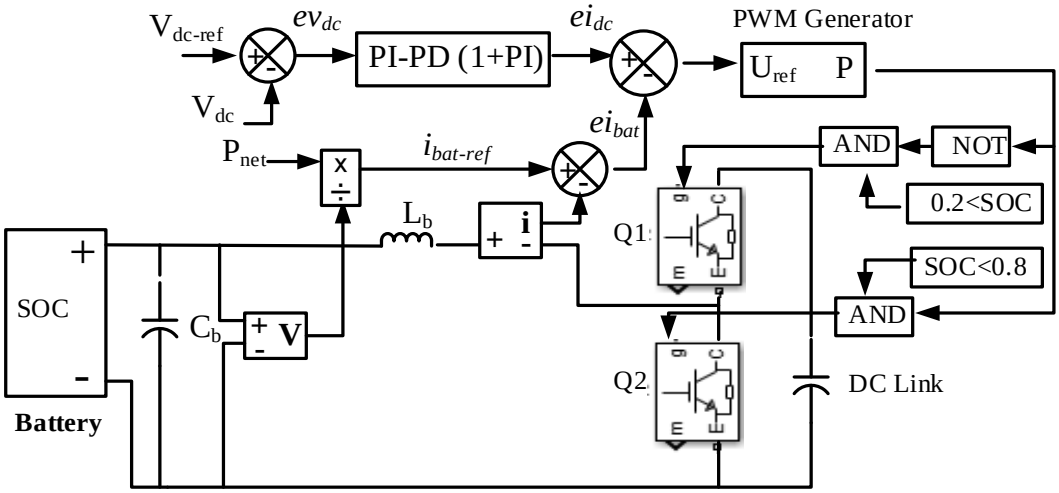

Figure.4.10. The proposed control for battery storage system (BSS)

The net power in the system (Pnet) can be calculated as (4.23):

$$P_{net} = P_l - (P_g + P_{pv} + P_w) \tag{4.23}$$

Where: Pnet: Battery power, P_l: load power, P_g: a grid power, P_{pv}: Solar power, P_w: wind power.

The reference battery current ($i_{bat\text{-}ref}$) is calculated by dividing Pnet in Equation (4.24) by V_{bat} as follows:

$$i_{bat-ref} = \frac{P_{net}}{v_{bat}} \tag{4.24}$$

The error in tracking the current of the battery is defined as:

$$e_{i_{bat}} = i_{bat-ref} - i_{bat} \tag{4.25}$$

Where the error in tracking the DC-link voltage is defined as (4.26):

$$e_{v_{dc}} = v_{dc\_ref} - v_{dc}$$

(4.26)

The inductor current is regulated with minimum steady-state error and determines the duty cycle of the buck-boost converter as shown in Equation 4.27:

$$D = e_{i_{dc}} - e_{i_{bat}} \tag{4.27}$$

While maintaining the state of the charge (SOC) as illustrated in the figure.4.5 (20%<SOC<80%).

2.1.5. Hybrid Renewable energy system analysis

A PD (1+PI) controller is combined with MPPT technology in order to reinforce the MPPT of the solar and wind power systems and to improve the power quality factor. Figures 4.11. and 4.12. illustrate the results obtained, which validate the efficiency of the suggested method. These outcomes support the research paper's proposed technology's effectiveness.

Solar irradiation, PV current output, voltage, and power response are presented in Figure 4.12. Variations in the weather (solar irradiation) affect the dynamic characteristics of the solar power generator. Furthermore, the PV output voltage use the P&O technique to get the reference value (V_{ref}). Particularly, at 1000 W/m^2, solar irradiation is when the generated energy reaches its maximum production level. This demonstrates how effectively the suggested approach tracks the MPP.

The wind power output and wind speed are shown in Figure 4.12. With wind speeds varying from 12 m/s to 6 kW, it is obvious that the power generated

varies with wind speed. It is also noticeable that the resultant energy is distortion-free and of excellent quality.

The results illustrate the effectiveness of the PD (1+PI) controller could be combined with MPPT methods for renewable energy generation systems that depend on solar and wind power.

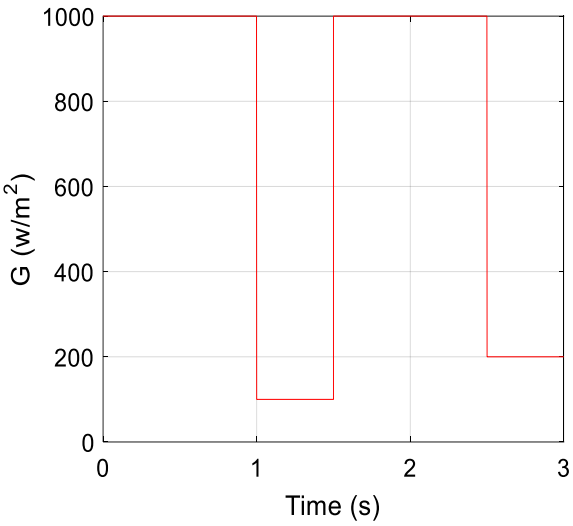

(a)

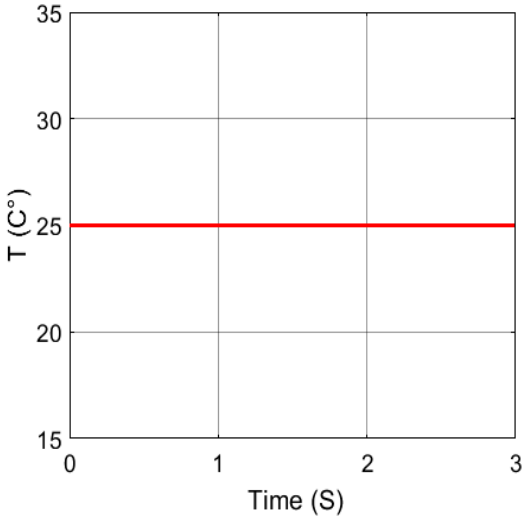

(b)

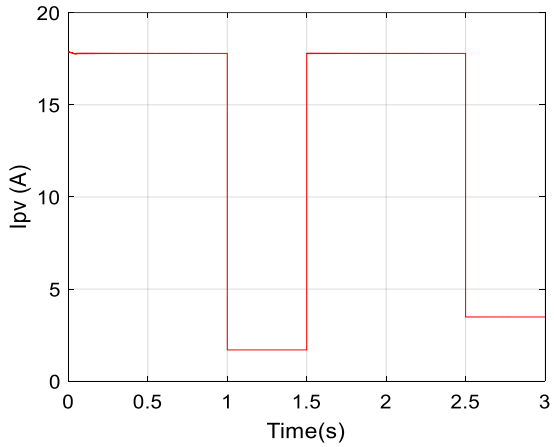

(c)

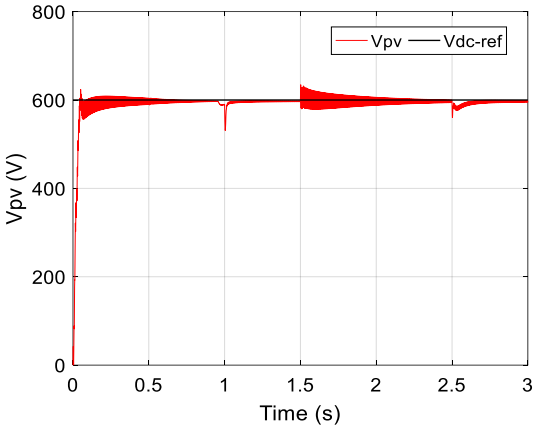

(d)

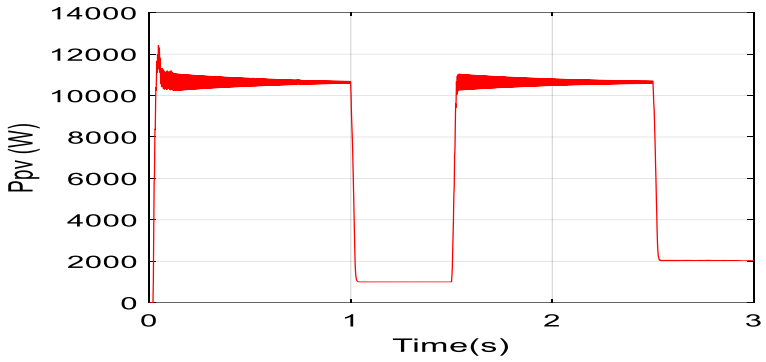

(e)

Figure.4.11. (a) :Solar irradiation profile, **(b)** :Temperature profile, **(c)** :PV voltage output,**(d)** : PV current output, **(e)** :Solar power

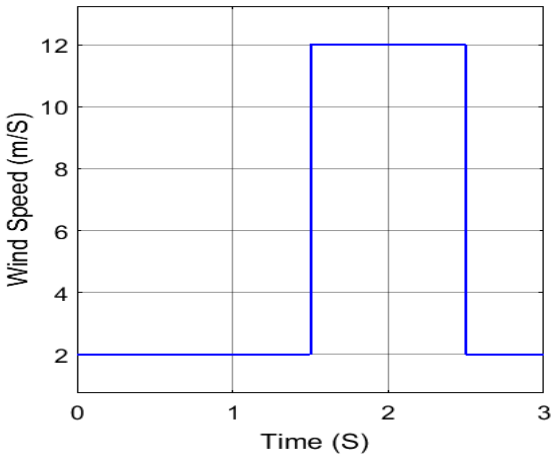

(a)

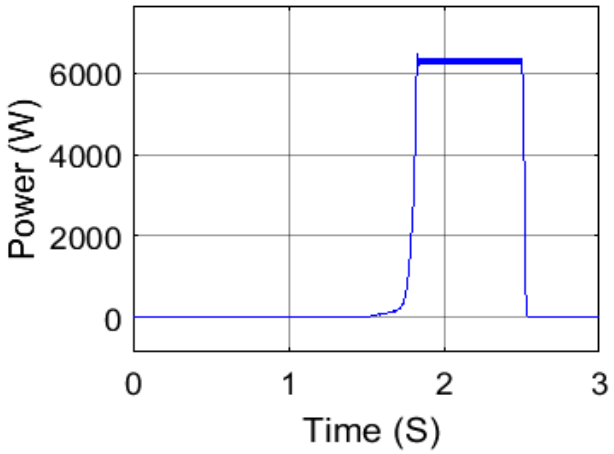

(b)

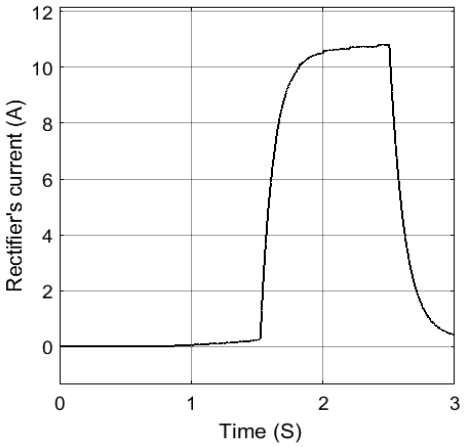

(c)

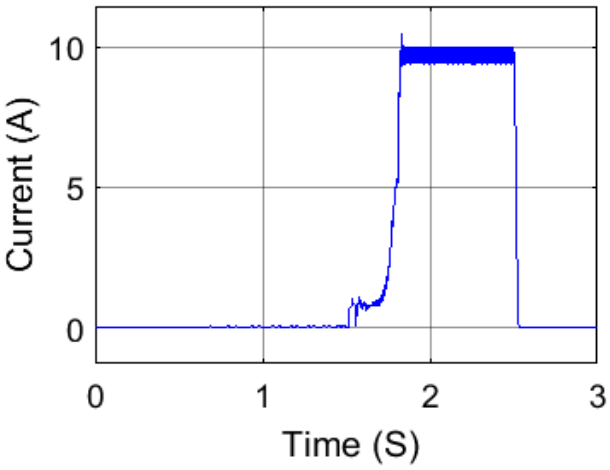

(d)

Figure.4.12. (a): Wind speed, (b): Wind power responses, (c): Current rectifier, (d): Output current

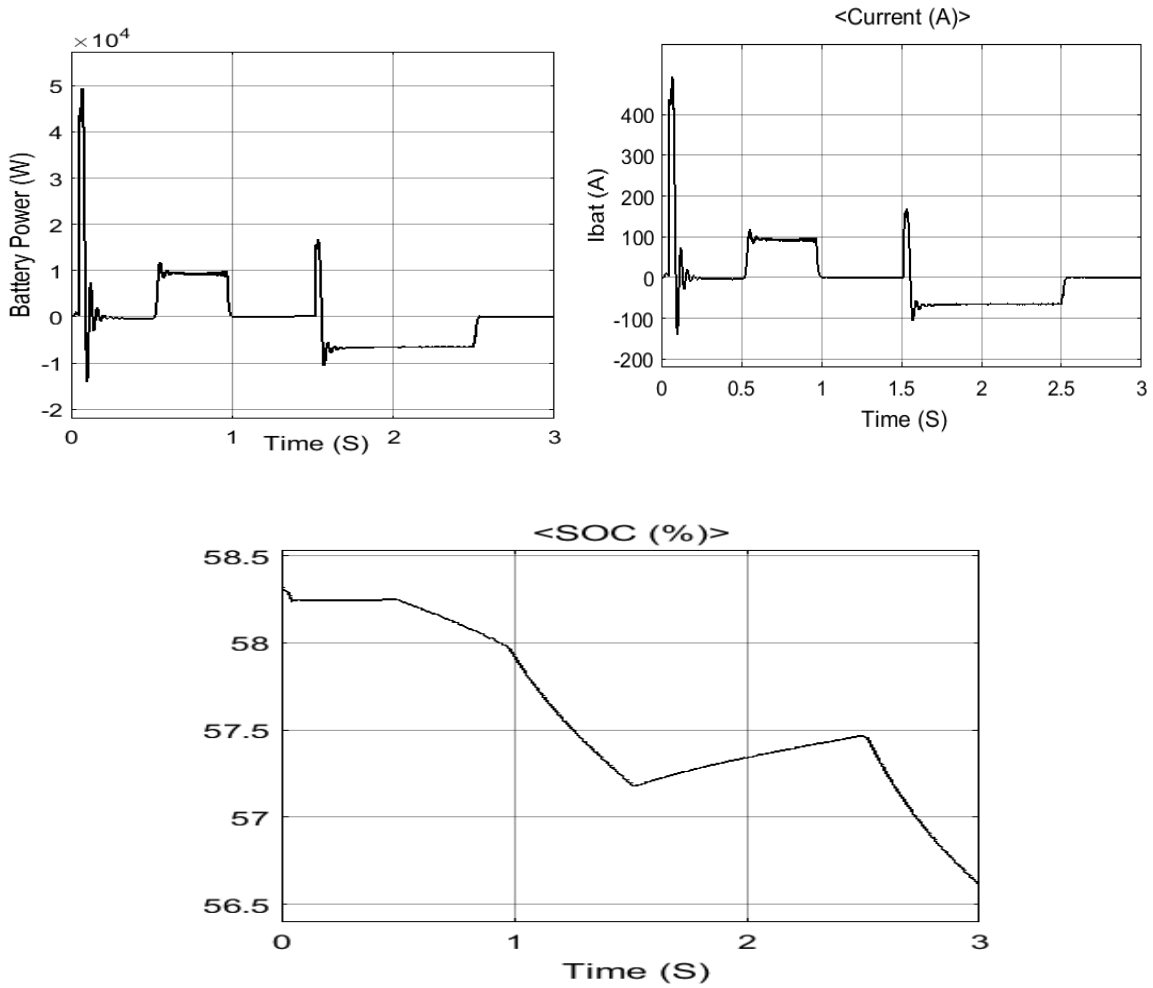

Figure.4.13. Battery characteristics

2.2. Electrical grid control

2.2.1.Direct power control strategy (PI-DPC)

The DPC concept is based on the use of predefined "voltage vectors," which are specified in a "switching table" and applied to the 3-phase PWM converter [68]. These voltage vectors correspond to sequences of switching states for the converter switches, namely "Sa, Sb, Sc" as presented in Figure 4.14. The selection of these vectors is determined by evaluating the discrepancies (Sp, Sq) between the desired references (P*, q*) and the actual measured values (P, q) of both "active power" and "reactive power." Additionally, the selection process considers the angular position θ of the flux vector for the Rotor Side Converter (RSC) and the grid voltage vector for the Grid Side Converter (GSC) [95].

The concept of DPC is visually presented in Figure 4.14. It relies on the comparison between the instantaneous reference values of active and reactive powers and their corresponding measurements. These comparisons are used as inputs for two hysteresis comparators. They are, in conjunction with the switching table and the grid voltage magnitude, determine the switching states of the switches. Furthermore, a PI controller is employed to regulate the voltage of the DC bus [35].

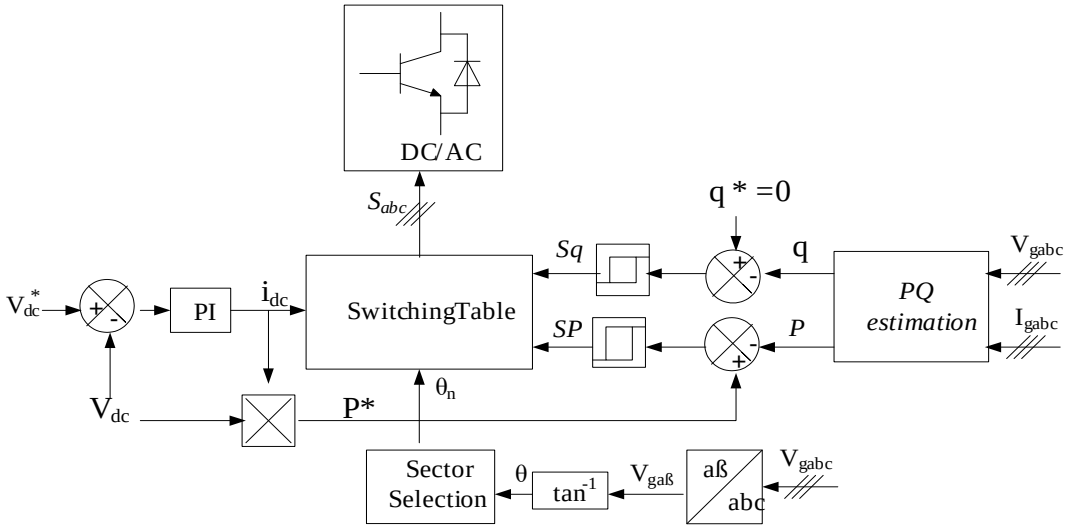

Figure.4.14. Block diagram for Classical DPC technique

$$V_g = Ri_g + L_g \frac{di_g}{dt} + V_{rec} \tag{4.28}$$

$$V_g = \frac{2}{3}\left(V_a + V_b e^{j(2\pi/3)} + V_c e^{j(4\pi/3)}\right) \tag{4.29}$$

$$i_g = \frac{2}{3}\left(i_a + i_b e^{j(2\pi/3)} + i_c e^{j(4\pi/3)}\right) \tag{4.30}$$

$$v_{rec} = \frac{2}{3}V_{dc}\left(S_a + S_b e^{j(2\pi/3)} + S_c e^{j(4\pi/3)}\right) \tag{4.31}$$

V_{dc}: is the DC-link voltage.

The rectifier control bases on the logic values S_i, where: Si=1, T_i is ON and T_i is OFF. S_i=0, T_i is OFF and T_i is ON. with: i= a, b, c.

It is a well-established fact that the calculation of "active" power "P" involves a "scalar" product between "voltages" and "currents," while the determination of "reactive" power "q" can be achieved through a "vector" product between them [37].

$$P = V_a i_a + V_b i_b + V_c i_c \tag{4.32}$$

$$q = \frac{1}{\sqrt{3}}\left[(V_b - V_c) i_a + (V_c - V_a) i_b + (V_a - V_b) i_c\right] \tag{4.33}$$

The instantaneous discrepancies in active and reactive powers are transformed into logic outputs, Sp and Sq, employing two two-level hysteresis comparators. If the error surpasses or falls below a specified band, the hysteresis output will assume states 1 or 0, respectively. When the errors fall within the acceptable range, the output remains unchanged. Thus, for hysteresis bands H_P and H_q corresponding to active and reactive powers, the outputs of the hysteresis comparators are as follows:

$$\begin{cases} Sp = 1 & if \quad P < P^* - H_p \\ Sp = 1 & if \quad P > P^* + H_p \end{cases} ; where \quad P^* = V_{dc}.i^*_{dc} \tag{4.34}$$

$$\begin{cases} Sq = 1 & if \quad q < q^* - Hq \\ Sq = 1 & if \quad q > q^* + H_q \end{cases} ; where \quad q^* = 0 \tag{4.35}$$

Note: The reference active power P^* is determined by a Proportional-Integral (PI) regulator controlling the DC voltage, while the reactive power q^* is set to zero to ensure operation at unity power factor.

To enhance precision and address issues that may arise at the boundaries of each control vector, the vector space is subdivided into twelve sectors, each spanning 30°.

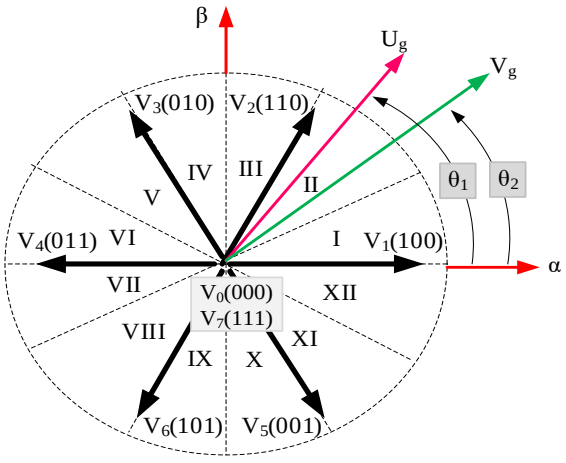

Figure 4.15. Six voltage vectors and 12 sectors in the αβ reference frame.

Based on the outputs of the hysteresis comparators Sp and Sq, and corresponding to the sector in which the voltage vector is situated, the selection of the voltage vector to be applied to the rectifier is determined according to the subsequent switching table [95].

Table.4.1. Switching Table

Sp	Sq	θ_1	θ_2	θ_3	θ_4	θ_5	θ_6	θ_7	θ_8	θ_9	θ_{10}	θ_{11}	θ_{12}
1	0	V_5	V_6	V_6	V_1	V_1	V_2	V_2	V_3	V_3	V_4	V_4	V_5
	1	V_3	V_4	V_4	V_5	V_5	V_6	V_6	V_1	V_1	V_2	V_2	V_3
0	0	V_6	V_6	V_6	V_6	V_6	V_6	V_6	V_6	V_6	V_6	V_6	V_6
	1	V_1	V_2	V_2	V_3	V_3	V_4	V_4	V_5	V_5	V_6	V_6	V_1

2.2.2.Proposed PD(1+PI) -P-DPC strategy

In the existing topology, the P-DPC technique [96] illustrated in Figure 4.17. is devised for the regulation of both active and reactive power levels exchanged with the grid. Additionally, it aims to compensate for undesired harmonic contents in the grid current by appropriately tuning the reference active Power P* by integrate PD(1+PI) controller. The fundamental concept behind this technique involves the minimization of a cost function, computed as the sum of squared differences between actual and predicted values of both active and reactive power [97].

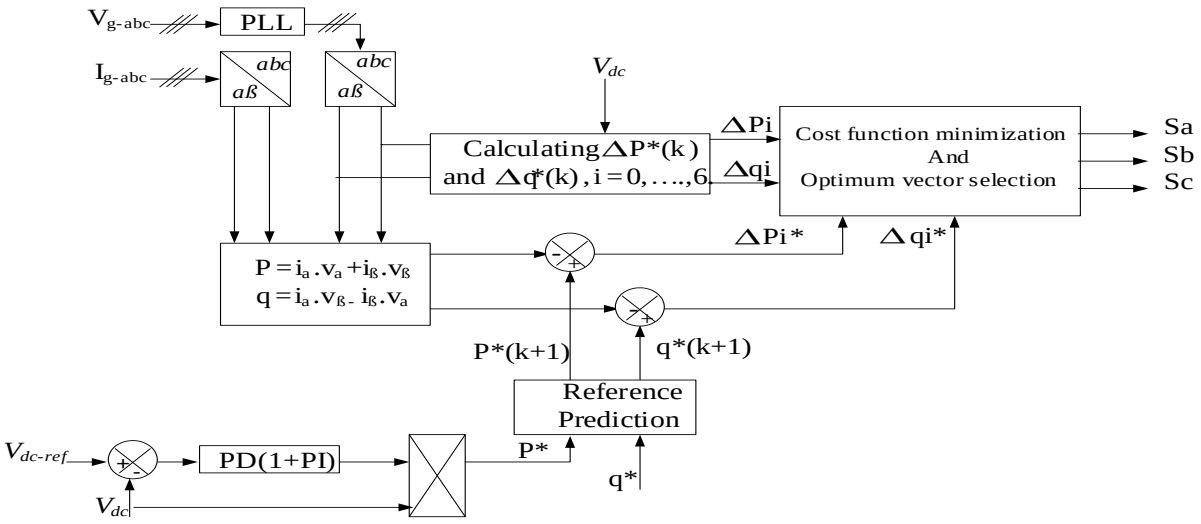

Figure.4.16. Block diagram proposed for P-DPC technique

To implement this strategy, the initial step involves establishing a forecasting model for the voltage inverter utilizing instantaneous power

quantities, as elucidated by the approach in α-β reference frame [98]. In this reference frame, the active and reactive power levels exchanged with the grid are expressed as follows:

$$\begin{cases} P = i_\alpha . e_\alpha + i_\beta . e_\beta \\ q = i_\alpha . e_\beta + i_\beta . e_\alpha \end{cases} \tag{4.36}$$

Assuming a sufficiently small sampling time Ts (Ts << T), the synthesis of active and reactive power at the subsequent sampling time can be expressed through the following equation:

$$\begin{bmatrix} P(K+1) \\ q(K+1) \end{bmatrix} = \begin{bmatrix} e_\alpha(K) & e_\alpha(K) \\ e_\beta(K) & -e_\beta(K) \end{bmatrix} . \begin{bmatrix} i_\alpha(K+1) \\ i_\beta(K+1) \end{bmatrix} \tag{4.37}$$

The changes in these magnitudes between two consecutive sampling moments are expressed as follows:

$$\begin{bmatrix} P(K+1) - P(K) \\ q(K+1) - q(K) \end{bmatrix} = \begin{bmatrix} e_\alpha(K) & e_\alpha(K) \\ e_\beta(K) & -e_\beta(K) \end{bmatrix} . \begin{bmatrix} i_\alpha(K+1) - i_\alpha(K) \\ i_\beta(K+1) - i_\beta(K) \end{bmatrix} \tag{4.38}$$

Furthermore, neglecting the influence of the series resistance of the coupling inductance at the inverter output, the change in the current vector is governed by a first-order differential equation:

$$\frac{d}{dt} \begin{bmatrix} i_\alpha \\ i_\beta \end{bmatrix} = \frac{1}{L_f} \begin{bmatrix} e_\alpha \\ e_\beta \end{bmatrix} - \begin{bmatrix} V_\alpha \\ V_\beta \end{bmatrix} \tag{4.39}$$

Discretizing Equation (4.36) over a sampling period Ts yields the change in the current vector between two successive instances 'k' and '(k + 1)', represented by:

$$\begin{bmatrix} i_\alpha(K+1) - i_\alpha(K) \\ i_\beta(K+1) - i_\beta(K) \end{bmatrix} = \frac{T_s}{L_f} \begin{bmatrix} e_\alpha(K) \\ e_\beta(K) \end{bmatrix} - \begin{bmatrix} V_\alpha(K) \\ V_\beta(K) \end{bmatrix} \tag{4.40}$$

Substituting Equation (4.39) into Equation (4.37) results in the predictive model at the inverter output, relying on the instantaneous active and reactive powers [94], expressed as:

$$\begin{bmatrix} P(K+1) \\ q(K+1) \end{bmatrix} = \begin{bmatrix} P(K) \\ q(K) \end{bmatrix} + \frac{T_s}{L_f} \begin{bmatrix} e_\alpha(K) & e_\alpha(K) \\ e_\beta(K) & -e_\beta(K) \end{bmatrix} \cdot \begin{bmatrix} e_\alpha(K) - V_\alpha(K) \\ e_\beta(K) - V_\beta(K) \end{bmatrix} \tag{4.41}$$

As observed, the predictive model system involves only two parameters: the coupling inductance (L_f) and the sampling period (T_s). Ideally, the controlled quantities converge to their set values when the following condition is satisfied:

$$\begin{cases} P^*(K+1) - P(K+1) = 0 \\ q^*(K+1) - q(K+1) = 0 \end{cases} \tag{4.42}$$

The condition stated in Equation (4.41) cannot be met unless the alterations in active and reactive power during the switching period assume the following values:

$$\begin{cases} \Delta P^*(K) = P^*(K+1) - P(K) \\ \Delta q^*(K) = q^*(K+1) - q(K) \end{cases} \tag{4.43}$$

The calculated predicted reference values for active power, P (k + 1), and reactive power, q (k + 1), are determined as follows:

$$\begin{cases} P^*(K+1) = 2.P^*(K) - P^*(K-1) \\ q^*(K+1) = q^*(K) \end{cases} \tag{4.44}$$

Thus, the optimal determination of the switching vector (Sa, Sb, Sc) is achieved by minimizing a quadratic cost function associated with errors in active and reactive power:

$$F = \varepsilon_p(K)^2 + \varepsilon_q(K)^2 \tag{4.45}$$

Where:
$$\begin{cases} \varepsilon_p(k) = \Delta P^*(K) - \Delta P_i \\ \varepsilon_q(k) = \Delta q^*(K) - \Delta q_i \end{cases} \quad i = 0,1,...,6 \tag{4.46}$$

2.2.3.Grid electrical analysis

The active (a) and reactive (b) power of the grid are shown, respectively, in Figure 4.17. The active power output response for the suggested and conventional techniques is shown in Figure (a). When a PI-DPC controller is used instead of a PD (1+PI)-P-DPC controller, there are more ripples in the

form, however the power precisely matches the reference in both techniques. More ripples can be observed with the classical technique than with the suggested technique at times [0.8s-1s] and [1.6s-1.7s]. In addition, the recommended method provides an energy reaction time that is more effective than the PI controller.

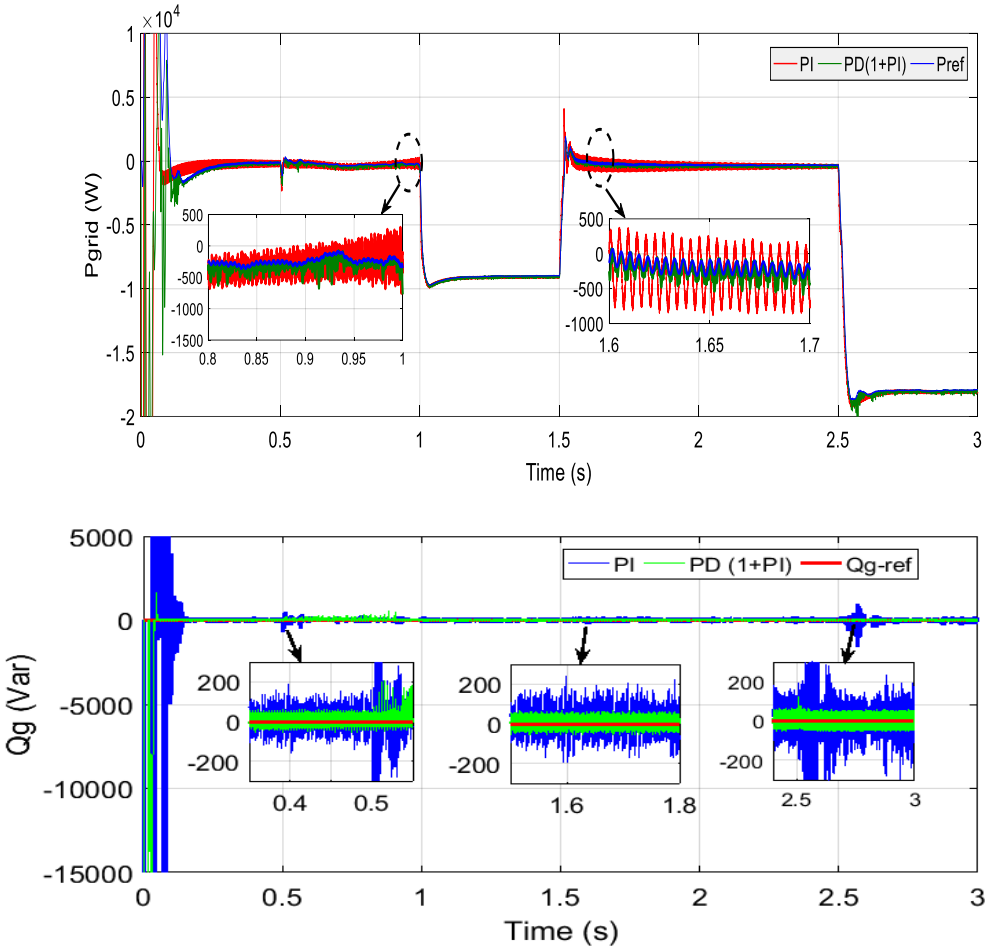

Figure.4.17. Grid active and reactive power

In figure 4.18 and 4.19 represent the first-phase grid voltage and three-phase grid currents output respectively. Through these figure, the voltage and the currents take on a sinusoidal for in the case of both traditional and proposed strategies, the figure 4.21 shows both the voltage and the electrical current of the load, as we can notice that they have taken the sinusoidal shape in an optimal way without ripples. Meanwhile, the figure 4.23 and the figure 4.24 illustrate the pulse values for both the traditional and proposed strategies. It can be observed that the THD values reach 0.39% and 0.35% when using the traditional method during periods when the power grid intervened to meet

demand requirements. However, with the proposed method, an improvement in THD values is noticeable, measured at 0.36% and 0.27%, respectively.

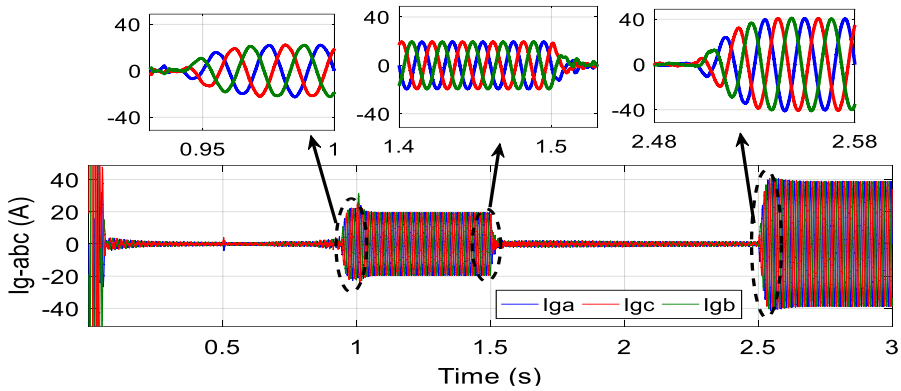

(a): PD (1+PI) -P-DPC technique

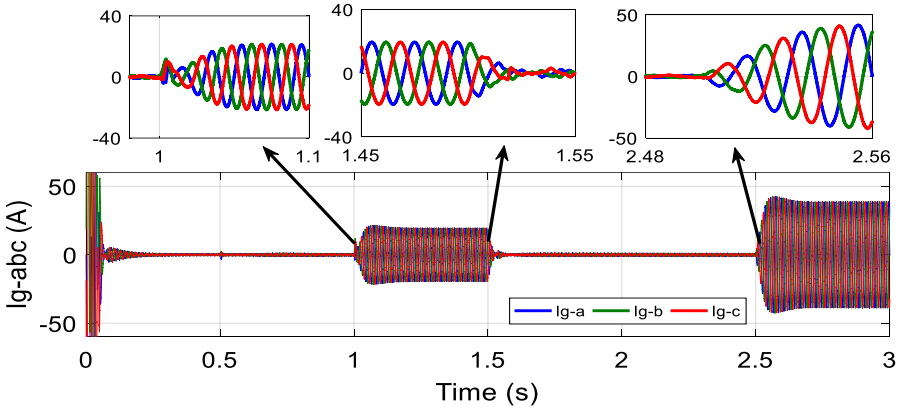

(b): PI-DPC technique

Figure.4.18. Three- phase grid currents

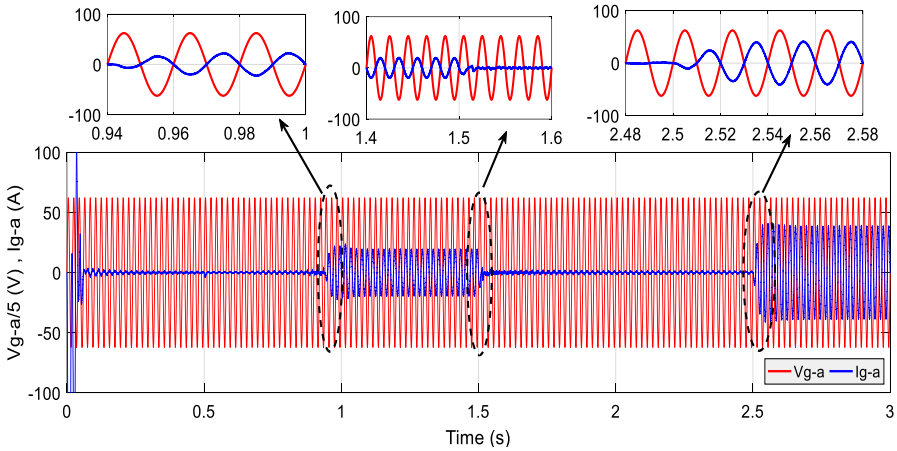

(a) : PD (1+PI) - P-DPC technique

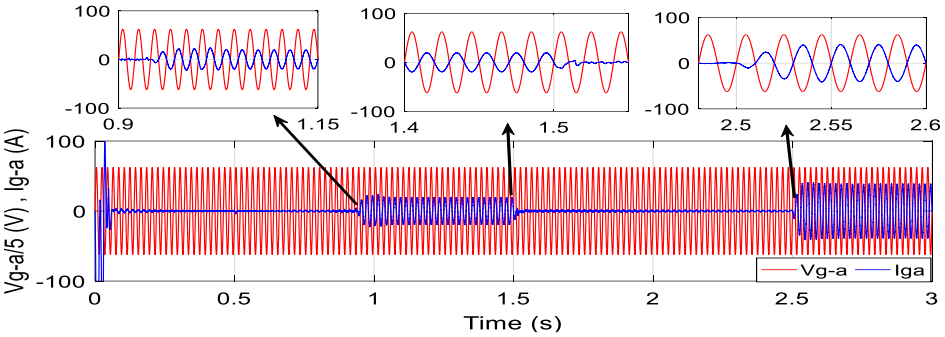

(b) : PI-DPC technique

Figure.4.19. The grid voltage and current of the First- phase

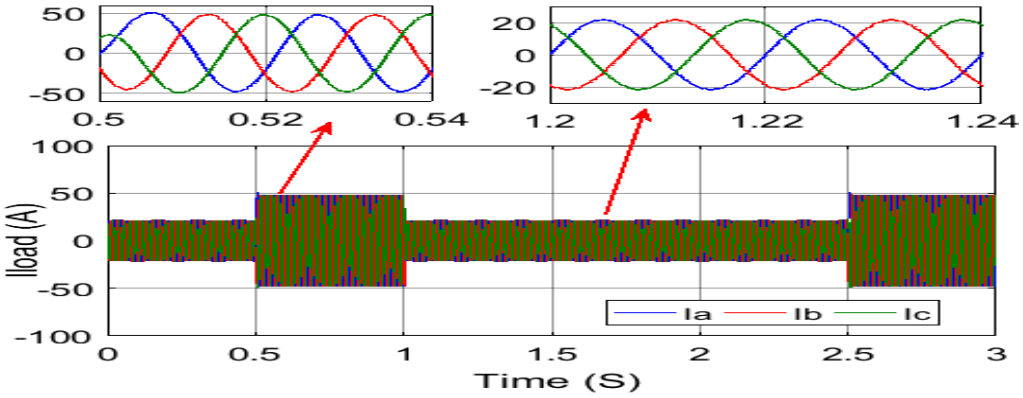

(a)

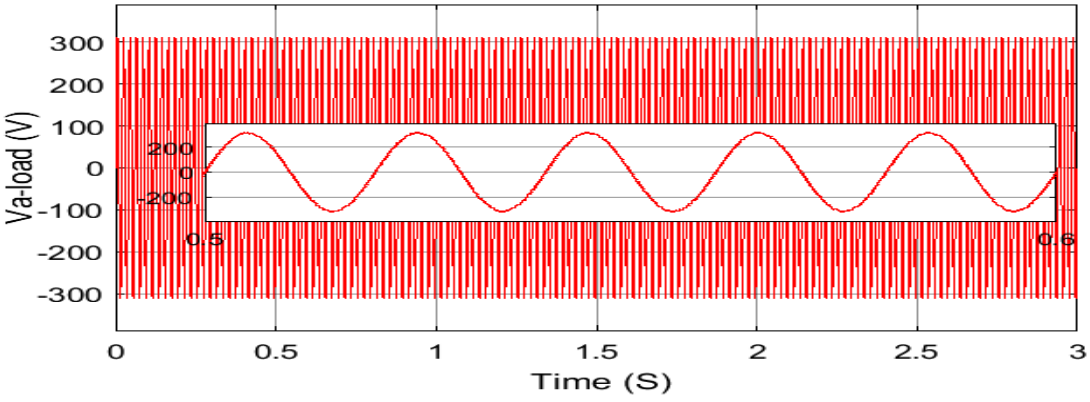

(b)

Figure.4.20. (a): A current load ;**(b):** First- phase load voltage

2.3. Various Operational Modes of the Hybrid System

Figure 4.22. shows a DC-link voltage, and it appears that both methods result in voltages that are within the 600-volt reference range. On the other hand, the recommended approach provides more accurate findings with no

distortion. For example, the ripples are much more apparent at 1seconds, 1.05 seconds, 2.6 seconds and nearly throughout the simulation time span when the traditional control scheme is used. This indicates that in order to align the DC voltage value with the reference value, the recommended method PD (1+PI) is required.

Figure 4.23. illustrates a power flow based on the PD (1+PI)-P-PDC technique. We have identified five modes for managing renewable energy in a grid-connected hybrid system, designed to supply a non-linear load under various climatic conditions:

Mode 01: It is clear that the photovoltaic system's power generation is sufficient to meet up to a 10-kilowatt load requirement between [0s and 0.5s]. This can be represented as $P_{pv}=P_l$ and does not require intervention from other production systems.

Mode 02: The energy demand increased from 0.5 s to 1 s, reaching 20 kW. This required the storage system to be discharged by approximately 9.9 kW in order to cover up for the production shortfall. This includes taking into account the fact that the photovoltaic system only produced roughly 10.1 kW, and the wind generator had no production at all because of the weather (extremely low wind speed). The formula for this is $P_l=P_{pv}+P_b$.

Modes 03 and 05: The RES is unable to supply the predicted load needs of 10 kW and 20 kW, respectively, within the time intervals [1 s - 1.5 s] and [2.5 s -3 s]. The photovoltaic system can only produce 1000 watts or 2000 watts, respectively, due to the following weather conditions: solar irradiation of 100 W/m² and 200 W/m² and wind speed deficiency of 6 m/s and 2 m/s. Furthermore, the storage system cannot discharge itself once more in order to keep the state of charge within the designated range (20% < SOC < 80%). This required the power grid to step in and cover the expected 9 kW to 18 kW of residual production, depending on the example analyzed. This situation can be expressed by: $P_l=P_g+P_{pv}$.

Mode 04: With the wind speed reaching 12 m/s during the time period, we observe the wind generator contributing to the production of power with an estimated quantity of 6 kW. In the meantime, about 10 kW were produced by the photovoltaic system. $P_l+P_b=P_{pv}+P_w$ is the extra energy that had to be

charged into the storage system because the production exceeded the 6 kW demand.

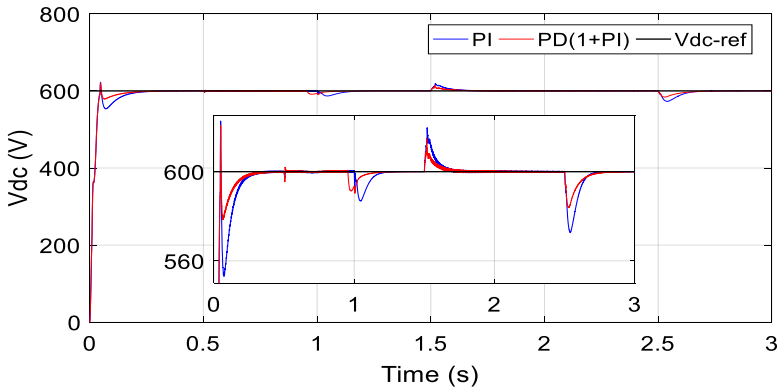

Figure.4.21. DC-Link voltage performance

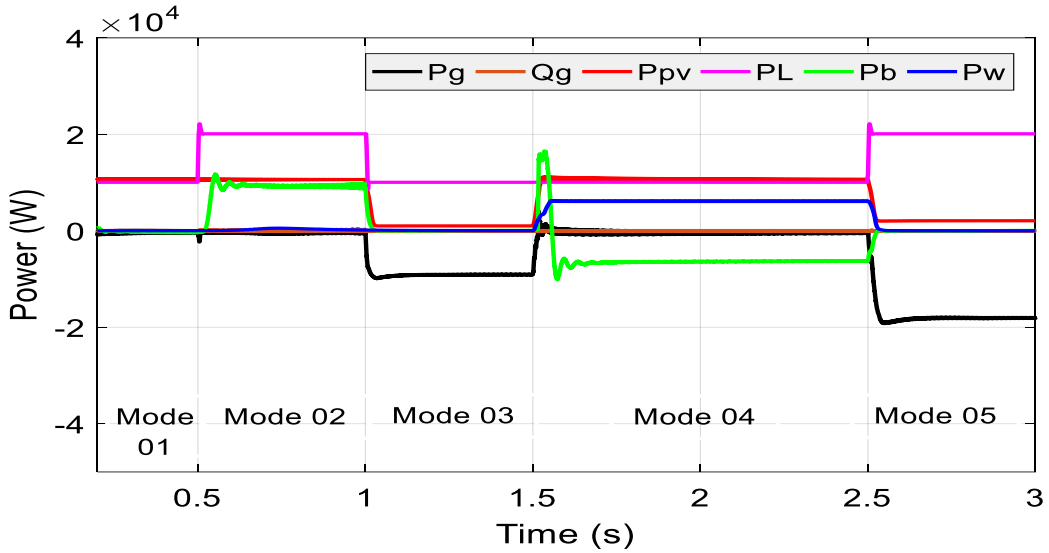

Figure 4.22. Power flow based on PD (1+PI)- P-DPC technique

3. THD analysis for the proposed system

This study compares pulse values for proposed and conventional techniques in terms of (THD). The results show that the proposed method enhances power quality. The reduction ratio for THD values decreases when solar irradiation equal to 1000 w/m², while the conventional method has a lower reduction ratio. However, the proposed method has a higher reduction ratio, reaching 0.02% for solar generators and 0.01% for wind generators. As solar irradiation and wind speed increase, the reduction ratio in THD current values also increases. The THD value for direct current (DC link) decreases from 0.9% in the proposed approach to 1.27% in the conventional method, and from 0.39% with the standard method to 0.27% with the proposed method.

This suggests that the proposed method is more successful in reducing harmonic distortion in grid voltage or current signals, ensuring grid stability and improving power quality. The observed drop in THD values demonstrates the efficacy of the suggested approach in enhancing power quality in RESs linked to the network.

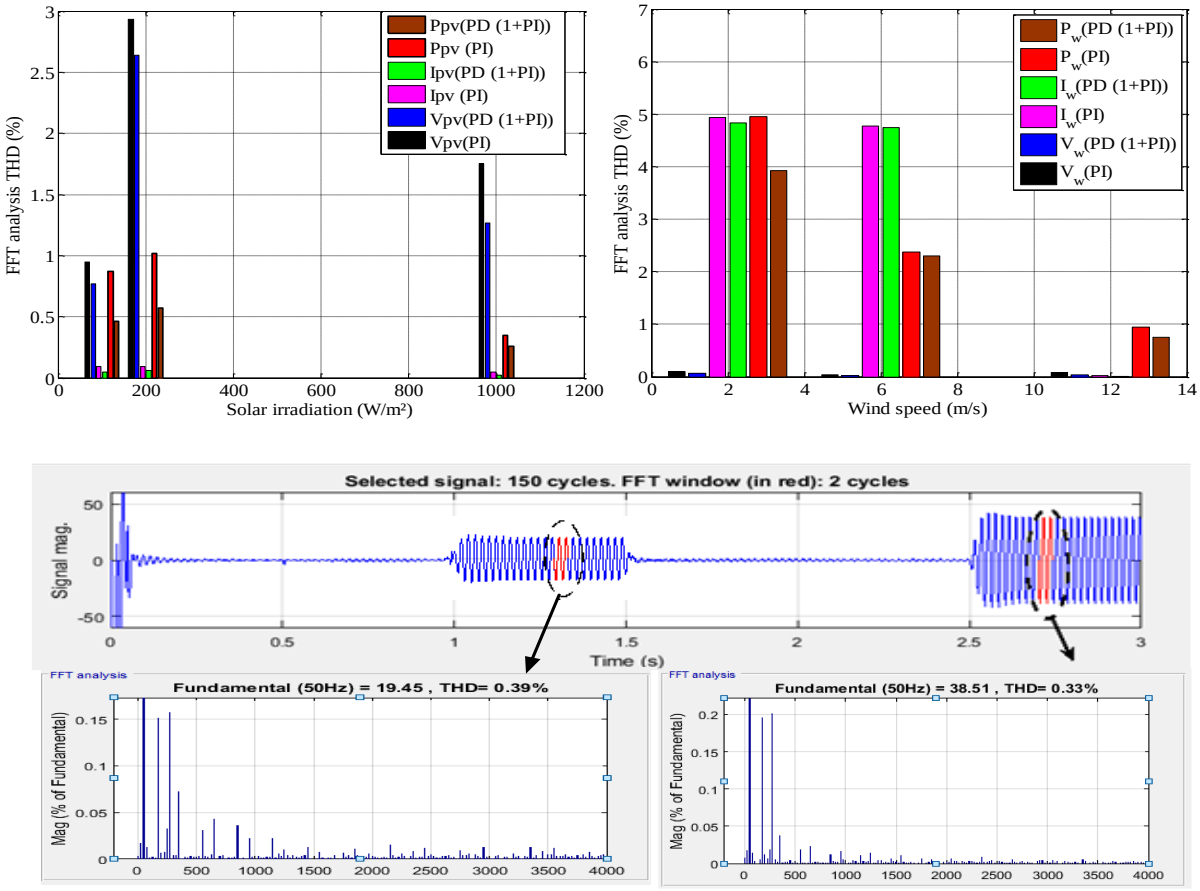

Figure 4.23. PI-DPC analysis of grid current phase

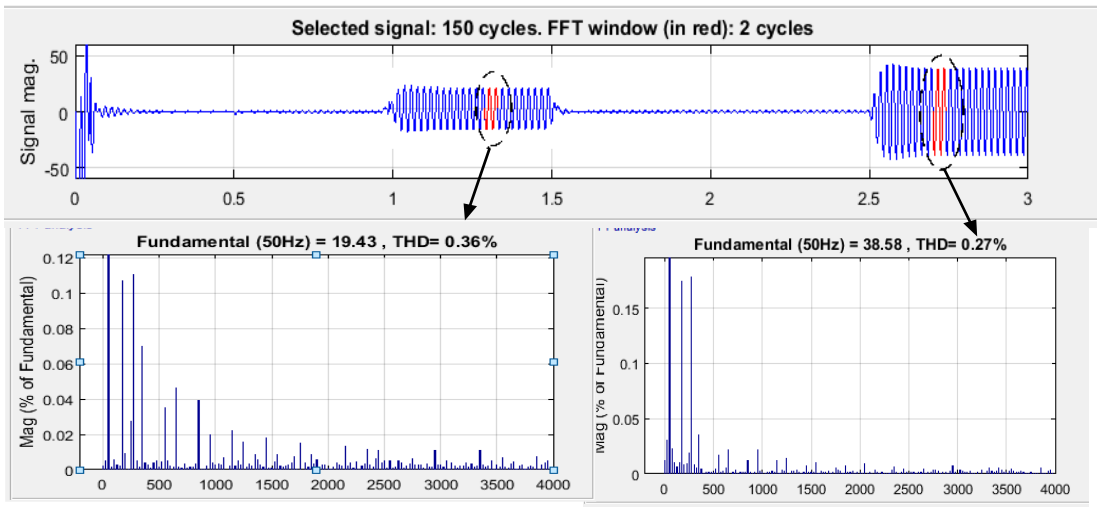

Figure 4.24. PD (1+PI)-P-DPC analysis of grid current phase

Table 4.3 presents quantitative analyses for the DC bus voltage, comparing the performance of the PD (1+PI) and PI control techniques across different time intervals.

- **Transient Time and Settling Time**: The PD (1+PI) technique generally exhibits shorter settling times compared to the PI technique. For example, in the time interval of 0-0.5 seconds, the settling time for the PD (1+PI) technique is 0.2 seconds, whereas it is slightly longer at 0.22 seconds for the PI technique. This indicates that the PD (1+PI) technique achieves stability faster in response to transient changes in the system.
- **Ripple**: The PD (1+PI) technique shows lower ripple values for the DC bus voltage compared to the PI technique. For instance, in the time interval of 0-0.5 seconds, the ripple for the PD (1+PI) technique is 0.07 volts, while it is slightly higher at 0.08 volts for the PI technique. This suggests that the PD (1+PI) technique produces a smoother and more consistent output voltage, which is desirable for stable operation.
- **Overshoot/Undershoot**: Both techniques exhibit some level of overshoot/undershoot in the DC bus voltage. In most cases, the PD (1+PI) technique shows lower overshoot/undershoot percentages compared to the PI technique. For example, in the time interval of 0-0.5 seconds, the overshoot/undershoot percentage for the PD (1+PI) technique is 1.6%, while it is higher at 2.43% for the PI technique. However, the absolute values of overshoot/undershoot (in volts) are higher for the PD (1+PI) technique in some cases.

The table's statistical analyses support the conclusion that the PD (1+PI) control approach exceeds the PI technique in terms of instantaneous response time, ripple reduction, and overshoot/undershoot control for the DC bus voltage in the provided hybrid system. These results give weight to the idea that the PD (1+PI) approach provide better dynamic performance and stability than the traditional PI technique for controlling such systems.

Table.4.2. Comparative THD

		THD (%)					
		PD (1+PI)			PI		
PV SYSTEM	$G\ (w/m^2)$	100	200	1000	100	200	1000
	P_{pv}	0.46	0.57	0.26	0.87	1.02	0.35
	I_{pv}	0.05	0.06	0.02	0.09	0.09	0.05
	V_{pv}	0.77	2.64	1.27	0.95	2.93	1.75
WIND SYSTEM	Wind speed (m/s)	2	6	12	2	6	12
	P_w	3.93	2.30	0.75	4.95	2.37	0.95
	V_w	4.84	4.74	0.01	4.94	4.77	0.02
	I_w	0.07	0.02	0.04	0.1	0.04	0.08
DC Link	**1 s**	0.4			0.89		
	1.5 s	0.72			0.92		
	2.5 s	1.43			1.86		

Table.4.3. Quantitative analyses for DC bus voltage.

Transiet Time (s)	Ripple (V)		Overshoot/Undershoot (%)		Settling time (s)	
	PD(1+PI)	PI	PD (1+PI)	PI	PD (1+PI)	PI
0 - 0.5	0.07	0.08	1.6	2.43	0.2	0.22
0.5 - 1	0.03	0.03	0.4	0.89	0.035	0.04
1 - 1.5	0.01	0.02	0.72	0.92	0.05	0.056
1.5 - 2.5	0.09	0.1	1.43	1.86	0.1	0.18
2.5 – 3	0.03	0.035	0	0	0.01	0.016

4. Comparative study with recent studies

As presented in table 4.3. PD (1+PI) control strategy demonstrates superior performance across several key metrics when compared to traditional and other advanced control strategies. Specifically, our method achieves an efficiency of 92%, outperforming the traditional Direct Power Control (DPC) approach, which achieves 88%, and slightly surpassing other advanced control strategies that achieve efficiencies between 90-91%.

In terms of Total Harmonic Distortion (THD), our system records a lower THD of 2.5%, which is better than the 3.0% observed with traditional DPC and comparable to other advanced strategies with THD values ranging from 2.6% to 2.8%. Furthermore, our approach provides exceptional voltage regulation at 98.5%, exceeding the performance of traditional DPC (95%) and other

advanced controls (97-98%). Additionally, our strategy results in energy savings of 15%, which is significantly higher than the 12% savings achieved with traditional DPC and slightly better than the 13-14% savings offered by other advanced strategies. These results highlight the effectiveness and benefits of our proposed control strategy in enhancing system performance and energy efficiency.

Table 4.4. Comparative study

Study	Control strategy	Efficiency (%)	THD (%)	Voltage regulation (%)	Energy savings (%)
Ours Study	PD (1+PI) Control	92	2.5	98.5	15
Study A (2022) [98]	Traditional DPC	88	3.0	95	12
Study B (2023) [99]	Advanced PI Control	90	2.8	97	13
Study C (2023) [100]	Hybrid Control	91	2.6	98	14

5. Conclusion

In the field of electrical energy, controlling a grid-connected hybrid system is considered complex. A thorough examination of renewable energy management systems using advanced monitoring systems, as demonstrated by several tests, underscores the importance of having effective and reliable methods in place. The proposed PD (1+PI) controller surpasses standard methods in terms of accuracy and performance, particularly in maintaining voltage stability and maximizing power flow under various environmental conditions. Additionally, the recommended approach effectively optimizes power output, reduces distortions, and maintains grid stability, as evidenced by testing under different conditions. These findings highlight the crucial role advanced control techniques play in improving the efficiency, reliability, and sustainability of RES. The integration of MPPT technology with the PD (1+PI) controller also appears to significantly enhance power quality and system performance, as indicated by the observed reduction in Total Harmonic Distortion.

General Conclusions and Perspectives

General Conclusions and Perspectives

In this work, we proposed a strategy for managing a RES linked to the network, primarily relying on two RES: wind power and solar energy. Additionally, a storage system was integrated as a secondary component to ensure the load demand is met regardless of changing weather conditions, while considering the battery state at specific values. The proposed strategy aims to optimize the energy output from various production sources as a first step, and then manage the different energy sources in the system by suggesting a control unit integrated with a bidirectional converter of a storage system, issuing charging commands to the battery as needed.

The strategy also aims to activate the role of the storage system and minimize the intervention of the electrical grid, allowing the grid to step in only in exceptional cases, such as when both the RE system and the storage system fail to meet the demand. This strategy was formulated based on an extensive study of a standalone hybrid system, which is described in detail in the third chapter. The first and second chapters provide an overview of the grid-connected hybrid system and its current importance in electricity production as a permanent element, including with mathematical modeling of the system's various parts.

The objectives of the study can be outlined in several points as follows:

- Ensure uninterrupted demand fulfillment regardless of weather conditions.
- Enhance the power quality produced from various production sources.
- Protect the battery and extend its lifespan.
- Automate the charging and discharging of the battery.
- Reduce the role of the electrical grid.
- Manage the generated energy optimally.

The results obtained in our study were compared with other methods discussed in different studies, and the results demonstrated the effectiveness of the proposed strategy in operating the system efficiently and optimally.

Perspectives:

Our study on this topic has led us to consider expanding the research points, as these points are no less important than the current study due to the topic's broad nature, which has been addressed by numerous studies. These points include:

- Using a test platform to verify the obtained results.
- Utilizing one of the sizing programs [**Hybrid2, HOMER** (Hybrid Optimization Model for Electric Renewables), **RAPSIM** (Remote Area Power Supply Simulator) to provide more accurate results.
- Determining the economic costs of production and developing a strategy to reduce costs.

The work presented in this thesis has given rise to the following publications and communications:

Publications :

1. *Fatima Menzri1, Tarek Boutabba2, Idriss Benlaloui2,3, Haneen Bawayan4, Mohmed I Mosaad,5 and Mohamed Metwally Mahmoud,6 "Applications of hybrid SMC and FLC for augmentation of MPPT method in a wind-PV-battery configuration », Wind Engineering Vol. 1(6), (2024)*

2. *Fatima Menzri 1, Tarek Boutabba 2,3, Idriss Benlaloui 3, * , Larbi Chrifi-Alaoui 4 , Abdulaziz Alkuhayli 5 ,Usama Khaled 6 and Mohamed Metwally Mahmoud, Applications of Novel Combined Controllers for Optimizing Grid-Connected Hybrid Renewable Energy Systems. 'Sustainability' Vol:16(16), 6825, (august2024)*

3. *Fatima MENZRI, Naamane DABDOUCHE, Brahim DEFFAF, Enhancing Grid Integration of Solar Energy: A Novel Approach Employing Sliding Mode Control (SMC) and Direct Power Control (DPC) Strategies, "International Journal of Electronics and Electrical Engineering Systems", Vol (7), Issue 1S (2024)*

International conferences :

1- *F. MENZRI, M l. Bechka, t. BOUTABBA AND R. CHENNI, Comparative study of an intelligent energy management of standalone hybrid generation power system 4th International Conference on Artificial Intelligence in Renewable Energetic Systems, December 22-24, 2020*

2- *Fatima Menzri; Tarek Boutabba; Idriss Benlaloui; Dalila Khamari; Optimization of Energy Management for Hybrid Renewable Energy Sources Using Particale Swarm Algorithm, ICAEE 2022,*

3- *Fatima Menzri; Tarek Boutabba; Mustafa Ergin Sahin; Optimal Energy Management System A Grid Connected Renewable Hybrid System with Direct Power Control, TICEMT's 23*

4- *Fatima Menzri**;** Anfal Lekmine; Amir Fatah; Tarek Boutabba; Idriss Benlaloui; Dalila Khamari, Improvement of energy management of standalone hybrid generation power system using Adaptive neuro fuzzy system, the First International Conference on Electrical Engineering and Advanced Technologies, ICEEAT23*

Annex

Parameters of the HES components

A.1. PV module SPR-305-WHT

Electrical and mechanical characteristics under typical conditions (1000 W/m² and 25°C)

Electrical characteristics		**Mechanical characteristics**	
Maximum power Pmax (Wc)	305	Cell type	Monocrystalline
Short-circuit current Icc (A)	5.96	Number of cells	96
Open-circuit voltage Voc (V)	64.2	Dimensions (mm/inches)	156 x 156 (6+)
Optimum current Iop (A)	5.58	Weight	24 Kg
Optimum voltage Vop (V)	54.7		

A.2. Wind system parameters

Wind system parameters		
Rated wind speed	V (m/s)	12
Nominal speed	Ω (rad/sec)	153
Rated power	P_t (Kw)	6
Pole pairs	P	5
Stator resistance	Rs (Ω)	0.425
Stator inductance	Ls (mH)	8.35
generator's inertia	J(kg.m^2)	0.01197

A.3. Nickel metal hydride battery parameters

Capacity	6.5 Ah
Nominal Voltage	200 V
Maximum Capacity	3.2308 Ah
Nominal Discharge Current	0.6 A
Exponential Voltage	216.9492 V
Internal Resistance	0.66667 Ω
Fully Charged Voltage	235.5932 V
Capacity Nominal Voltage	2.8846 Ah
Exponential Capacity	0.6 Ah

Bibliographic references

[1] P. K. Oanh, “Renewable energy, the inevitable trend of the world and the future direction for Vietnam,” Vietnam Institute of Strategy and Policy for Industry and Trade, Industry and Trade Research Review - VIOIT, 2023.

[2] A. Sabonadiére, et al., “Nouvelle technologies de l’énergie 1 : les énergies renouvelables,” Edition Lavoisier, 2006.

[3] Recherche ECRIN Entreprise, “L’électronique de puissance vecteur d’optimisation pour les énergies renouvelables,” Rapport de Synthèse, May 2002.

[4] M. Mladjao and M. Al Anfaf, “Contribution à la modélisation et a l’optimisation de systèmes énergétiques multi-sources et multi charge,”.

[5] Statista, "Global electricity production by energy source 2022," Statista, 2022. https://www.statista.com/statistics/269811/world-electricity-production-by-energy-source/.

[6] A. El Khadimi, L. Bchir, and A. Zeroual, “Dimensionnement et optimisation technico économique d’un système d’énergie hybride photovoltaïque-éolien avec système de stockage,” Revue des Energies Renouvelables, vol. 7, pp. 73-83, 2004.

[7] W. López-Castrillón, H. H. Sepúlveda, and C. Mattar, "Off-Grid Hybrid Electrical Generation Systems in Remote Communities: Trends and Characteristics in Sustainability Solutions," *Sustainability*, vol. 13, no. 11, p. 5856, May 2021.

[8] I. Vechiu, “Modélisation et analyse de l‟intégration des énergies renouvelables dans un réseau autonome,” Doctoral Thesis, University of Havre, 2005.

[9] D. Abbes, “Contribution au dimensionnement et à l'optimisation des systèmes hybrides éoliens-photovoltaïques avec batteries pour l'habitat résidentiel autonome,” Doctoral Thesis, University of Poitiers, 2012.

[10] M. A. El-Hadidy, “Performance evaluation of hybrid wind/solar/diesel power systems,” Renewable Energy, vol. 26, pp. 401–413, 2002.

[11] C. Wang and M. Hashem Nehrir, “Power Management of a Stand-Alone Wind/Photovoltaic/Fuel Cell Energy System,” IEEE Transactions on Energy Conversion, vol. 23, no. 3, September 2008.

[12] J. M. Guerrero, J. C. Vasquez, J. Matas, L. G. de Vicuña, and M. Castilla, “Hierarchical control of droop-controlled AC and DC microgrids—A general approach toward standardization,” IEEE Transactions on Industrial Electronics, vol. 58, no. 1, pp. 158-172, Jan. 2011.

[13] Aouichak, S. Jacques, S. Bissey, C. Reymond, T. Besson, and J.-C. Le Bunetel, "A Bidirectional Grid-Connected DC–AC Converter for Autonomous and Intelligent Electricity Storage in the Residential Sector," *Energie*s, vol. 15, no. 3, p. 1194, Feb. 2022.

[14] D. J. van de Ven, et al., “The potential land requirements and related land use change emissions of solar energy,” Scientific Reports, vol. 11, 2021.

[15] A. Adnan, et al., “Comparison of Ground-Based Global Horizontal Irradiance and Direct Normal Irradiance with Satellite-Based SUNY Model,” Energies, vol. 15, no. 7, 2022.

[16] D. H. Kambezidis and B. E. Psiloglou, “Estimation of the Optimum Energy Received by Solar Energy Flat-Plate Convertors in Greece Using Typical Meteorological Years. Part I: South-Oriented Tilt Angles Solar Radiation: Measurements and Modelling,” Effects and Applications, vol. 2, Feb. 2021.

[17] Y. Rizwana, X. Yao, I. U. Haq Padda, W. U. H. Shah, and W. Jie, “Exploring the role of solar energy and foreign direct investment for clean environment: Evidence from top 10 solar energy consuming countries,” Renewable Energy, vol. 185, Feb. 2022.

[18] C. Sicard, “Les énergies solaire et éoliennes en Algérie,” Tome III – OCS 81 DZ 232, 2011.

[19] M. Dida et al., "Promotion of Solar Energies in Southern Algeria: Strategies and Perspectives," SpringerLink, 2023.”

[20] A. Tebib, “La Production Electrique a` partir de la Biomasse Oleicole: le Potentiel Algerien,” MED Énergie Maghreb, p. 28, 2014.

[21] T. J. Coutts, K. A. Emery, and J. A. Gordon, “Solar Cell and Module Measurement Techniques,” in Handbook of Photovoltaic Science and

Engineering, A. Luque and S. Hegedus, Eds., 2nd ed. Hoboken, NJ: John Wiley & Sons, 2011, ch. 5, pp. 289-350.

[22] M. Zandi, “Contribution au pilotage des sources hybrides d’énergie électrique,” Doctoral Thesis, Nancy University - Institut National Polytechnique de Lorraine, 2010.

[23] T. Abdulkader, “Modelling, control and supervision of multi-source system connected to the network with a buffer storage of electrical energy via hydrogen vector,” Doctoral Thesis, University of Belfort–Montbéliard, 2015.

[24] Ritchie, H., & Roser, M. (2020). "Renewable Energy." Our World in Data

[25] A. Larbaoui, “Renewable energy technologies potential contribution to sustainable development: the case of Algeria,” Journal of Political Orbits, vol. 6, no. 1, pp. 216–226, 2022.

[26] Global Wind Energy Council, *Global Wind Report 2022*. Brussels, Belgium: GWEC, Apr. 2022. https://gwec.net.

[27] M. Belhamel, S. Moussa, and A. Kaabeche, “Production d’Electricité au Moyen d’un Système Hybride (Eolien-Photovoltaïque-Diesel),” Revue des Energies Renouvelables, pp. 49-54, 2002.

[28] T. Burton, D. Sharpe, N. Jenkins, and E. Bossanyi, “Horizontal Axis Wind Turbine Technology,” in Wind Energy Handbook, 2nd ed. Hoboken, NJ: John Wiley & Sons, 2011, ch. 4, pp. 147-253.

[29] B. Cheikh, “Commande d’une machine asynchrone à double alimentation en vue de son application dans le domaine de l’énergie éolienne étude et expérimentation,” Doctoral Thesis, University of Mohamed Boudiaf-Oran, 2007.

[30] R. Ortega González, "Comparison of Power Coefficients in Wind Turbines Considering the Tip Speed Ratio and Blade Pitch Angle," *Energies*, vol. 16, no. 6, p. 2774, Mar. 2023.

[31] E. Aitor, “Microgrid Hybrid Energy Storage Integration and Three Level NPC converter,” Doctoral Thesis, University of Bordeaux 1, 2012.

[32] N. Mohan, T. M. Undeland, and W. P. Robbins, “Power Electronics: Converters, Applications, and Design,” 3rd ed. Hoboken, NJ: John Wiley & Sons, 2003.

[33] R. W. Erickson and D. Maksimovic, “Fundamentals of Power Electronics,” 2nd ed. Norwell, MA: Kluwer Academic Publishers, 2001.

[34] M. H. Rashid, “Power Electronics: Circuits, Devices, and Applications,” 4th ed. Upper Saddle River, NJ: Pearson Prentice Hall, 2013.

[35] H. Kanchev, “Gestion des flux énergétiques dans un système hybride de sources d’énergie renouvelable : Optimisation de la planification opérationnelle et ajustement d’un micro réseau électrique urbain,” Doctoral Thesis, PRES Université Lille Nord-de-France.

[36] V. Courtecuisses, “Supervision d’une centrale multi sources à base d’éoliennes et de stockage d’énergie connectée au réseau électrique,” Doctoral Thesis, Laboratoire d'Electrotechnique et d'Electronique de Puissance de Lille, 2008.

[37] O. Richardo, “Réglage coordonné de Tension dans les Réseau de Distribution à l’aide de la Production Décentralisée,” Doctoral Thesis, 10 Oct. 2006.

[38] T. Ackermann, G. Andersson, and L. Söder, “Distributed generation: a definition,” Electric Power Systems Research, vol. 57, no. 3, pp. 195-204, Apr. 2001.

[39] A. Blatter, “Placement optimal de centrales de production et de stockage d'énergie électrique décentralisées dans un réseau

[40] O. Richardo, “Réglage coordonné de Tension dans les Réseau de Distribution à l’aide de la Production Décentralisée,” Doctoral thesis, 10 octobre 2006.

[41] T. Ackermann, G. Andersson, and L. Söder, "Distributed generation: a definition," *Electric Power Systems Research*, vol. 57, no. 3, pp. 195-204, Apr. 2001.

[42] A. Blatter, “Placement optimal de centrales de production et de stockage d'énergie électrique décentralisées dans un réseau électrique,” Travaux d'étudiants réalisés au LRE, Responsable(s): Stéphane Gerbex, Prof. Alain Germond, 2003.

[43] E. F. Mogos, "Production décentralisée dans les réseaux de distribution," Doctorat génie électrique ENSAM, soutenue le 20 juillet 2005.

[44] A.A. Al-shamma'a and K.E. Addoweesh, “Optimum Sizing of Hybrid PV/Wind/Battery/Diesel System Considering Wind Turbine Parameters Using Genetic Algorithm,” in *IEEE International Conference on Power and Energy (PECon), Kota Kinabalu Sabah, Malaysia, 25 December 2012.

[45] A. EL Khadimi, L. Bchir, and A. Zeroual, “Dimensionnement et Optimisation Technico-économique d'un Système d'Energie Hybride Photovoltaïque-Eolien avec Système de stockage,” *Revue des Energies Renouvelables*, vol. 7, 2004.

[46] A.A. Khan, A.F. Minai, R.K. Pachauri, et al., “Optimal Sizing, control, and management strategies for hybrid renewable energy systems: A comprehensive review,” Energies, vol. 15, no. 6249, 2022.

[47] M. M. Ibrahim, “Energy management strategies of hybrid renewable energy systems: A review,” *Wind Engineering*, 2023.

[48] B. Madaci, R. Chenni, E. Kurt, and K.E. Hemsas, “Design and control of a stand-alone hybrid power system,” *International Journal of Hydrogen Energy, pp. 1-12, 2016.

[49] A. Benjemaa, “Coopération méta heuristique et logique floue pour le dimensionnement d'une installation hybride,” Doctoral thesis, University of Reims Champagne-Ardenne, 2015.

[50] W. Cao, Y. Xie, and Z. Tan, “Wind Turbine Generator Technologies,” Advances in Wind Power, 2012.

[51] T. Suzuki, H. Okitsu, and T. Kawahito, “Characteristics of a small wind-power system with DC generator,” IEEE Proceedings Electric Power Applications B, vol. 129, no. 4, pp. 217-220, 1982.

[52] H. Ma, L. Chen, P. Ju, H. Liu, N. Jiang, and C. Wang, “Feasibility research on DC generator-based wind power generation system,” in *International Conference on Sustainable Power Generation and Supply (SUPERGEN), April 1-5, 2009.

[53] H. S. Kim and D. D. C. Lu, “Review on wind turbine generators and power electronic converters with the grid-connection issues,” in 20th Australasian Universities Power Engineering Conference (AUPEC)*, pp. 1-6, 2010.

[54] M. R. Ruviaro, F. S. Runcos, N. Sadowski, and I. M. Borges, “Analysis and test results of a brushless doubly fed induction machine with rotary transformer,” IEEE Transactions on Industrial Electronics, vol. 59, no. 6, pp. 2670-2677, 2012.

[55] X. Li, Y. Zhou, L. Han, D. Zhang, J. Zhang, Q. Qiu, et al., “Design of a high temperature superconducting generator for wind power applications,” IEEE Transactions on Applied Superconductivity, vol. 21, part 2, pp. 31155-11580, 2011.

[56] H. Li and Z. Chen, “Overview of different wind generator systems and their comparisons,” IET Renewable Power Generation, vol. 2, no. 2, pp. 123-138, 2008.

[57] F. Valenciaga, P. F. Puleston, P. E. Battaiotto, and R. J. Mantz, “Passivity/sliding mode control of a stand-alone hybrid generation system,” IEE Proc.-Control Theory Appl., vol. 147, no. 6, pp. 680-686, November 2000.

[58] J. Rico-Melgoza, J. P. Suarez, E. Barrera-Cardiel, and M. M. Martinez, “Modeling and Analysis of Three-phase Diode Bridge Rectifiers as Linear Complementarity Systems,” Electric Power Components and Systems, vol. 40, pp. 1639–1655, 2012.

[59] B. Mebarki, L. Rahmani, D. Belkacem, and B. Allaoua, “Electric Automobile Ni-MH Battery Investigation in Diverse Situations,” Energy Procedia, vol. 36, pp. 130-141, 2013.

[60] A. Pradhan and B. Panda, “A Simplified Design and Modeling of Boost Converter for Photovoltaic System,” International Journal of Electrical and Computer Engineering (IJECE), vol. 8, no. 1, pp. 141-149, February 2018.

[61] S. Dimitar, L. Vladimir, R. Daniel, Z. Zahari, and M.A. Omar, “Modélisation Des Convertisseurs Statiques DC-DC Pour Des Applications Dans Les Energies Renouvelables En Utilisant MATLAB/SIMULINK,” in Conférence EF UTC, Compiègne, 24-25 Septembre 2009.

[62] M. T. Vaïtchemé, “Modelisation et simulation d'un système de stockage intégré dans un micro-réseau autonome solaire-éolien,” University of Québec En Abitibi Témiscamingue, 2019.

[63] Z. Laid, “étude technique d’un système d’énergie hybride photovoltaïque-éolien hors réseau,” Doctoral thesis, University of Constantine, 2010.

[64] B. Subudhi and R. Pradhan, “A Comparative study on maximum power point tracking techniques for photovoltaic power systems,” IEEE Transactions on Sustainable Energy, vol. 4, no. 1, pp. 89-98, January 2013.

[65] L. Zhang, W. Zhang, and D. Xu, "LCL Filter Design with the Inductor Nonlinear Behavior Consideration in the Three Phase Grid-Connected Inverter," *in Proc. IEEE Conf. on Energy Conversion Congress and Exposition*, Montreal, Canada, Sep. 2018, pp. 3141-3148.

[66] J. Lettl, J. Bauer, and L. Linhart, “Comparison of different filter types for grid connected inverter,” in Progress in Electromagnetics Research Symposium Proceedings (PIERS), Marrakesh, MOROCCO, pp. 1426–1429, May 20–23, 2011.

[67] Ch. Ammari, Dj. Belatrache, B. Touhami, and S. Makhloufi, “Sizing, optimization, control and energy management of hybrid renewable energy system,” Energy and Built Environment, vol. 3, no. 4, October 2022.

[68] I. S. Mohamed, S. A. Zaid, M. F. Abu-Elyazeed, and H. M. Elsayed, “Classical methods and model predictive control of three–phase inverter with output LC filter for UPS applications,” in IEEE International Conference on Control, Decision and Information Technologies (CoDIT’13), Hammamet, Tunisia, 6–8 May 2013.

[69] N. L. Manuel and N. İnanç, “Sliding Mode Control-Based MPPT and Output Voltage Regulation of a Stand-alone PV System,” Power Electron. Drives, vol. 7, no. 1, pp. 159–173, 2022, doi: 10.2478/pead-2022-0022.

[70] S. Motahhir, A. El Hammoumi, and A. El Ghzizal, “The most used MPPT algorithms: Review and the suitable low-cost embedded board for each algorithm,” Journal of Cleaner Production, vol. 246, 2020.

[71] H. Abouobaida and S. El Beid, "Practical performance evaluation of maximum power point tracking algorithms in a photovoltaic system," International Journal of Power Electronics and Drive System (IJPEDS), vol. 8, no. 4, pp. 1744-1755, 2017.

[72] D. Rekioua, A. Y. Achour, and T. Rekiouaa, “Tracking power photovoltaic system with sliding mode control strategy,” in Energy Procedia, pp. 219–230, 2013.

[73] E. A. Kisame, M. J. Gatari, D. M. Mulati, and M. Iavi, “An improved perturb and observe maximum power point tracking technique using fuzzy logic controller,” JAGST, vol. 17, no. 1, 2016.

[74] O. Zebraoui and M. Bouzi, “Improved MPPT controls for a standalone PV/wind/battery hybrid energy system,” International Journal of Power Electronics and Drive Systems (IJPEDS), vol. 11, no. 2, pp. 988–1001, 2020.

[75] H. Kahal, R. Taleb, Z. Boudjemaa, and A. Bouyekni, “Super Twisting Sliding Mode Control of Dual Star Induction Generator for Wind Turbine,” *The Mediterranean Journal of Measurement and Control (MEDJMC)*, vol. 13, no. 3, pp. 788-794, 2017.

[76] A. Yahdou, B. Hemici, and Z. Boudjema, “Second Order Sliding Mode Control of a Dual-Rotor Wind Turbine System by Employing a Matrix Converter,” *Journal of Electrical Engineering*, vol. 16, no. 3, pp. 89-100, 2016.

[77] A. Polyakov and L. Fridman, "Stability notions and Lyapunov functions for sliding mode control systems," *IFAC Proceedings Volumes*, vol. 45, no. 9, pp. 431-435, 2012.

[78] A. Levant, “Higher-Order Sliding Modes, Differentiation and Output Feedback Control,” *International Journal of Control*, vol. 76, no. 9-10, pp. 924-941, 2003.

[79] O. Zebraoui and M. Bouzi, “Robust sliding mode control based MPPT for a PV/Wind hybrid energy system,” *International Journal of Intelligent Engineering Systems (IJIES)*, vol. 11, no. 5, pp. 290–300, 2018, doi: 10.22266/IJIES2018.1031.27.

[80] Z. Boudjema, R. Taleb, A. Yahdou, and H. Rahal, “High Order Sliding Mode Control of a DFIM Supplied by Two Power Inverters,” *Carpathian Journal of Electronic and Computer Engineering*, vol. 8, no. 1, pp. 23-30, 2015.

[81] I. Eker and Ş. A. Akinal, "Sliding mode control with integral augmented sliding surface: design and experimental application to an electromechanical system," *Electrical Engineering*, vol. 90, pp. 189-197, 2008.

[82] E. H. Mamdani and W. J. M. Kickert, "Analysis of a fuzzy logic controller," *Fuzzy Sets and Systems*, vol. 1, no. 1, pp. 29–114, 1978.

[83] E. H. Mamdani, "Application of fuzzy algorithms for control of simple dynamic plant," *Proceedings of the Institution of Electrical Engineers*, vol. 121, no. 12, pp. 1585–1588, Dec. 1974, doi: 10.1049/PIEE.1974.0328.

[84] L. A. Zadeh, "A fuzzy-set-theoretic interpretation of linguistic hedges," *Journal of Cybernetics*, vol. 3, pp. 4–34, Jan. 1972.

[85] B. Kumar, N. Agrawal, S. K. Singh, and A. Agarwal, “A comparative analysis of wind energy conversion systems based on PMSG for maximum power extraction,” in 2022 IEEE 10th Power India International Conference (PIICON), 2022.

[86] F. Menzri, A. Lekmine, A. Fatah, T. Boutabba, I. Benlaloui, and D. Khamari, “Improvement of energy management of standalone hybrid generation power system using adaptive neuro-fuzzy system,” in 2023 IEEE First International Conference on Electrical Engineering and Advanced Technologies (ICEEAT23), Batna, Algeria, Nov. 5-7, 2023.

[87] C. Nicola, M. Nicola, S. Popescu, and M. Duță, "Power factor correction and sensorless control of PMSM using FOC strategy," in *2019 International Conference on Electromechanical and Energy Systems (SIELMEN)*, pp. 1-6, 2019.

[88] M. Khalilpour, K. Valipour, H. Shayeghi, and N. Razmjooy, "Designing a robust and adaptive PID controller for gas turbine connected to the generator," *Res. J. Appl. Sci. Eng. Technol.*, vol. 5, pp. 1544–1551, 2013.

[89] H. Shayeghi and A. Rahnama, "Designing a PD-(1+PI) controller for LFC of an entirely renewable microgrid using PSO-TVAC," *Int. J. Techn. Phys. Prob. Eng. (IJTPE)*, vol. 12, no. 45, pp. 19–27, 2020.

[90] H. Shayeghi, A. Rahnama, and H. H. Alhelou, "Frequency control of fully-renewable interconnected microgrid using fuzzy cascade controller with demand response program considering," *Int. Conf. Clean Energy*, 2022.

[91] H. Shayeghi, A. Rahnama, N. Takorabet, P. Thounthong, and N. Bizon, "Designing a multi-stage PD(1+PI) controller for DC–DC buck converter," in *7th Int. Conf. Advances Clean Energy Res. (ICACER)*, Barcelona, Spain, Apr. 2022.

[92] L. M. Shankareppagol, S. N. Dodamani, and S. Hampannavar, "Performance analysis of P&O and INC MPPT for WECS," in 2018 IEEE 3rd International Conference for Convergence in Technology (I2CT), 2018.

[93] Y. Charan, S. Teja, and Y. Pradeep Kumar, "Energy management of grid connected rooftop solar system with battery storage," in 2016 IEEE Innovative Smart Grid Technologies - Asia (ISGT-Asia), 2016.

[94] M. Hoon, M. A. Mohd Radzi, M. K. Hassan, and N. F. Mailah, "DC-link capacitor voltage regulation for three-phase three-level inverter-based shunt active power filter with inverted error deviation control," Energies, 2016.

[95] W. Bu and L. Xu, “Direct power control strategy of PWM rectifier based on improved virtual flux-linkage observer,” Journal of Control Science and Engineering, vol. 2017.

[96] S. Ouchen, S. Abdeddaim, A. Betka, and A. Menadi, “Experimental validation of sliding mode-predictive direct power control of a grid connected photovoltaic system, feeding a nonlinear load,” Solar Energy, vol. 136, pp. 328-336, 2016.

[97] S. Aurtenechea, M. A. Rodríguez, E. Oyarbide, and J. R. Torrealday, “Predictive control strategy for DC/AC converters based on direct power control,” IEEE Transactions on Industrial Electronics, vol. 54, pp. 1261–1271, 2007.

[98] S. Mahjoub, L. Ch. Alaoui, S. Drid, and N. Derbel, "Control and implementation of an energy management strategy for a PV–wind–battery microgrid based on an intelligent prediction algorithm of energy production," Energies, vol. 16, p. 1883, 2023, doi: 10.3390/en16061883.

[99] Z. Gadouche, C. Belfedal, T. Allaoui, M. Denai, and M. Bey, "Hybrid renewable energy system controlled with intelligent direct power control," Journal Européen des Systèmes Automatisés, vol. 55, no. 4, pp. 467-475, 2022, doi: 10.3166/jesa.55.467-475.

[100] M. Z. Oskouei, et al., "A critical review on the impacts of energy storage systems and demand-side management strategies in the economic operation of renewable-based distribution network," Sustainability, vol. 14, no. 4, 2022, doi: 10.3390/su14041883.